# *Tectonic evolution and deep mantle structure of the eastern Tethys since the latest Jurassic*

**Authors**

Sabin Zahirovic[a,*], Kara J Matthews[a,#], Nicolas Flament[a], R Dietmar Müller[a], Kevin C Hill[b], Maria Seton[a] and Michael Gurnis[c]

[a] EarthByte Group, School of Geosciences, The University of Sydney, NSW 2006, Australia

[b] Oil Search Limited, Sydney, NSW 2000, Australia

[c] Seismological Laboratory, California Institute of Technology, Pasadena, CA 91125, USA

* Corresponding author at: EarthByte Group, School of Geosciences, The University of Sydney, NSW 2006, Australia. E-mail address: sabin.zahirovic@sydney.edu.au (S. Zahirovic)

[#] Present address: Department of Earth Sciences, University of Oxford, South Parks Road, Oxford OX1 3AN, UK

Invited review submitted to *Earth-Science Reviews*

**Abstract**

The breakup of Pangea in the Jurassic saw the opening of major ocean basins at the expense of older Tethyan and Pacific oceanic plates. Although the Tethyan seafloor spreading history has been lost to subduction, proxy indicators from multiple generations of Tethyan ribbon terranes, as well as the active margin geological histories of volcanism and ophiolite obduction events can be used to reconstruct these ancient oceanic plates. The plate reconstructions presented in this study reconcile observations from ocean basins and the onshore geological record to provide a regional synthesis, embedded in a global plate motion model, of the India-Eurasia convergence history, the accretionary growth of Southeast Asia and the Tethyan-Pacific tectonic link through the New Guinea margin.

The global plate motion model presented in this study captures the time-dependent evolution of plates and their tectonic boundaries since 160 Ma, which are assimilated as surface boundary conditions for numerical experiments of mantle convection. We evaluate subducted slab locations and geometries predicted by forward mantle flow models against P- and S-wave seismic tomography models. This approach harnesses modern plate reconstruction techniques, mantle convection models with imposed one-sided subduction, and constraints from the surface geology to address a number of unresolved Tethyan geodynamic controversies. Our synthesis reveals that north-dipping subduction beneath Eurasia in the latest Jurassic consumed the Meso-Tethys, and suggests that northward slab pull opened the younger Neo-Tethyan ocean basin from ~ 155 Ma. We model the rifting of 'Argoland', representing the East Java and West Sulawesi continental fragments, as a northward transfer of continental terranes in the latest Jurassic from the northwest Australian shelf – likely colliding first with parts of the Woyla intra-oceanic arc in the mid-Cretaceous, and accreting to the Borneo (Sundaland) core by ~ 80 Ma. The Neo-Tethyan ridge was likely consumed along an intra-oceanic subduction zone south of Eurasia from ~ 105 Ma, leading to a major change in the motion of the Indian Plate by ~ 100 Ma, as observed in the Wharton Basin fracture zone bends.

We investigate the geodynamic consequences of long-lived intra-oceanic subduction within the Neo-Tethys, requiring a two-stage India-Eurasia collision involving first contact between Greater India and the Kohistan-Ladakh Arc sometime between ~ 60 and 50 Ma, followed by continent-continent collision from ~ 47 Ma. Our models suggest that the Sunda slab kink beneath northwest Sumatra in the mantle transition zone results from the rotation and extrusion of Indochina from ~ 30 Ma. Our results are also the first to reproduce the enigmatic Proto South China Sea slab beneath northern Borneo, as well as the Tethyan/Woyla slab that is predicted at mid-mantle depths south of Sumatra. Further east, our revised reconstructions of the New Guinea margin, notably the evolution of the Sepik composite terrane and the Maramuni subduction zone, produce a better match with seismic tomography than previous reconstructions, and account for a slab at ~ 30°S beneath Lake Eyre that has been overridden by the northward advancing Australian continent. Our plate reconstructions provide a framework to study changing patterns of oceanic circulation, long-term sea level driven by changes in ocean basin volume, as well as major biogeographic dispersal pathways that have resulted from Gondwana fragmentation and accretion of Tethyan terranes to south- and southeast-Eurasia.

Keywords:
Tethys, Pangea, Tectonics, Geodynamics, Sundaland, Southeast Asia

## 1 Introduction

Southern Eurasia, Southeast Asia and New Guinea represent a unique example of long-term tectonic convergence between multiple tectonic domains that has resulted in a complex assemblage of continental fragments, intra-oceanic arcs, ophiolite belts and marginal basins (Figs. 1 and 2). The Southeast Asian continental promontory, known as Sundaland, has grown through successive accretionary episodes resulting from the breakup of Pangea (Acharyya, 1998; Audley-Charles, 1988; Metcalfe, 1994), and subsequent northward transfer of Gondwana-derived continental ribbon terranes and microcontinents on the Tethyan oceanic "conveyors" towards Eurasia. Importantly, the region records a complex interaction between the Tethyan and (proto-) Pacific tectonic domains, which has opened and consumed successive oceanic basins and gateways (Metcalfe, 1999), and has had major consequences for biogeographic dispersal pathways such as the origin of the Wallace Line (Burrett et al., 1991; de Bruyn et al., 2014; Lohman et al., 2011; Monod and Prendini, 2015; Rolland et al., 2015), oceanic circulation (Gaina and Müller, 2007; Gourlan et al., 2008; Heine et al., 2004), global climate and sea level (Herold et al., 2014; Huber and Goldner, 2012; Lee et al., 2013; Morley, 2012b; Müller et al., 2008; Scotese et al., 1999; Spasojevic and Gurnis, 2012; van der Meer et al., 2014; Wang, 2004; Xu et al., 2012), and the development of economic resources (Goldfarb et al., 2014; Zaw et al., 2014).

Plate tectonic reconstructions play a pivotal role in unravelling the complexity of this region and provide a platform to address long-standing geological questions in a geodynamic context. We apply a modern approach of modelling entire plates, their evolving plate boundaries and the terranes they carry. This study aims to synthesise previously published onshore and offshore geological constraints, as well as incorporate decades of developments in plate tectonic reconstructions, into a modern plate motion model to document the post-Pangea geodynamic evolution of southern Eurasia,

Southeast Asia and New Guinea since the Late Jurassic in a regional and global context. Despite significant technological and methodological advancements in plate reconstruction approaches, very few reconstructions of the eastern Tethys exist in an open-access digital form that can be tested and expanded by the scientific community.

As part of this work, we release detailed plate reconstructions for the eastern Tethys (from the India-Eurasia collision zone eastward to Papua New Guinea, Figs. 1-3) that are embedded in a self-consistent global plate motion model, as a collection of digital geometry files and rotation parameters compatible with the open-source and cross-platform plate reconstruction tool, GPlates (www.gplates.org). We provide a brief background to previous regional tectonic reconstructions in Section 1.1, as well as tomographic and numerical modelling approaches in Sections 1.2-1.3 that have been used to gain insight into the tectonic and geodynamic processes controlling the regional evolution. In Sections 2 to 4, we outline our approach of building modern plate reconstructions for the three key regions that comprise the eastern Tethys, including i) the India-Eurasia convergence zone, ii) Southeast Asia, and iii) the New Guinea margin, and compare our approach and findings with previous work. In Section 5, we show how modern plate reconstructions that incorporate evolving plate boundaries can be used with numerical models of mantle flow to predict mantle structure, study the distribution of ancient slabs, and test alternative plate motion scenarios where geological constraints are vague or interpretation is ambiguous. In Sections 6 and 7 we highlight the implications of our work in a regional and global context, and provide some key findings from our modelling of the tectonic and geodynamic evolution of the entire eastern Tethyan domain.

The coupled global plate reconstructions and mantle flow models provide a context for better understanding the latest Jurassic rifting events from northern Gondwana (Metcalfe, 1994; Pigram and Panggabean, 1984), which opened the Neo-Tethys at the expense of the Meso-Tethys ocean basin (Fig. 4A). This rifting episode transferred the 'Argoland' ribbon continent, which included East Java, West Sulawesi and Mangkalihat (Hall, 2012; Zahirovic et al., 2014), north towards Eurasia, while also marking the onset of major intra-oceanic subduction systems along southern Eurasia and

154 northern New Guinea. In the absence of preserved seafloor spreading histories for Neo-Tethyan
155 evolution, we test alternative scenarios of subduction using geodynamic models of mantle flow that
156 are compared with the present-day mantle structure interpreted from seismic tomography.

157 The improvement in the methods applied to plate reconstructions and increasing data coverage
158 in complex regions have implications for linking plate tectonic evolution with the deep mantle and
159 other Earth systems. Improved plate tectonic reconstruction techniques have enabled the
160 quantification of time-dependent convergence rates (Lee and Lawver, 1995; Sdrolias and Müller,
161 2006; Whittaker et al., 2007), and inferences of regional and global plate re-organization events
162 (Matthews et al., 2011; Matthews et al., 2012), as well as providing insight into the size distribution
163 of tectonic plates (Morra et al., 2013) and factors controlling the speed of tectonic plates (Zahirovic
164 et al., 2015). The plate reconstructions presented in this work have important implications for our
165 understanding of the mid-Cretaceous seafloor spreading pulse (Seton et al., 2009) that may have led
166 to higher eustatic sea levels (Müller et al., 2008), and the proposed major regional and global plate
167 reorganization at ~ 105-100 Ma (Matthews et al., 2012) that may be linked to the subduction of the
168 Neo-Tethyan mid-oceanic ridge. In addition, plate reconstructions of the Tethyan domain have
169 consequences for understanding the atmospheric carbon budget resulting from the initiation and
170 abandonment of major Andean-style and intra-oceanic Tethyan subduction zones (Jagoutz et al.,
171 2016; van der Meer et al., 2014).

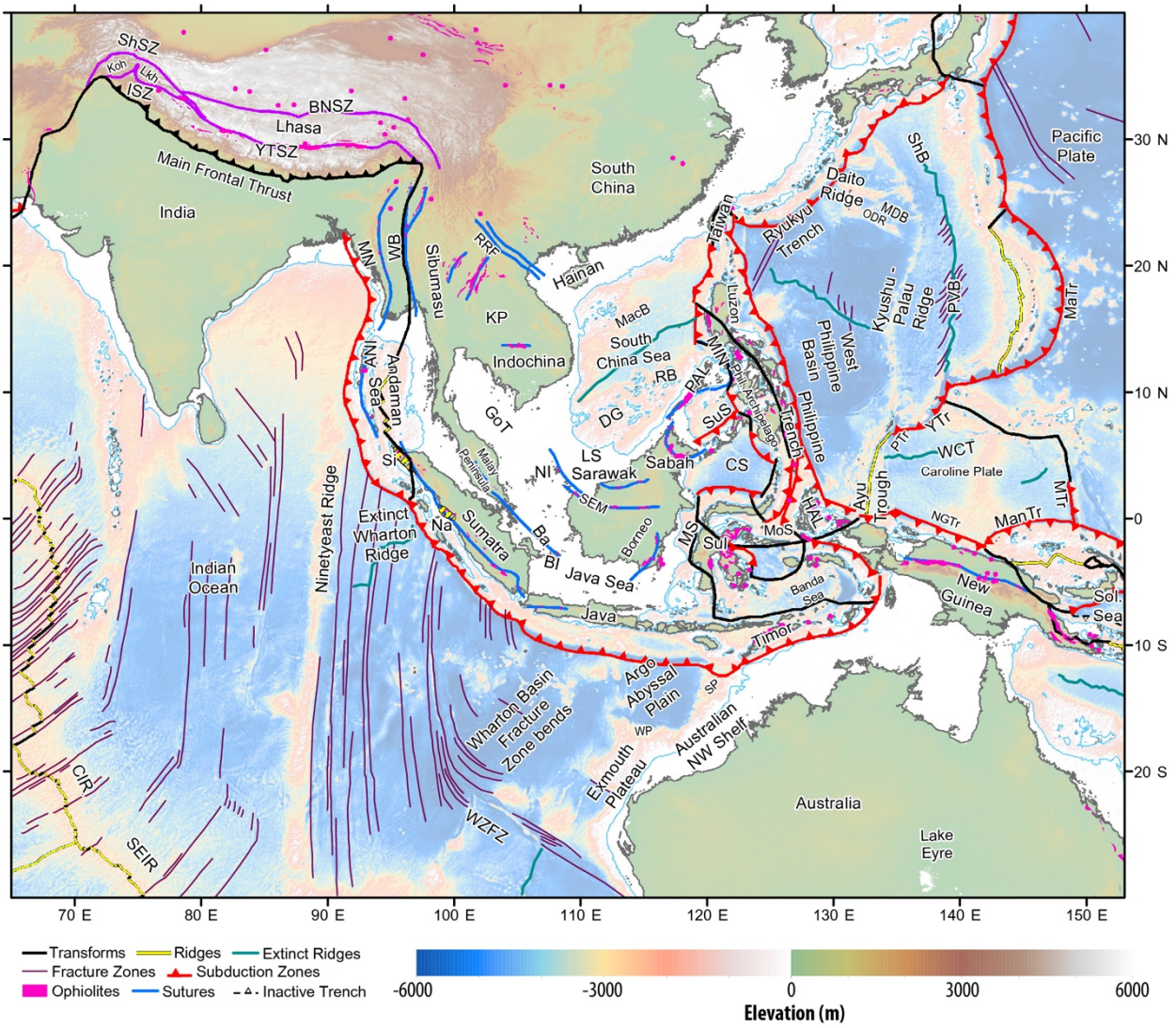


**Fig. 1.** Regional tectonic setting of southern Eurasia, Southeast Asia and New Guinea. The plate boundaries are modified from Bird (2003), the topography is from Amante et al. (2009), and the seafloor fabric is from Matthews et al. (2011). Southeast Asian sutures (blue) and ophiolites are modified from Hutchison (1975), with additional ophiolites for New Guinea from Baldwin et al. (2012), and for Southeast Asia from Pubellier et al. (2004). The Tethyan sutures in the Indian segment of the margin (violet lines) are from Yin and Harrison (2000). ANI – Andaman-Nicobar Islands, Ba – Bangka Island, BI – Billiton Island, BNSZ – Bangong-Nujiang Suture Zone, CIR – Central Indian Ridge, CS – Celebes Sea, DG – Dangerous Grounds, GoT – Gulf of Thailand, HAL – Halmahera, ISZ – Indus Suture Zone, Koh-Lkh – Kohistan-Ladakh, KP – Khorat Plateau, LS – Luconia Shoals, ManTr – Manus Trench, MaTr – Izu-Bonin-Mariana Trench, MDB – Minami Daito Basin, MIN – Mindoro, MN – Mawgyi Nappe, MoS – Molucca Sea, MP – Malay Peninsula, MS – Makassar Straits,

MTr – Mussau Trench, Na – Natal, NGTr – New Guinea Trench, NI – Natuna Island, ODR – Oki Daito Ridge, PA – Philippine Arc, PAL – Palawan, PTr – Palau Trench, PVB – Parece Vela Basin, RB – Reed Bank, RRF – Red River Fault, SEIR – Southeast Indian Ridge, SEM – Semitau, ShB – Shikoku Basin, ShSZ – Shyok Suture Zone, Si – Sikuleh, Sol. Sea – Solomon Sea, SP – Scott Plateau, Sul – Sulawesi, SuS – Sulu Sea, WB – West Burma, WCT – West Caroline Trough, WP – Wombat Plateau, WZFZ – Wallaby Zenith Fracture Zone, YTr – Yap Trench, YTSZ – Yarlung-Tsangpo Suture Zone.

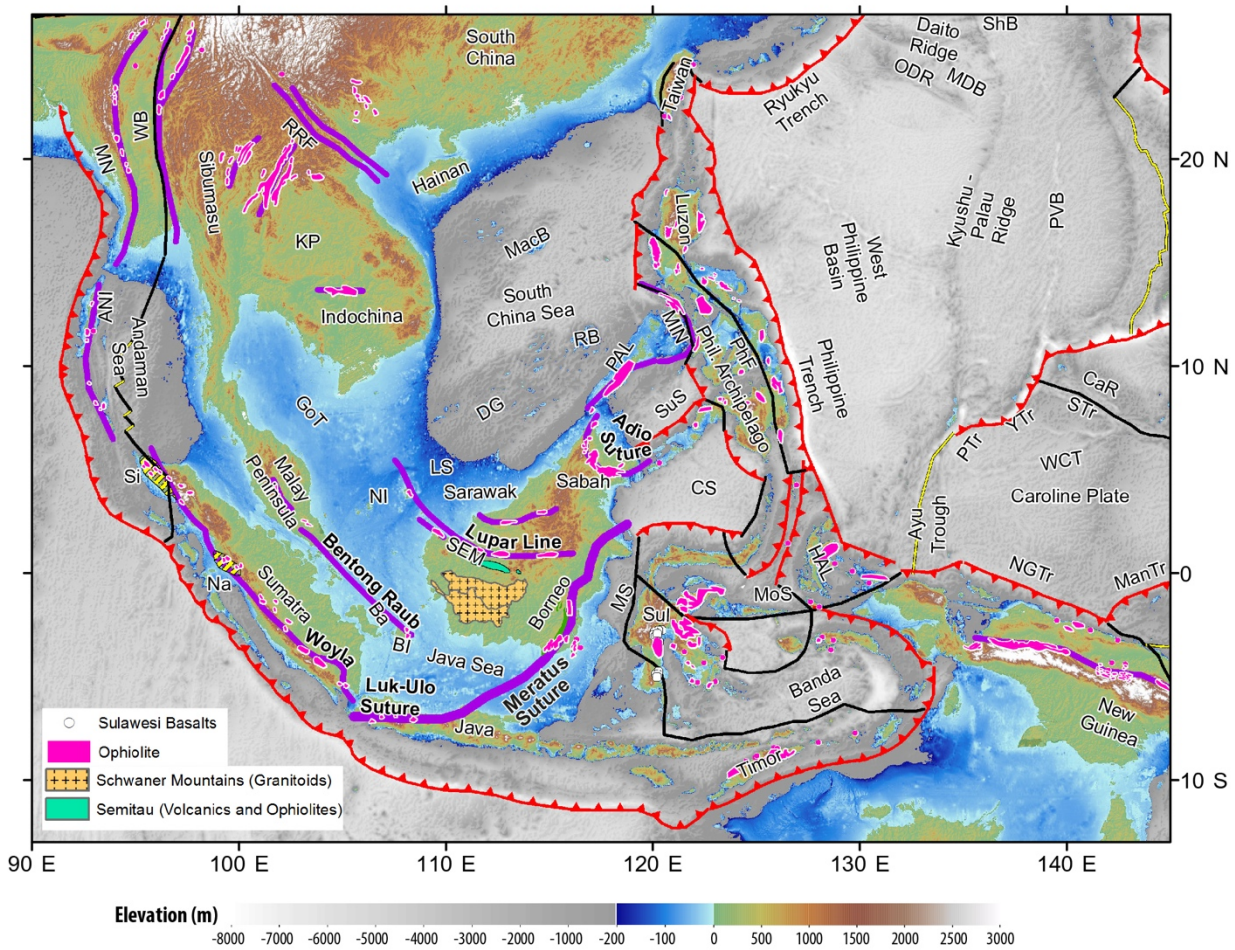


**Fig. 2.** Regional tectonic framework of Southeast Asia and New Guinea, with high-resolution Global Multi-Resolution Topography of depths shallower than 200 m from Ryan et al. (2009). Abbreviations and plate boundary symbology follow those used in Fig. 1.

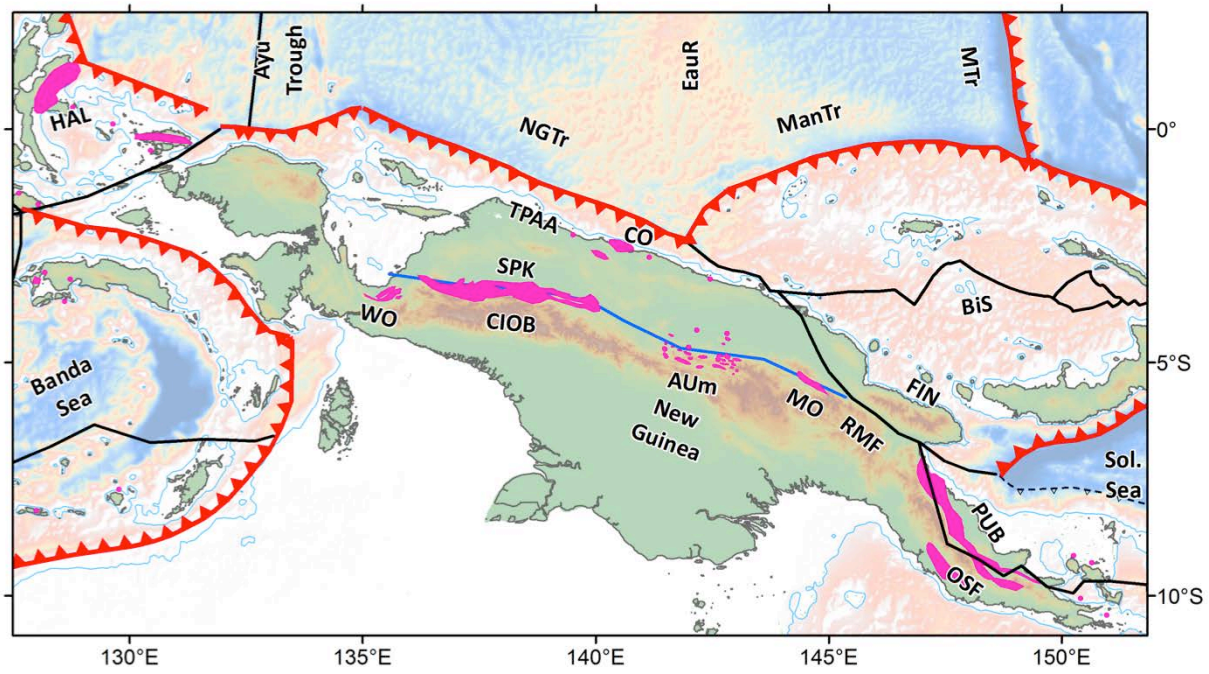


**Fig. 3.** Tectonic framework and topography of New Guinea. AUm – April Ultramafics, BiS – Bismarck Sea, CIOB – Central Irian Ophiolite Belt, CO – Cyclops Ophiolite, EauR – Eauripik Rise, FIN – Finisterre Terrane, MO – Marum Ophiolite, OSF – Owen Stanley Fault, PUB – Papuan Ultramafic Belt, SPK – Sepik Terrane, Sol. Sea – Solomon Sea, TPAA – Torricelli-Prince Alexander Arc, WO – Weyland Overthrust. Other abbreviations and plate boundary symbology follow those used in Fig. 1.

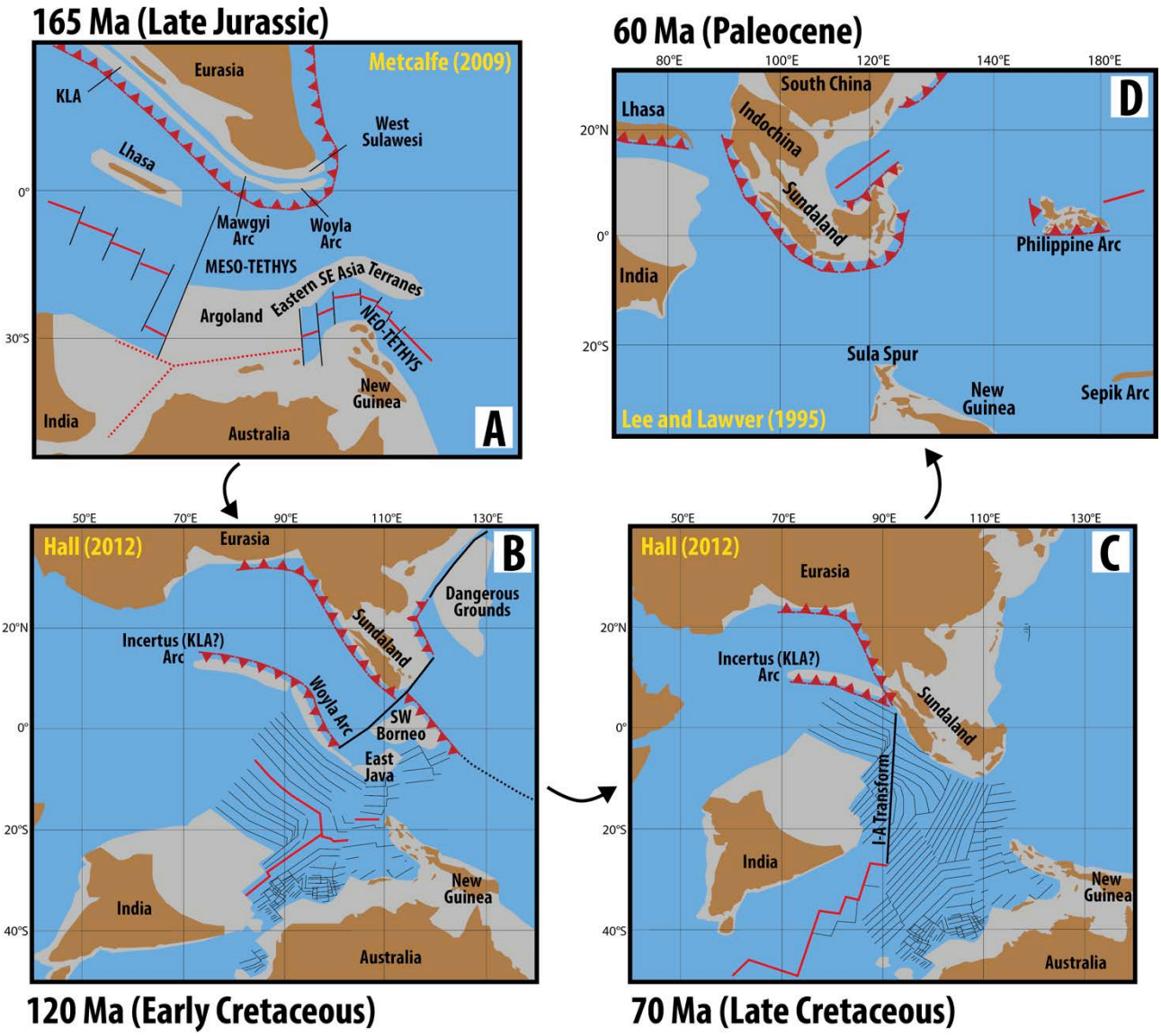


**Fig. 4.** A wide range of tectonic reconstructions have been proposed for the eastern Tethys between the India-Eurasia convergence zone and New Guinea. A) The Late Jurassic rifting event along northern Gondwana has been modelled as a westward propagating rift from New Guinea towards Argoland, and joining up as a triple junction between India and Australia in the model of Metcalfe (2009). The rifting mechanism is implied as northward slab pull from Tethyan subduction along southern Eurasia. B) The model of Hall (2012) instead invokes a south-dipping subduction zone along northern Gondwana in the latest Jurassic, leading to the opening of the Neo-Tethys as a large back-arc basin. The related Incertus Arc likely represents the Kohistan-Ladakh (KLA) and Woyla arc systems in the Neo-Tethys. C) By the Late Cretaceous, subduction polarity reverses across the Incertus Arc to produce northward slab pull along a north-dipping intra-oceanic subduction zone. The

Hall (2012) model imposes a subduction hiatus along southern Sundaland between 90 and 45 Ma, which requires the segmentation of the Neo-Tethys across a transform that cross-cuts Tethyan seafloor fabric at ~ 90°E (I-A Transform). D) The model of Lee and Lawver (1995) presents eastern Tethyan plate reconstructions since 60 Ma in a South China fixed reference frame. The size of Greater India is similar as proposed in Hall (2012), but is about twice the northward extent presented in this study, largely to accommodate an India-Eurasia continent-continent collision at ~ 55 Ma. The Lee and Lawver (1995) model also presents all plate rotation parameters, which enables the reproducibility and testability of this model. A common feature between the models (A-D) is relatively less detail for the New Guinea region, which has been difficult to reconstruct due to the lack of data and the dominance of complex interactions between Asian and Pacific subduction systems.

### 1.1 Plate tectonic models of the eastern Tethys

As many generations of plate reconstructions have been proposed for the eastern Tethyan tectonic domain, it is useful to understand the historical context and help categorize successive generations of models that have been proposed. Even before the acceptance of plate tectonic principles, Southeast Asian geology was of great interest due to significant hydrocarbon (Halbouty et al., 1970; Wennekers, 1958) and metallogenic (Brown, 1951; Leith, 1926; Matthews, 1990; Penrose, 1903) discoveries. Early attempts to explain the geology of Southeast Asia led to a large number of competing hypotheses. Fairbridge (1963) explained the geological affinities between Southeast Asia and Gondwana by invoking a range of mechanisms from now-abandoned ideas of mantle contraction, mantle expansion, rising and sinking land bridges, and galactic expansion, to then emerging ideas of continental drift. A few years on, Audley-Charles (1966) provided the first synthesis of stratigraphic evidence to describe the region's Mesozoic paleogeographic evolution in

241 the context of continental drift, with special reference to paleo-latitude indicators from paleo-climatic
242 and paleo-magnetic data.

243 It was only in the 1970s that plate tectonic principles of subduction, seafloor spreading and
244 transform tectonic boundaries (Forsyth and Uyeda, 1975; Le Pichon, 1968; McKenzie, 1969;
245 McKenzie and Parker, 1967) were invoked in first-generation continental reconstructions (Table 1)
246 to explain the present-day tectonic complexity of the eastern Tethys (Fitch, 1972; Hamilton, 1979;
247 Katili, 1971). These models were subsequently used to create the first schematic "plate
248 reconstructions" (Katili, 1975) that largely focused on the dominance of active volcanic arcs and
249 associated subduction zones in controlling the tectonic complexity of the region. Importantly, the
250 work of Katili (1975) identified a number of parallel and arcuate paleo-arc systems, which recorded
251 post-Permian subduction of Tethyan oceanic crust. Pioneering work in the 1970s and 1980s applied
252 paleomagnetic techniques to infer that parts of Southeast Asia originated from the northern
253 Gondwana margin (McElhinny et al., 1981), and more specifically somewhere between north Africa
254 and Greater India (the portion of India currently under-thrust beneath Eurasia) (Stauffer, 1983).
255 Although the origin of Southeast Asian continental fragments from Arabia or Africa in the Paleozoic
256 has since been discounted (see Metcalfe, 1988; Metcalfe, 1994; Metcalfe, 1999; Veevers, 2004), these
257 early works established the wider notion of Southeast Asian crustal accretion via the northward
258 transfer of continental fragments originating from the northern Gondwana margins (Fig. 4A).

259 Pioneering reconstructions of Gondwana breakup, and the northward transfer of crustal
260 fragments towards Asia, were largely presented as schematic scenarios portraying the drift of
261 continents with consideration of some major regional plate boundaries. Pigram and Panggabean
262 (1984) and Audley-Charles (1988) combined regional stratigraphic composite wells to identify a
263 major Late Jurassic breakup unconformity across the NW Australian margin, which suggested that a
264 number of continental fragments had detached to form the north Gondwana passive margin and open
265 the "Mesozoic Tethys" ocean basin. Based on the interpretation of rift-drift sedimentary sequences,
266 including the timing of the post-breakup unconformity, Pigram and Panggabean (1984) provided

schematic reconstructions of the Late Jurassic drifting episode and concluded that seafloor spreading initiated sometime in the Early Jurassic along New Guinea and Middle Jurassic along the NW Australian shelf. The generally northward transfer of Gondwana terranes opened successive Tethyan ocean basins including the rifting of a ribbon continent comprising Iran, North Tibet (Qiangtang) and Indochina to open "Tethys II" in the late Permian (Audley-Charles, 1988). A subsequent major rifting phase in the Late Jurassic opened the "Tethys III", detaching fragments including South Tibet (Lhasa), West Burma, Malaya, Borneo, Sulawesi, and Sumatra and a number of Banda allochthons (Audley-Charles, 1988). Importantly, the work of Audley-Charles (1988) and Audley-Charles et al. (1988) introduced a paleogeographic reconstruction framework using the computerised University of Cambridge Atlas plotting workflow, which we classify as a second generation reconstruction methodology (Table 1). This early generation of reconstructions assessed the prior continental affinities and inferred major rifting phases using biostratigraphic constraints, as well as made use of paleomagnetic syntheses and structural interpretations from seismic sections to infer rift and drift histories.

The third generation of plate reconstructions, largely developed in the late 1980s and throughout the 1990s (e.g., Besse and Courtillot, 1988; Daly et al., 1991; Jolivet et al., 1989; Lee and Lawver, 1994; Lee and Lawver, 1995), made use of extensive identifications of marine magnetic anomalies from the Indian Ocean and West Pacific calibrated to a geological timescale (e.g., Taylor and Hayes, 1980; Taylor and Hayes, 1983). The seafloor spreading histories, supplemented with paleomagnetic data from the continental blocks (e.g., Haile et al., 1977), were applied to make plate reconstructions using rigid body motions on the surface of a sphere (i.e., Euler rotations). The Jurassic to recent plate reconstructions of Besse and Courtillot (1988) and Scotese et al. (1988) were an important benchmark for subsequent plate motion models, as the work synthesised marine magnetic anomalies and continental paleomagnetism, yet also took into account the plate boundary evolution. Pertinent to this study, the work of Besse and Courtillot (1988) and Scotese et al. (1988) enabled reproducibility by providing finite rotation parameters.

293 Although the plate reconstructions of Lee and Lawver (1994) and Lee and Lawver (1995)
294 covered only the Cenozoic evolution of Southeast Asia (Fig. 4D), these were the first detailed regional
295 reconstruction that published testable and reproducible finite rotation parameters that quantitatively
296 described the motion of Southeast Asian crustal elements, building on the more regional approach
297 presented in Jolivet et al. (1989). The relative plate motions, provided as finite rotations, were linked
298 into a plate motion hierarchy that tied back to the South China block, and thus only provide a regional
299 perspective (Lee and Lawver, 1994; Lee and Lawver, 1995). However, the provision of Euler
300 rotations significantly increased their utility even over more recent models as they allow for
301 reproducibility and refinement by subsequent researchers.
302 A major improvement in regional plate reconstructions was presented in Hall (1996), and
303 subsequent works by the same author (Hall, 2002; Hall, 2012) (Fig. 4B–C), where the regional plate
304 reconstructions were embedded in a global plate circuit – that links Australia and India back to Africa,
305 and Asian fragments through Eurasia, North America and Africa. Using a global plate circuit
306 combines relative plate motions with a frame of reference with respect to the mantle using a hotspot
307 frame (e.g., Müller et al., 1993), which enables linkages between the plate-mantle system. In the
308 absence of hotspot tracks (i.e., before ~ 120 Ma), plate reconstructions make use of paleomagnetic
309 reference frames (e.g., Hall and Spakman, 2015), which enable the reconstruction of paleo-latitudes
310 of climate-sensitive data, and can be corrected for True Polar Wander to create more explicit links
311 between the plate-mantle system in deep time. The reconstructions presented in Hall (1996) and Hall
312 (2002) provide a regional post-Jurassic evolution of the India-Eurasia convergence zone, Southeast
313 Asia and New Guinea embedded in a detailed synthesis of relevant data, and are presented in 1 Myr
314 interval snapshots. Such high temporal resolution is important for capturing major plate boundary
315 reconfigurations and resulting changes in plate motion magnitudes and directions, such as the change
316 in India's plate motions and northward advance from ~ 100 Ma (Gibbons et al., 2015; Matthews et
317 al., 2012; van Hinsbergen et al., 2011). Although the reconstructions are presented in 1 Myr intervals,

no relative or absolute plate rotation parameters have been provided, which limits the testability of such models.

These first- to fourth-generation plate reconstructions provide considerable detail and insight into the tectonic evolution of the eastern Tethys, but cannot be easily linked to methods that take into account the geodynamic evolution of the plate-mantle system. Schematic reconstructions cannot be linked to numerical models of convection as they usually lack the continuous network of plate boundaries through time that enables the use of plate velocities as surface boundary conditions. As plate motions are inextricably linked to mantle convection (Hager and O'Connell, 1981; Turcotte and Oxburgh, 1972), and since much of the Tethyan seafloor spreading history has since been subducted (Hutchison, 1975; Şengör et al., 1988), some authors have inferred plate motion histories from high velocity seismic anomalies as given by mantle tomography models (Hall and Spakman, 2003; Hall and Spakman, 2015; Replumaz et al., 2004; van der Voo et al., 1999b; Wu et al., 2016). We expand on these approaches and make use of our most recent plate reconstructions coupled to numerical models of mantle convection which are then validated using seismic tomographic images and a suite of onshore and offshore geological constraints.

Table 1. Generations of continental and plate reconstructions depicting the kinematic and geodynamic evolution of Southeast Asia.

| **Generation of reconstruction** | **Description** | **Examples** |
|---|---|---|
| First | Schematic reconstructions of continental motions. | Pigram and Panggabean (1984)<br>Metcalfe (1988) |
| Second | Continental reconstructions are made using digital approaches, with schematic paleo-plate boundaries. | Audley-Charles et al. (1988)<br>Rangin et al. (1990) |
| Third | Additionally provide regional reconstructions using seafloor spreading histories, constraints from onshore geology (paleomagnetism, stratigraphy, seismic, structural, biogeography, | Besse and Courtillot (1988)<br>Scotese et al. (1988)<br>Jolivet et al. (1989) |

| | | |
|---|---|---|
| | etc.) and an incomplete network of plate boundaries. Although these models are classified as 3rd generation reconstructions, they have a significant advantage over any other reconstructions that do not provide Euler rotation parameters that are provided in the 5th generation models. These models are important examples of reproducible and testable plate reconstructions of Southeast Asia. | Lee and Lawver (1994)<br>Lee and Lawver (1995) |
| Fourth | Regional reconstructions embedded in a global rotation hierarchy, constraining relative plate motions using seafloor spreading histories that are tied to an absolute hotspot or paleomagnetic reference frame. Synthetic seafloor spreading histories are generated in regions and times where seafloor has been subducted. | Hall (1996)<br>Hall (2002)<br>Hall (2012)<br>Stampfli and Borel (2002)# |
| Fifth | A continuous global network of evolving plate boundaries is modelled, with complete model rotation parameters and digital geometry files released for testability and reproducibility. Such models can be linked to regional and global geodynamic numerical calculations that link plate tectonics with underlying mantle convection. Some of these models incorporate regional refinements that include retro-deformation of continental crust to provide better full-fit reconstructions of Pangea. | Gurnis et al. (2012)<br>Seton et al. (2012)<br>Zahirovic et al. (2012)<br>Zahirovic et al. (2014)<br>Domeier and Torsvik (2014)^<br>Gibbons et al. (2015)<br>This study |
| Future | Build on previous approaches with stronger emphasis on quantifying uncertainties, and using ensemble computer modelling that incorporates all constraints (offshore and onshore) simultaneously and all relevant uncertainties to derive a quantitative "best-fit" plate reconstruction that is fully consistent with plate boundary forces and mantle convection models. Global plate reconstructions incorporate all major regions of deformation to provide better full-fit reconstructions and address the oversimplification of plate rigidity assumptions. | Such models are not yet available, and represent an aspirational goal to produce better plate tectonic reconstructions. |

336 ^ The Domeier and Torsvik (2014) reconstructions cover the Late Paleozoic global plate motion history, and include
337 major blocks of Southeast Asia.

338 [#] The model of Stampfli and Borel (2002) has linked plate boundaries and synthetic seafloor spreading histories, which
339 are important components of the 5th-generation models, but only provides snapshots without rotation parameters or
340 (evolving plate boundary) geometries.
341

342 **1.2 Seismic tomography constraints**

343

344 Seismic tomographic techniques have provided an important link between the present-day
345 arrangement of plate boundaries and deep mantle structure around Southeast Asia that has resulted
346 from long-term subduction of Tethyan and Pacific lithosphere. High-resolution P-wave seismic
347 tomographic models have demonstrated that the Sunda slab from the subduction of the Indo-
348 Australian oceanic plate penetrates to depths of ~ 1500 km (Li et al., 2008; Widiyantoro and van der
349 Hilst, 1996), and that it is distinct from the older and deeper Tethyan slabs (Widiyantoro and van der
350 Hilst, 1996). Due to the complexity of Tethyan convergence, and the lack of preserved seafloor
351 spreading histories, interpretations of mantle structure provide an important additional insight into
352 the past geometry and evolution of active margins in the region. For example, Hall and Spakman
353 (2002; 2003) used a P-wave seismic tomographic model to infer Cenozoic subduction histories in the
354 vicinity of the northern Australian margin. Hall and Spakman (2003) interpreted the Bijwaard and
355 Spakman (2000) P-wave seismic tomographic model to suggest that north-dipping subduction north
356 of Australia along the Philippine Archipelago occurred between 45 and 25 Ma, and inferred that little
357 subduction occurred north of Australia since 25 Ma due to the likelihood of a margin dominated by
358 strike-slip motion rather than convergence. Hall and Spakman (2015) recently attributed the 1600 km
359 deep Sunda slab to subduction since 45 Ma, but discounted the possibility that the Proto South China
360 Sea slab is in the upper mantle, and concluded that it is instead likely in the lower mantle at ~ 1200
361 km depth. Further south, a large east-west slab beneath Australia (including Lake Eyre) at ~ 800-
362 1200 km depths has been interpreted to be the result of north-dipping subduction that ceased

following accretion of the Sepik Terrane along New Guinea at ~ 50 Ma (Schellart and Spakman, 2015).

The India-Eurasia Tethyan mantle structure was interpreted in van der Voo et al. (1999b) where a global P-wave seismic tomographic model (Bijwaard et al., 1998) was used to infer the subduction history related to post-Jurassic subduction (Fig. 5). The large slabs, with a generally northwest-southeast trend and largely at mid-mantle depths, were interpreted to be the result of two simultaneous north-dipping subduction zones in the Neo-Tethys (van der Voo et al., 1999b), a scenario which requires a two-stage India-Eurasia collision. Hafkenscheid et al. (2006) elaborated on this approach by quantifying Tethyan slab volumes and inferring average slab sinking rates in the mantle. Hafkenscheid et al. (2006) tested end-member scenarios of Neo-Tethyan convergence, including a model for long-lived Andean-style subduction along southern Eurasia following Norton (1999) and Şengör and Natal'in (1996). Instead, the analysis by Hafkenscheid et al. (2006) suggested that an additional intra-oceanic subduction zone, following Stampfli and Borel (2002), could better reproduce the volume and distributions of slabs interpreted from 3D seismic tomography. The preferred scenario in Hafkenscheid et al. (2006) invoked an arc-continent collision between Greater India and the Spong Arc, likely contemporaneous with the Kohistan-Ladakh Arc (McDermid et al., 2002), at ~ 65-60 Ma, with continent-continent collision occurring at ~ 48 Ma, and infers a “free sinking rate” (i.e., when not attached to a subducting plate) of 3 and 2 cm/yr in the upper and lower mantle, respectively.

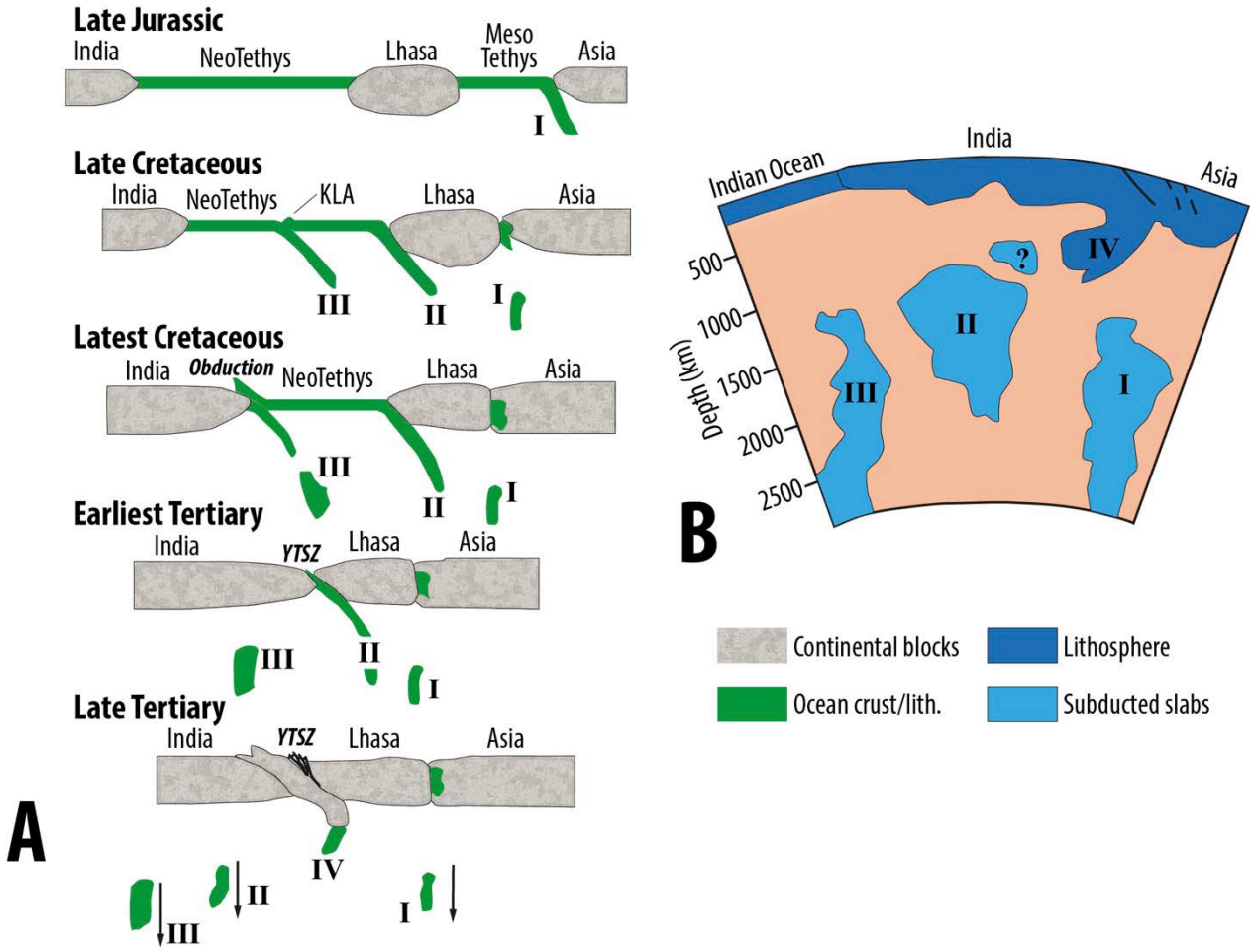


**Fig. 5.** A) Schematic synthesis of Tethyan subduction history accommodating India-Eurasia convergence, as interpreted from P-wave seismic tomography by van der Voo et al. (1999b). B) The three slab volumes in the lower mantle are interpreted as representing intra-oceanic subduction and a two-stage India-Eurasia collision. Figure adapted from van der Voo et al. (1999b). Note that the Tethyan ocean basin nomenclature in van der Voo et al. (1999b) differs slightly from the terminology used in this study. KLA – Kohistan-Ladakh Arc, YTSZ – Yarlung Tsangpo Suture Zone.

Incorporating 3D seismic tomographic interpretations, Replumaz et al. (2004) combined an assumption of vertical slab sinking with a tectonic reconstruction of Southeast Asia in a Siberia reference frame, and interpreted the pre-collision geometry of the southern Eurasian active margin using tomographic depth slices. The analysis of tomography linked to a "retro-deformation" model of block motions in Southeast Asia (using available fault offsets and slip rates) for Cenozoic times

suggests that the India-Eurasia continental collision occurred sometime between 55 and 40 Ma, based on changes in slab morphology, and suggests a sinking rate of 5 cm/yr in the upper mantle and 2 cm/yr in the lower mantle. The resulting upper mantle sinking rates are slightly higher than the values suggested by Hafkenscheid et al. (2006). A similar approach of age-coding slabs in P- and S-wave seismic tomographic depth slices, assuming constant and vertical slab sinking was used in Zahirovic et al. (2012; 2014) as an estimate of the location of Tethyan subduction zones that were then implemented into a global plate motion model. One important distinction was the use of multiple P- and S-wave seismic tomographic models, which is an important consideration in determining the distribution of Tethyan slabs. To supplement the assumption of vertical slab sinking, Zahirovic et al. (2012) used numerical mantle convection models kinematically driven by time-dependent plate reconstructions, and found that an intra-oceanic subduction scenario, as suggested by van der Voo et al. (1999b), Hafkenscheid et al. (2006) and Aitchison et al. (2007), better reproduced the Tethyan mantle structure than Andean-style subduction alone.

More generally, the approach of age-coding slabs in seismic tomographic depth slices has been applied globally to derive average slab sinking rates (Butterworth et al., 2014; van der Meer et al., 2010), and to propose a subduction reference frame using the assumption of vertical sinking and constant sinking rates (van der Meer et al., 2010). The cataloguing of global slab volumes by van der Meer et al. (2010) suggests that an ~ 15 to 20° longitudinal global shift of all continents is required to account for the observed distribution of post-Jurassic slabs in the mantle. Such an observation is an important first-order constraint of paleo-longitude in the absence of preserved hotspot tracks during the Late Jurassic and Early Cretaceous, and provides an estimated average global slab-sinking rate of 1.2 ± 0.3 cm/yr. A similar synthesis of slabs interpreted from seismic tomography in Butterworth et al. (2014) suggests a comparable average sinking rate of 1.3 ± 0.3 cm/yr for the whole mantle. However, such an approach does not take into account the contrasting viscosities of the upper and lower mantle, or the effects of slab stagnation and lateral slab advection from mantle flow, which may be an important factor contributing to Tethyan mantle structure (Becker and Faccenna, 2011;

422 Zahirovic et al., 2012). To address this, Butterworth et al. (2014) made use of global numerical
423 modelling of mantle flow to test competing absolute reference frames against present-day seismic
424 tomographic constraints, and suggest that the longitudinal correction argued in van der Meer et al.
425 (2010) is likely too large. The numerical modelling approach in Butterworth et al. (2014) highlighted
426 the need to account for variable slab sinking rates resulting from factors such as oblique convergence,
427 diachronous collisions and suturing, as well as two orders of magnitude increase in viscosity between
428 the upper and lower mantle. The slab sinking rates from numerical mantle convection models in
429 Butterworth et al. (2014) suggest a global mantle sinking rate of 1.5 to 2.0 cm/yr, which is also
430 consistent with the 2.0 ± 0.8 cm/yr mantle sinking rate inferred from mantle flow modelling
431 (Steinberger et al., 2012). More generally, studies applying mantle flow modelling highlight the time-
432 varying nature of slab sinking rates, which is an important consideration when interpreting slabs from
433 the present-day snapshot in seismic tomography (Bower et al., 2013).
434

435 **1.3 Numerical modelling of Tethyan geodynamics**

436

437 The evolution of the Tethyan realm has been the focus of decades of research to better
438 understand the India-Eurasia collision and the complex tectonics of Southeast Asia and New Guinea.
439 A wide range of physical (analogue) and numerical experiments at crustal, lithosphere and mantle
440 scales has revealed important aspects of the plate-mantle system that are responsible for the
441 geodynamics of the Tethyan, Eurasian and Pacific tectonic domains. Since our approach requires
442 modelling in a spherical domain with assimilation of plate reconstructions, only numerical methods
443 are appropriate to study the long-term eastern Tethyan subduction history in a regional and global
444 framework.

445 Wide ranges of numerical approaches exist to model mantle behaviour – including forward or
446 backward advection models (including inverse and adjoint approaches), forward models with data
447 assimilation, and fully geodynamic models that do not have imposed boundary conditions. Forward

448 models assume that the plate motion histories are a reasonably good recorder of plate-mantle
449 evolution, and use the plate motions as a surface kinematic boundary condition to predict mantle
450 structure that can be compared to seismic tomography (Bower et al., 2015; Bunge et al., 2002;
451 Richards et al., 2000; Zahirovic et al., 2012). Backward advection models use seismic tomography
452 (as a present-day snapshot of the mantle) as an input where the seismic velocity anomalies are
453 converted to density perturbations, assuming that the bulk of the anomaly has a thermal source, and
454 the sign of gravity and time reversed to compute the past position of the mantle material (Bunge et
455 al., 2003; Conrad and Gurnis, 2003; Glišović and Forte, 2014; Liu and Gurnis, 2008; Steinberger and
456 O'Connell, 1998). The backward advection models take into account the complex present-day mantle
457 structure, but can only be successfully used for times since ~ 70 Ma due to the inherent issues of
458 irreversible thermal diffusion and the interaction of the boundary layers with internal flow (Bunge et
459 al., 2003; Conrad and Gurnis, 2003; Steinberger and O'Connell, 1998). More advanced approaches
460 using adjoint models overcome the limitations of irreversible backward advection (Liu and Gurnis,
461 2008; Spasojevic et al., 2009), but have yet to be applied to the Tethyan domain. Since our region of
462 interest requires deeper time considerations, we use forward geodynamic flow experiments that are
463 tested against mantle tomography.
464

465 ***1.3.1 Numerical models of India-Eurasia convergence***
466

467 Following the interpretation of discrete Tethyan slab volumes at mid-mantle depths beneath
468 India in P-wave seismic tomographic models by van der Voo et al. (1999b), a numerical approach
469 using a 2D box (with 16.5 km mesh resolution) was used by Jarvis and Lowman (2005) to interpret
470 the inferred Tethyan mantle structure (Fig. 6). A number of experiments were conducted, specifically
471 varying the poorly-constrained viscosity contrast between the upper and lower mantle, with the results
472 requiring a lower mantle that was at least 30 times more viscous than the upper mantle to maintain
473 Tethyan slabs at mid-mantle depths (Jarvis and Lowman, 2005). The resulting upper and lower mantle

viscosity contrast from Jarvis and Lowman (2005) was also consistent with earlier estimates of a 10 to 30 times more viscous lower mantle from global models fitting geoid anomalies over slabs (Hager, 1984).

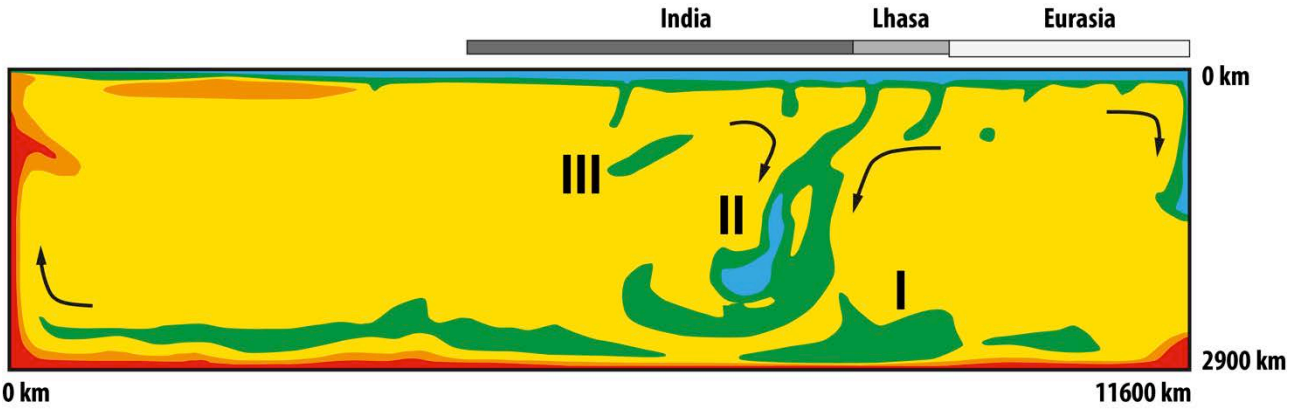


**Fig. 6.** Numerical 2D box model of India-Eurasia convergence, adapted from Jarvis and Lowman (2005), provided an important benchmark for quantifying and testing tectonic reconstruction scenarios of India-Eurasia convergence and Tethyan geodynamics. Slabs I to III represent discrete volumes of subducted Tethyan lithosphere, with blue and green colours indicating cooler mantle temperatures, as opposed to the hotter upwelling orange and red regions.

Due to the limitation of a 2D box set-up, the India-Eurasia convergence modelled by Jarvis and Lowman (2005) required a simplified convergence history along a single transect despite a complex active margin with periods of oblique convergence. The applied velocity boundary condition led to symmetric downwellings rather than one-sided subduction. However, the work of Jarvis and Lowman (2005) highlighted the need for quantitative approaches to test plate reconstructions, while suggesting a lower limit on the viscosity contrast between the upper and lower mantle. The approach utilised simple kinematic boundary conditions for the convergence velocities, which were assumed to be ~ 17 and 6 cm/yr (Besse and Courtillot, 1988) before and after the India-Eurasia collision, respectively, at 42 Ma. Their subsequent numerical approach made use of a simple sinking slab in a 2D and 3D Cartesian box (Jarvis and Lowman, 2007), which suggested a viscosity contrast of a factor

of 100 to 300 between the upper and lower mantle to maintain Tethyan slabs in the mid-mantle. These results suggested that Jurassic slabs likely retain a thermally anomalous signature with respect to the ambient mantle, enabling their detection by seismic tomographic techniques.

Becker and Faccenna (2011) used a 3D global approach to investigate the plate driving forces acting on the circum-Tethyan regions, and converted P- and S-wave seismic tomographic models to density anomalies to drive instantaneous mantle flow models. They found that there was a dominant first-order mantle conveyor belt with northward velocities in the shallow mantle beneath India, sinking of mantle material near the suture zone, and accompanying southward flow that is interrupted by mantle upwelling in the region of the Carlsberg and Central Indian ridges. The work highlights the power of global models in capturing the complexity of slab interactions from circum-Tethyan subduction, with results suggesting that large-scale mantle flow and an associated Tethyan conveyor support ongoing indentation by India. Similarly, a 3D global spherical approach using CitcomS (Zhong et al., 2000) was applied in Zahirovic et al. (2012), where plate kinematic boundary conditions were applied from 140 Ma to test end-member subduction scenarios accommodating India-Eurasia convergence. The forward numerical model predictions were compared to slabs interpreted from seismic tomography (Zahirovic et al., 2012), and showed that the mantle structure could be better reproduced when taking into account intra-oceanic subduction and a two-stage India-Eurasia collision (Aitchison et al., 2007; Hafkenscheid et al., 2006; van der Voo et al., 1999b). This earlier work highlights the need to test end-member plate reconstruction scenarios using mantle flow models, and comparisons to mantle structure from seismic tomography as an additional criterion for reconciling surface geology.

More recently, a 3D approach was also employed in Yoshida and Hamano (2015), who ran a forward convection model from Pangea times, but without applying a kinematic boundary condition or being able to incorporate one-sided subduction. Although many of the experiments failed to reproduce present-day arrangements of continents (such as predicting a problematic fit of Antarctica with South America), one aspect of the models reproduced the approximate present position of India

and highlights the requirement of long-lived subduction along southern Eurasia since Pangea breakup (Yoshida and Hamano, 2015). When considering the motion of India towards Eurasia, the anomalously high velocities (> 14 cm/yr) of India between ~ 80 and 65 Ma can be modelled numerically through a viscous coupling mechanism between two simultaneous north-dipping subduction zones in the Neo-Tethys prior to India-Eurasia collision (Jagoutz et al., 2015). This modelling approach suggests that two subduction zones in the Neo-Tethys are required to account for the high convergence rates as long-lived (~ 20 Myr) accelerations cannot be explained by plume influences, which are likely to diminish over a shorter timeframe of several millions of years (van Hinsbergen et al., 2011).

When considering the mantle-surface interaction from Tethyan tectonics, the work of Pusok and Kaus (2015) used a 3D numerical box model that captured both subduction processes and the resulting topographic response to the India-Eurasia collision, providing insight on the formation of oroclines in the eastern and western syntaxes of the convergence zone, as well as the uplift of the Tibetan Plateau and lateral expulsion of continental material. Major advances are also being made in reducing the uncertainties in the rheology of the mantle and lithosphere in such numerical models, with the recent work (Baumann and Kaus, 2015) highlighting a new, and currently computationally-intensive, approach of parallel inversion of observables including the gravity field, topography and GPS velocities to better model the lithospheric and crustal rheology. Other advances in inverse methods have the potential to fully incorporate the details of slabs and their coupling to lithospheric plates with fault-zones between plates with fully non-linear rheologies, which remains one of the largest uncertainties in mantle convection modelling (Ratnaswamy et al., 2015; Worthen et al., 2014). Such approaches provide a framework for geodynamic computations that capture realistic non-linear rheologies, including strain rate weakening and yielding, to better account for plate velocity observations, complex slab-trench interactions, and intra-plate deformation that goes beyond the simplifying assumption of plate rigidity (Alisic et al., 2012; Alisic et al., 2010).

### *1.3.2 Numerical modelling of Southeast Asia and New Guinea geodynamics*

Few geodynamic models of mantle-, lithospheric- and crustal-scale evolution exist for the tectonically complex and less constrained Sundaland and New Guinea regions than for other parts of the Tethyan tectonic domain. For example, the synthesis by van Ufford and Cloos (2005) of at least six competing proposed scenarios for the Cenozoic evolution of New Guinea highlights the uncertain chronology of major tectonic events, as well as poorly-constrained subduction polarities. As a result, much of the numerical modelling has been restricted to understanding the present-day geodynamic character of the region. Ghose et al. (1990) used focal mechanism solutions to build a 3D finite element numerical experiment of subducted slabs and generalised mantle structure in the Sundaland region to compute the flow and stress field acting on the overriding continental promontory. The results indicate significantly higher plate coupling across the Sumatra segment of the Sunda Trench, resulting in a higher seismogenic potential than the Java region. This may be due to lower coupling assumed to be due to the lubricating effect of soft sediments in the trench (e.g., Clements and Hall, 2011), as well as the subduction of older Indian Ocean crust than along the Sumatra segment (Ghose et al., 1990).

North of New Guinea, the geodynamic significance of the Philippine Sea Plate has been the subject of a number of studies that employ numerical modelling to quantify the effects of Izu-Bonin-Mariana subduction initiation (Gurnis et al., 2004; Hall et al., 2003; Leng and Gurnis, 2015) on the Pacific Plate boundary forces, and its contribution to a change in Pacific Plate motion between ~ 50 and 40 Ma based on force balance calculations (Faccenna et al., 2012). Temporally linked to the inception of (proto-) Izu-Bonin-Mariana subduction, major changes in subduction along New Guinea in the Eocene have been invoked to explain the acceleration of Australia's northward motion (Schellart and Spakman, 2015; Zahirovic et al., 2014) from ~ 43 Ma (Williams et al., 2011). Schellart and Spakman (2015) identified a subducted slab at depths between ~ 800 and 1200 km beneath Lake Eyre in eastern Australia, and argued based on a simple Stokes flow model that the topographic

depression is caused by dynamic subsidence induced by the sinking of a slab that detached along New Guinea at ~ 55-45 Ma. However, the complex interaction of slabs from regional subduction zones plays an important role that can only be tested in regional and global geodynamic numerical simulations that capture the time-dependent evolution of Southeast Asian plate boundaries.

## 2 Methods

### 2.1 Plate tectonic reconstructions

Reconstructions of the Tethyan domain have taken many forms over decades of research (see Section 1.1, Table 1, Fig. 4), with the post-Pangea plate reconstruction timeframe (since ~ 200 Ma) generally associated with lower uncertainties than earlier times due to greater preservation of oceanic crust (Zahirovic et al., 2015). Due to the ambiguity in reconstructing regions with no preserved seafloor spreading records and/or poor geological constraints, testing alternative scenarios becomes an avenue to evaluate the uncertainty inherent in plate reconstructions. In this study we present a new post-Jurassic plate motion model spanning the Tethyan region from the westernmost India-Eurasia convergence segment, in the vicinity of Kohistan-Ladakh, eastward to Southeast Asia (including Sundaland and the proto-South China Sea) and Papua New Guinea. The model is also compared to the previous synthesis of the region presented in Zahirovic et al. (2014) for Southeast Asia and New Guinea, and in Gibbons et al. (2015) for the India-Eurasia convergence zone, highlighting the alternative kinematic scenarios that can account for the constraints from marine and onshore data (Supplementary Animation 1). The refinements presented in this study focus on an alternative model for the Neo-Tethys, transferring the East Java-West Sulawesi blocks from the Argo Abyssal Plain on the NW Australian shelf towards Sundaland, as well as refinements to the evolution of the Kohistan-

Ladakh, Woyla, and Philippine intra-oceanic arcs, in the context of the evolving Sundaland and New Guinea continental margins (see Section 3).

Relative plate motions are derived from preserved seafloor spreading histories (as in third and fourth generation reconstructions from Table 2), where seafloor magnetic anomalies are identified and combined with directional constraints from fracture zones to compute the Euler rotation that defines the relative rigid body motions on the surface of a sphere. We use the Global Seafloor and Magnetic Lineation Database of previously-published magnetic anomaly picks (Seton et al., 2014) and fracture zone geometries (Matthews et al., 2011), which were combined to compute relative plate motion parameters in previous studies (see discussion and references in Seton et al., 2012), preferably using the least-squares best-fit statistical method following Hellinger (1981) and Royer and Chang (1991). The rotation parameters are calibrated to the geomagnetic polarity reversal timescale of Gee and Kent (2007), which is an updated timescale compared to the one used in our previous plate reconstruction of the Tethyan region in Zahirovic et al. (2014) and Gibbons et al. (2015). In the absence of preserved seafloor spreading histories, we use onshore geological constraints to estimate the pre-rift position of continental fragments, the timing and trajectory of rifting, as well as the age and location of the accretion events (Tables 2-3). We construct synthetic oceanic plates that are consistent with plate tectonic driving mechanisms and reasonable relative plate motions across plate boundaries (e.g., convergence across subduction zones, divergence across mid-oceanic ridges, strike-slip motion along transform faults).

The relative plate motions form a chain that is hierarchical and typically ties all plate motions back to Africa, largely due to the central position of Africa within Pangea and relative stability because it is surrounded by mid-oceanic ridges (Torsvik et al., 2008). The motion of Africa is expressed with respect to the underlying mantle, using Indo-Atlantic or global hotspot tracks since ~ 100 Ma to derive a frame of reference for the global plate motion model. For earlier times when no hotspot tracks are available, the True Polar Wander- (TPW) corrected paleomagnetic reference frame of Steinberger and Torsvik (2008) is used. Due to the lack of paleo-longitudinal constraints in a

623 paleomagnetic reference frame resulting from the radial symmetry of the Earth's magnetic dipole, we
624 apply a 10° longitudinal shift gradually between 70 and 105 Ma to the TPW-corrected reference
625 frame, following Butterworth et al. (2014) and van der Meer et al. (2010) to provide a better paleo-
626 longitudinal link between subduction zones and Jurassic and Cretaceous subducted slabs interpreted
627 from seismic tomography.

628 The combination of relative plate motions with an absolute reference frame enables the
629 computation of absolute plate motions through time, modelled using the GPlates software (Boyden
630 et al., 2011). Evolving plate boundaries are constructed using continuously-closing plate polygon
631 algorithm (Gurnis et al., 2012), which provides global coverage of plates through time in 1 Myr
632 intervals. The Tethyan plate motions are embedded in a global model, which is based on the synthesis
633 in Seton et al. (2012) with regional refinements that are documented in Müller et al. (2016). The time-
634 dependent plate boundaries, seafloor age-grids and plate velocities are assimilated into the numerical
635 models of mantle convection, described in Section 2.3. By considering the evolution of the entire
636 plate (Gurnis et al., 2012; Stampfli and Borel, 2002) rather than only focusing on continental blocks,
637 plate reconstructions can be linked to geodynamic models (Conrad and Lithgow‐Bertelloni, 2004;
638 Lithgow‐Bertelloni and Richards, 1998). The coupling of plate kinematics to geodynamic models
639 provides the opportunity to reproduce the mantle structure interpreted from seismic tomography as
640 well as reconstruct past mantle flow using the present-day surface geology and tectonics as
641 constraints.

642

643 Table 3. Constraints used to construct plate motion model.

| **Region** | **Event** | **Timing** | **Dating method/ interpretation** | **Interpretations based on data and models** |
|---|---|---|---|---|
| Australian NW Shelf | Onset of rifting | Sometime in Late Jurassic | Stratigraphic rift-drift sequences | Pigram and Panggabean (1984) |

| | | | | |
|---|---|---|---|---|
| | Triple junction mid-oceanic ridge configuration | Latest Jurassic | Geometrical requirement, and evidence of possible plume influence | Audley-Charles (1988), Audley-Charles et al. (1988), Gibbons et al. (2012), Rohrman (2015) |
| | Onset of seafloor spreading | 155 ± 3.4 Ma | K-Ar of basaltic basement | Gradstein and Ludden (1992) |
| West Sulawesi, East Java, Mangkalihat and easternmost Borneo | Onset of rifting | Late Jurassic | Biostratigraphic constraints in Paremba Sandstone and shallow marine sandstones in Bantimala Complex | Sukamoto and Westermann (1992), Wakita (2000) |
| | Onset of seafloor spreading | ~ 158-155 Ma | K–Ar of diorite, microgabbro and basaltic dyke | Polvé et al. (1997) |
| | Oldest seafloor spreading magnetic anomalies | M25A<br>M26<br>(~ 153-155 Ma) | Magnetic anomaly identifications from shiptracks | Heine and Müller (2005)<br>Gibbons et al. (2012) |
| | Youngest preserved seafloor spreading magnetic anomaly in the Argo Abyssal Plain region | M10Ny, 128.9 Ma | Magnetic anomaly identifications from shiptracks | Gibbons et al. (2012) |
| | Suturing of 'Argoland' to southwest Borneo core | ~ 80 Ma | Stratigraphy, K–Ar and U–Pb of metamorphics, synthesis of previous studies | Wakita (2000)<br>Clements and Hall (2011) |

| | | | | |
|---|---|---|---|---|
| New Guinea | Rifting on northern New Guinea (opening of Sepik ocean basin) | Late Jurassic<br>172 Ma<br><br>~ 157 ± 16 Ma | Jurassic granite in Bena Bena Terrane<br><br>SSZ ophiolites in Central Ophiolite Belt | Davies (2012)<br><br>Permana (1998) |
| | Subduction influence on eastern New Guinea | Early Cretaceous | Kondaku Tuffs | Dow (1977), Rickwood (1954) |
| | Onset of Sepik ocean basin subduction | Maastrichtian<br>(~ 71 to 66 Ma)<br><br>68 Ma | Stratigraphic correlation and dating using foraminifera<br><br>High-temperature metabasites on West Papuan Ophiolite | Worthing and Crawford (1996)<br><br>Davies (2012) |
| | Sepik Terrane docking with New Guinea | 35-31 Ma<br><br>~ 30 Ma | Ar-Ar age of Emo metamorphics<br><br>Cooling histories from exhumation | Worthing and Crawford (1996)<br><br>Crowhurst et al. (1996) |
| | South-dipping subduction | ~ 18-8 Ma | Maramuni Arc volcanics | Hill and Hall (2003), Page (1976) |
| | Halmahera Arc collision | ~ 14 Ma | Compression in PNG Mobile Belt, apatite fission track geochronology | Hill and Raza, (1999), Kendrick (2000) |
| Lhasa | Onset of Neo-Tethyan subduction | ~ 170 Ma (to 137 Ma) | Calc-alkaline granites and granitoids | Zhang et al. (2012) |
| | Onset of intra-oceanic subduction | ~ 154 Ma | Matum Das tonalite | Schaltegger et al. (2003) |

| | | | | |
|---|---|---|---|---|
| | along Kohistan-Ladakh Arc | | | |
| | Subduction along Zedong Terrane | 161.0 ± 2.3 Ma, ~ 156 Ma, 152.2 ± 3.3 Ma | Dacite breccia, Andesite dyke/breccia, Quartz diorite, Andesitic dyke | McDermid et al. (2002) |
| | Magmatic hiatus on Lhasa | ~ 137 to 109 Ma, ~ 75 to 60 Ma | Magmatic gap in Gangdese Batholith | Ji et al. (2009), Wen et al. (2008), Chung et al. (2005) |
| | Initiation of Kohistan-Ladakh back-arc basin subduction along Lhasa | ~ 109 Ma | Resumption of arc volcanism in Gangdese Batholith | Ji et al. (2009), Wen et al. (2008) |
| | Maximum southward position of Kohistan-Ladakh Arc | ~ 100 Ma | Equatorial paleo-latitudes from mid- to Late Cretaceous red beds | Zaman and Torii (1999) |
| | Kohistan-Ladakh collision with Greater India | ~ 60 to 50 Ma | Cessation of calc-alkaline magmatism, stratigraphic constraints of collision, slowdown in Indian Ocean seafloor spreading at ~ 52 Ma, change in arc magma chemistry by ~ 50 Ma | Khan et al. (2009) Hu et al. (2015) Cande et al. (2010) Bouilhol et al. (2013) |

| | | | | |
|---|---|---|---|---|
| | Kohistan-Ladakh collision with Eurasia | ~ 47 to 40 Ma | Slowdown in India-Africa seafloor spreading, Indian Ocean microplate formation, completion of Andean-style subduction (Linzizong), change in arc magma chemistry by ~ 40 Ma | Cande and Patriat (2015)<br>Matthews et al. (2016)<br>Chung et al. (2005)<br>Bouilhol et al. (2013) |
| West Burma | Onset of Neo-Tethyan subduction | ~ 163-152 Ma | Jadeite geochronology | Shi et al. (2008, 2014) |
| | Onset of Neo-Tethyan intra-oceanic subduction | ~ 156-150 Ma | Biostratigraphic ages of cherts constraining age of Naga Ophiolite formation | Baxter et al. (2011) |
| | Subduction of Woyla back-arc basin | ~ 113-110 Ma (Albian)<br>~ 105-90 Ma<br>95 ± 2 Ma | Albian unconformity on West Burma<br>Wuntho-Popa Arc<br>SSZ formation of Andaman Ophiolite | Morley (2012a)<br>Mitchell et al. (2012)<br>Pedersen et al. (2010) |
| Sumatra | Onset of Neo-Tethyan subduction | ~ 170 Ma<br>~ 165-140 Ma (?) | Onset of arc volcanism in Sumatra segment<br>Minor UHP/VHP metamorphism | McCourt et al. (1996)<br>Parkinson et al. (1998) |

| | | | | |
|---|---|---|---|---|
| | Subduction of Woyla back-arc basin | From ~ 115 Ma<br><br>~ 105-75 Ma | Peak in UHP/VHP metamorphism in Meratus and Luk Ulo sutures<br><br>Wuntho-Popa Arc volcanism to the west, and Woyla intrusions | Parkinson et al. (1998)<br><br>Mitchell et al. (2012), McCourt et al. (1996), Wajzer et al. (1991) |
| | Woyla Arc accretion | ~ 75-62 Ma | Magmatic gap of arc volcanics on Sumatra | McCourt et al. (1996) |
| | Onset of Sunda subduction | 62 Ma | Arc volcanism on Sumatra | McCourt et al. (1996) |
| West Java/ East Borneo | Onset of NeoTethyan subduction | ~ 180-165 Ma<br><br>~ 170 Ma (Bajocian)<br><br>~ 160 Ma | Schist in Meratus Complex<br><br>Radiolarians<br><br>Zircon age spectra | Wakita et al. (1998)<br><br>Wakita et al. (1998)<br><br>Clements and Hall (2007) |
| | Late stage of Woyla/Barito back-arc basin subduction along Sunda continental margin | ~ 100 Ma<br><br>~ 100-93 Ma | Peak in zircon age spectra<br><br>Cenomanian/Turonian Meratus Ophiolite obduction | Clements and Hall (2007)<br><br>Pubellier et al. (2004), Yuwono et al. (1988) |
| | Suturing of East Java | ~ 80 Ma | Stratigraphy, K–Ar and U–Pb of metamorphics, | Wakita (2000) Clements and Hall (2011) |

| | | | | |
|---|---|---|---|---|
| | | | synthesis of previous studies | |
| | Onset of Sunda subduction | 65 Ma | Subduction-related rocks on Sulawesi | Guntoro (1999), van Leeuwen (1981) |
| Philippine Arc | Onset of south-dipping subduction along New Guinea (Sepik) | 156.3 ± 2.0 Ma and 150.9 ± 3.3 Ma<br><br>142 ± 4 Ma | SSZ ophiolitic crust from the Lagonoy Ophiolite<br>Ophiolite crystallisation from Gag Island, Halmahera | Encarnación (2004) |
| | Continued arc volcanism | 126 ± 3 Ma and 119 ± 2 Ma<br><br>99.9 ± 7.0 Ma<br><br>100 ± 4 Ma | SSZ volcanics from Cebu Island<br><br>Ar-Ar age of the Calaguas Ophiolite<br><br>Arc rocks reported from Obi Island on Halmahera | Deng et al. (2015)<br><br>Geary et al. (1988), Geary and Kay (1989)<br><br>Hall et al. (1995b) |

## 2.2 Insights from seismic tomography

The distribution of ophiolites, intra-oceanic arc fragments and a complex network of sutures within southern Eurasia (Figs. 1-3), Southeast Asia and New Guinea preserves the remnants of oceanic basins that have been lost to subduction. Although the consumption of oceanic basins leaves physical evidence in the form of arc volcanics, accreted seamounts and ocean floor sediments, and ophiolites, the present-day mantle structure illuminated using seismic tomographic methods holds

652 additional clues to the geodynamic evolution of these regions (Hafkenscheid et al., 2006; Replumaz
653 et al., 2004; van der Voo et al., 1999a; van der Voo et al., 1999b).

654 As an estimate of the location of subduction through time, depth slices of fast seismic velocity
655 anomalies are age-coded according to an assumption of vertical slab sinking with an average sinking
656 rate. In this study we compare our revised plate reconstructions with the publicly-available P-wave
657 seismic tomography depth slices from Li et al. (2008), assuming a sinking rate of 3 and 2 cm/yr in
658 the upper and lower mantle, respectively, following Hafkenscheid et al. (2006). Hafkenscheid et al.
659 (2006) also noted that the upper mantle sinking rates are likely to be similar to the convergence rate
660 at the trenches, which may suggest even higher sinking rates for the circum-Tethyan region in the
661 context of Australia's 6-8 cm/yr, the Pacific's ~ 8 cm/yr, and India's ~ 5 cm/yr root mean square
662 velocities since ~ 40 Ma (Zahirovic et al., 2015). To investigate, we test a higher end-member sinking
663 rate of 8 cm/yr in the upper mantle, which is likely only meaningful for the Cenozoic as constrained
664 by seafloor spreading histories and detailed hotspot tracks for the Pacific. The sinking rates applied
665 in this study are significantly higher than the ~ 1.2-1.3 cm/yr whole-mantle average global slab
666 sinking rates (Butterworth et al., 2014; van der Meer et al., 2010), with a similar slower and constant
667 sinking rate scenario applied to age-coding of slabs in P- and S-wave seismic tomography models in
668 Zahirovic et al. (2014). However, a faster sinking rate, with differential rates in the upper and lower
669 mantle, was found to better reproduce the evolution of major Tethyan and Southeast Asian subduction
670 zones (Zahirovic et al., 2014). Importantly, we note that the assumption of vertical and temporally
671 constant sinking rates along a single subduction zone, not to mention across a range of subduction
672 zones in a region, is likely an oversimplification and requires testing using numerical simulations of
673 mantle flow, as was carried out in Butterworth et al. (2014).

674 We compare our numerical mantle flow predictions to a number of P- and S-wave seismic
675 tomography models, because tomographic models are typically constructed using a variety of
676 methods, which incorporate different seismic phases and parameterisations (Grand, 2002;
677 Romanowicz, 2008). P-wave models tend to have higher resolutions than S-wave models, due to the

678 limited number of S-wave phases that can be used in seismic tomographic inversions (Widiyantoro
679 et al., 1998). Beyond the inherent higher resolution of P-wave models in well-sampled continental
680 regions, the Li et al. (2008) global seismic tomography model has additional coverage by
681 incorporating coverage using the Chinese Seismographic Network, leading to a better sampling of
682 the Tethyan and Asian mantle.

683 The limitation of P-wave models is that they tend to bias their sampling of the mantle beneath
684 continental crust, leading to lower seismic velocity anomaly amplitudes beneath oceanic regions. For
685 example, a subducted slab that may straddle oceanic and continental regions (such as the Tethyan
686 slabs) may appear "faded" beneath the oceanic regions. Although S-wave models tend to have lower
687 resolution, they offer more equal sampling of the mantle beneath oceans and continents (Grand,
688 2002). Due to the lack of permanent seismic stations in the oceans (except for some stations located
689 on islands) and over Antarctica, the coverage and sampling for both P- and S-wave seismic
690 tomography models is poorer for the southern hemisphere and all oceanic regions (Romanowicz,
691 2008). As regional tomographic models can have edge artefacts (Foulger et al., 2013), and typically
692 are not represented as seismic velocity anomalies with respect to the global mantle, we focus on using
693 only global tomographic models in our comparisons.

694

695 **2.3 Coupled plate reconstructions and mantle convection numerical models**

696

697 To better understand the geodynamic implications of the plate reconstructions, and go beyond
698 the assumption of constant and vertical slab sinking used in simple interpretations of mantle structure,
699 we couple the plate kinematics to computations of mantle flow. We use the mantle convection
700 modelling code CitcomS (Zhong et al., 2000) (https://geodynamics.org/cig/software/citcoms/),
701 modified to incorporate a time-dependent surface boundary condition using plate velocities from our
702 plate motion model, and progressively assimilate the thermal structure of the lithosphere and the
703 shallow thermal structure of subducting slabs (Bower et al., 2015) (Fig. 7A). The temperature and

thickness of the lithosphere are derived using a half-space cooling model and the synthetic age of the ocean floor. Slabs are assimilated into the mantle to a depth of 350 km but convection is entirely dynamic away from slabs and below the lithosphere. We computed numerical models from 230 Ma to the present to capture the post-Pangea mantle evolution, with global plate reconstructions of the pre-Late Jurassic described in Müller et al. (2016). However, we analyse the mantle evolution since the latest Jurassic (~ 160 Ma) for which time the plate reconstructions are regionally refined, and the mantle flow models have reached a dynamic equilibrium from the synthetic initial condition (Flament et al., 2014). Initially at 230 Ma, slabs are inserted down to 1400 km depth, with a 45º dip down to 425 km and 90º below 425 km. In the initial conditions, slabs are twice as thick in the lower mantle than in the upper mantle to account for advective thickening observed in tests in which slabs are only initially inserted in the upper mantle. The initial condition includes a basal thermochemical layer 113 km thick just above the core–mantle boundary (CMB) that consists of material 3.6% denser than ambient mantle. This condition suppresses the formation of plumes, but does not impede the formation of large-scale mantle upwellings. The surface and CMB are isothermal at 273 K and 3100 K, respectively (Fig. 7B). Subduction zones that appear (initiate) during the model run are progressively inserted as slabs in the uppermost mantle (Bower et al., 2015). The kinematic boundary conditions, generated in GPlates, and the thermal volume conditions for the lithosphere and shallow subduction, are assimilated in 1 Myr intervals, as described in Bower et al. (2015). The average model resolution, obtained with ~ $13 \times 10^6$ nodes and radial mesh refinement, is ~ 50 × 50 × 15 km at the surface, ~ 28 × 28 × 27 km at the core–mantle boundary (CMB), and ~ 40 × 40 × 100 km in the mid-mantle.

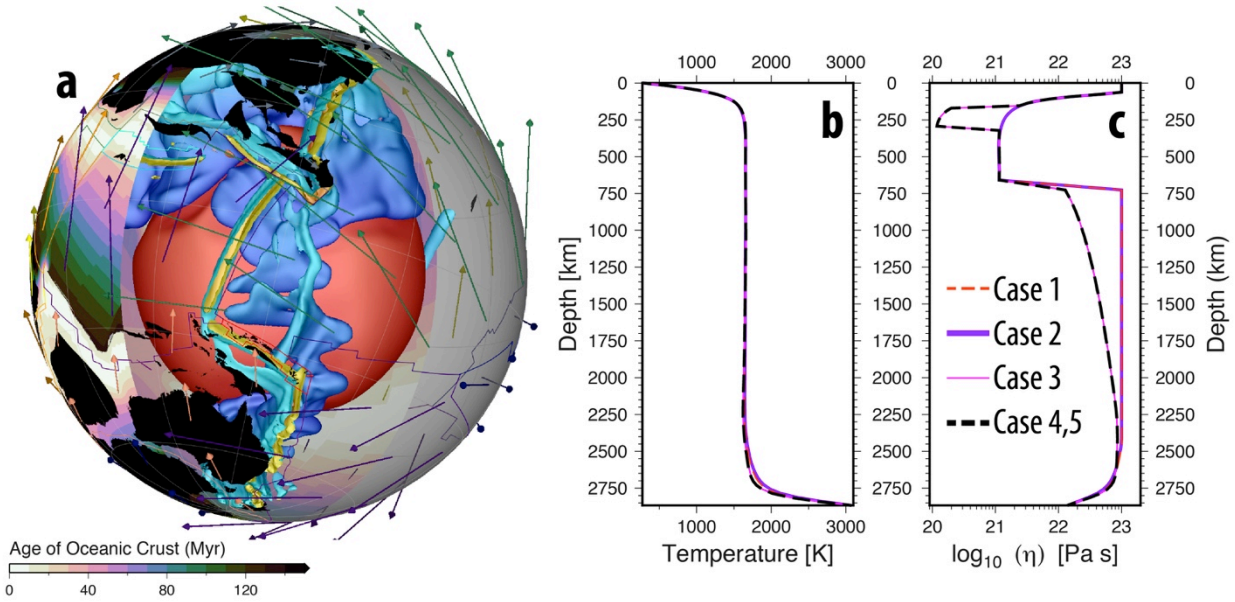


**Fig. 7.** a) Assimilation of plate velocities (arrows), subduction zones (yellow) and thermal lithospheric thickness based on the age of the seafloor from plate reconstructions in GPlates, with 3D volume contours of dynamic cold slabs (blue) and hotter upwellings (red) predicted by the mantle convection code CitcomS (here using Case 5, see Section 2.3). Reconstructed present-day coastlines (black) are provided as a reference. Slab colouring is a function of depth from light blue (shallow mantle) to darker blue (deep mantle). Seafloor age-grid is applied globally, but is cut out in this schematic to highlight the internal mantle structure. b) Horizontally-averaged present-day mantle temperature, and c) present-day average viscosity in the five numerical cases (see Section 2.3).

The vigour of mantle convection is defined by the Rayleigh number, Ra, where:

$$Ra = \frac{\alpha_0 \rho_0 g_0 \Delta T h_M^3}{\kappa_0 \eta_0},$$

in which $\alpha$ is the coefficient of thermal expansion, $\varrho$ the density, $g$ the acceleration of gravity, $\Delta T$ the temperature difference between surface and CMB, $h_M$ the thickness of the mantle, $\varkappa$ the thermal diffusivity, and $\eta$ the viscosity; the subscript "0" indicates reference values (see Table 4). The viscosity of the slabs and mantle is stress- and temperature-dependent, following

$$\eta = \eta_0(r)\exp\left(\frac{E_\eta}{R(T+T_\eta)} - \frac{E_\eta}{R(T_b+T_\eta)}\right)$$

where $\eta_0(r)$ is a depth-dependent pre-factor defined with respect to the reference viscosity, $\eta_0$, $E_\eta$ is the dimensional activation energy ($E_{UM}$ in the upper mantle and $E_{LM}$ in the lower mantle), $R$ is the universal gas constant, $T$ is the temperature, $T_\eta$ is a temperature offset, and $T_b$ is the ambient mantle temperature outside the thermal lithosphere, slabs or the basal thermal boundary layer (see Table 4). Although the viscosity of the upper mantle can be estimated in studies of post-glacial rebound (Fjeldskaar et al., 2000; Gasperini and Sabadini, 1989; Lambeck et al., 1998), the viscosity of the lower mantle is less well constrained, which has resulted in a wide range of proposed viscosity profiles. Previous approaches have argued for a factor of 10 increase in viscosity between the upper and lower mantle (Paulson et al., 2007), while others have argued for a factor of 30 (Hager, 1984) or 100 (Forte and Mitrovica, 1996; Steinberger and Calderwood, 2006). We vary the viscosity profile (Fig. 7C, Table 5) with cases 1 to 4 based on the plate reconstructions from Zahirovic et al. (2014) and Gibbons et al. (2015), and a fifth case based on the refined plate reconstructions presented in this study. The viscosity of the lower mantle in each case is either 100 times more viscous than the upper mantle, or increases gradually with depth from a factor of 10 at the base of the transition zone (660 km) to a maximum of 100 in the lowermost mantle (Steinberger and Calderwood, 2006). Cases 3, 4 and 5 also incorporate a low-viscosity asthenosphere, which has been suggested to be an important decoupling layer that enables the elevated velocities of typically oceanic plates (Becker, 2006; Debayle and Ricard, 2013). Since paleo-longitudes are less well constrained earlier than ~ 100 Ma, we incorporate the van der Meer et al. (2010) subduction reference frame and their time-dependent longitudinal shift into Case 3. Using a variety of radial viscosity profiles, different absolute reference frames, and plate reconstructions between the five cases, allow us to capture some of the uncertainties involved in our approach of modelling deep-time plate reconstructions and mantle convection, and help test end-member plate reconstructions of the Tethyan region.

The time-dependent mantle structure is presented in 3D visualisations made with GPlates and as a series of vertical cross-sections that are reconstructed with the overriding plate to capture the evolution of subduction, plotted using Generic Mapping Tools (Wessel et al., 2013). The predicted

present-day mantle structure is qualitatively compared to equivalent slices of P- and S-wave seismic tomography models, where fast seismic velocity anomalies are compared to slab contours (10% colder than ambient mantle, representing temperatures colder than ~ 1270°C) from the mantle convection models.

**Table 4.** Parameters common to all model cases. Subscript "0" denotes reference values.

| **Parameter** | **Symbol** | **Value** | **Units** |
|---|---|---|---|
| Rayleigh Number | $Ra$ | $7.84 \times 10^{7}$ | |
| Thermal expansion coefficient | $\alpha_0$ | $3 \times 10^{-5}$ | $K^{-1}$ |
| Density | $\varrho_0$ | 4000 | kg $m^{-3}$ |
| Gravity acceleration | $g_0$ | 9.81 | m $s^{-2}$ |
| Temperature change | $\Delta T$ | 2825 | K |
| Temperature offset | $T_\eta$ | 452 | K |
| Background mantle temperature | $T_b$ | 1685 | K |
| Mantle thickness | $h_M$ | 2867 | km |
| Thermal diffusivity | $\varkappa_0$ | $1 \times 10^{-6}$ | $m^2$ $s^{-1}$ |
| Reference viscosity | $\eta_0$ | $1 \times 10^{21}$ | Pa s |
| Activation energy (upper mantle) | $E_{UM}$ | 100 | kJ $mol^{-1}$ |
| Activation energy (lower mantle) | $E_{LM}$ | 33 | kJ $mol^{-1}$ |
| Activation temperature | $T_\eta$ | 452 | K |
| Universal gas constant | $R$ | 8.31 | J $mol^{-1}$ $K^{-1}$ |
| Radius of the Earth | $R_0$ | 6371 | km |

775

776 **Table 5.** Model set-up for Case 1 – 5. Also refer to Fig. 7b-c.

| | **Case 1** | **Case 2** | **Case 3** | **Case 4** | **Case 5** |
|---|---|---|---|---|---|
| Mesh nodes | 129 × 129 × 12 (nodes on the surface) × 65 (depth levels) | | | | |
| Viscosity relative to Reference Viscosity (Lithosphere 0-160 km depth, Asthenosphere 160-310 km depth, Upper mantle 310-660 km depth, Lower Mantle > 660 km depth) | 1,0.1,1,100 | 1,1,1,100 | 1,0.1,1,10→100 linear increase of viscosity from 10 to 100 with depth in the lower mantle to approximate the viscosity profile of Steinberger and Calderwood (2006) | | |
| Plate reconstructions for the eastern Tethys | Zahirovic et al. (2014) | | Slab-calibrated longitudinal positions from van der Meer et al. (2010) and using the relative plate motions from Zahirovic et al. (2014) | Zahirovic et al. (2014) | This Study |

777

778 # 3 Regional tectonic evolution

779 ## 3.1 Late Jurassic plate boundary configuration and rifting mechanism along northern

780 ### Gondwana

781

782 The Late Jurassic is marked by a major rifting event along northern Gondwana (Pigram and
783 Panggabean, 1984) (Figs. 4A and 8), which transferred a number of continental blocks (including
784 East Java, West Sulawesi, Mangkalihat and east Borneo) northward towards Eurasia (Hall, 2012;
785 Zahirovic et al., 2014), with the only portions of the seafloor spreading system preserved in the Argo
786 Abyssal Plain on the NW Australian shelf (Gibbons et al., 2013). Beyond the oldest preserved oceanic
787 crust, the plate configuration can only be inferred from proxy indicators found on continents. One
788 pertinent argument is that Audley-Charles (1988) and Audley-Charles et al. (1988) required a triple
789 junction plate boundary configuration in the Late Jurassic and Early Cretaceous in the vicinity of the
790 NW Australian shelf where northward slab pull from subduction along southern Eurasia was the
791 driving mechanism for detaching the Neo-Tethyan ribbon terrane (also in Fig. 4a). This northward
792 slab pull detached the continental fragments forming passive margins along the northern and southern
793 boundaries of the ribbon terrane, the preferred scenario presented here. An alternative scenario has
794 south-dipping subduction along northern Gondwana in the Late Jurassic, leading to the opening of
795 the Neo-Tethys and transfer of continental fragments northward through slab rollback (Hall, 2012)
796 (Fig. 4B). Both mechanisms are thought to be capable of detaching continental fragments (see
797 Stampfli and Borel, 2002), but, the south-dipping subduction end-member requires continuous arc
798 volcanism, some of which ought to be preserved on the drifting ribbon terranes.
799

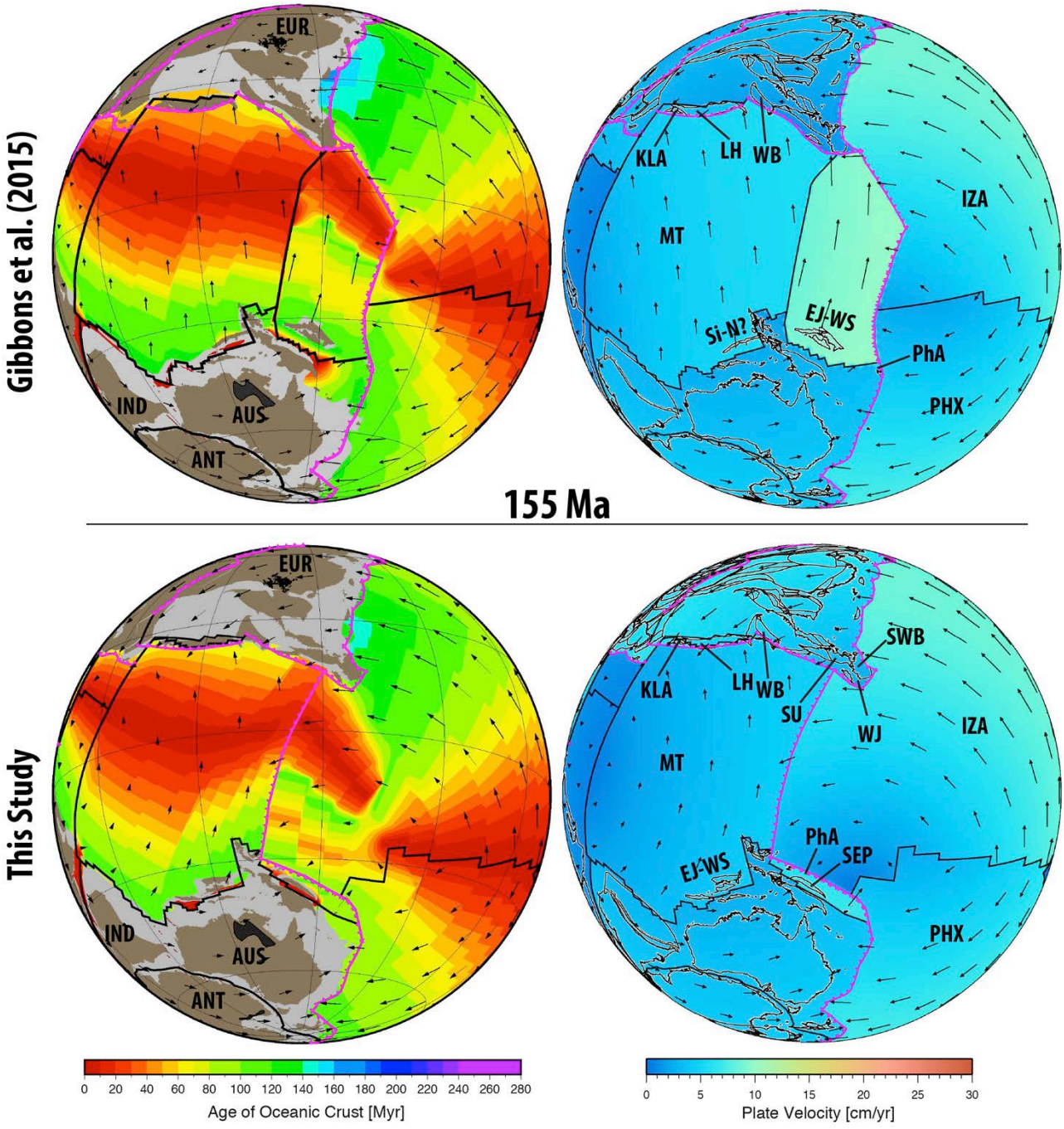


800

801 **Fig. 8.** Reconstruction of Neo-Tethyan ocean basin opening along northern Gondwana in the latest
802 Jurassic. Both the Zahirovic et al. (2014) and Gibbons et al. (2015) models (top) invoke East Java
803 and West Sulawesi rifting from New Guinea, as the simplest tectonic scenario to transfer the blocks
804 northwards towards Southeast Asia, and a possible origin of the Sikuleh and Natal (Si-N) fragments
805 from the Argo Abyssal Plain. Southwest Borneo (SWB), West Java (WJ), Sumatra (SU), West Burma
806 (WB) and Lhasa (LH) form the active Eurasian continental margin. Seafloor spreading in the Neo-
807 Tethys is driven by north-dipping subduction along southern Eurasia (EUR), consuming the Meso-

808 Tethyan (MT) oceanic crust and resulting in the incipient formation of the Kohistan-Ladakh Arc
809 (KLA). In the revised reconstructions, East Java and West Sulawesi (EJ-WS) are the 'Argoland'
810 continental fragment originating in the Argo Abyssal Plain on the NW Australian shelf. South-
811 dipping subduction along New Guinea is modelled to detach the Sepik Terrane (SEP) from the New
812 Guinea margin through slab rollback, generating the embryonic components of the Philippine
813 Archipelago (PhA). The colour scales are relevant to all plate reconstruction figures. Grey regions
814 represent the extent of continental crust, dark grey represents large igneous provinces and other plume
815 products, and thin brown lines represent reconstructed fracture zones. ANT – Antarctica, AUS –
816 Australia, IND – India, IZA – Izanagi Plate, PHX – Phoenix Plate. Orthographic reconstructions are
817 centred on 115°E, 15°S. See Supplementary Animation 2, 3 and 4.
818
819 The NW Australian shelf, the putative source of the Argoland ribbon terrane records some Late
820 Jurassic and Early Cretaceous volcanic plateaus (e.g., Scott and Wombat plateaus and Joey Rise –
821 see Fig. 1), as well as rift-related volcanics and seaward dipping reflectors (Heine and Müller, 2005;
822 Rohrman, 2015; von Rad et al., 1992). An earlier phase of rhyolitic volcanism between ~ 213 and
823 190 Ma erupted on the Wombat Plateau (von Rad and Exon, 1983; von Rad et al., 1992), but cannot
824 be temporally linked to the latest Jurassic (~ 155 Ma) rifting and seafloor spreading phase recorded
825 on the NW Australian shelf. Although the latest Jurassic NW Australian margin was volcanic, little
826 evidence exists that it was dominated by an Andean-style active margin (von Rad and Exon, 1983;
827 von Rad et al., 1992). Although the seismic interpretations by Hopper et al. (1992) of the margin's
828 volcanic history do not indicate widespread plume activity, the recent work of Rohrman (2015)
829 suggests a plume origin for the large volume of underplated material and widespread sills interpreted
830 from seismic sections in the Exmouth Plateau region (Fig. 1). One critical aspect of the latest Jurassic
831 event is that the onset of seafloor spreading is well-constrained by a 155 ± 3.4 Ma K-Ar age of the
832 oldest seafloor in the Argo Abyssal Plain (Gradstein and Ludden, 1992), consistent with rapid tectonic
833 subsidence in the latest Jurassic on the NW Australian shelf (Heine and Müller, 2005; Rohrman,

834 2015; Tovaglieri and George, 2014), and the identification of M25A (Heine and Müller, 2005) or
835 M26 (Gibbons et al., 2012) as the oldest magnetic anomalies (~ 153-155 Ma) in the seafloor spreading
836 record.

837 Due to the lack of latest Jurassic arc volcanics on the NW Australian Shelf, together with strong
838 indicators of north-dipping subduction initiation along southern Eurasia (see following sections), we
839 prefer northward slab pull as the driving mechanism for rifting and seafloor spreading to open the
840 Neo-Tethys from ~ 155 Ma. Although more work is required to test whether a plume model can
841 explain the volcanism on the NW Australian shelf in the latest Jurassic (Rohrman, 2015), such a
842 scenario would be consistent with the triple junction scenario invoked for this region (Audley-
843 Charles, 1988; Audley-Charles et al., 1988; Gibbons et al., 2015; Gibbons et al., 2012; Zahirovic et
844 al., 2014), and the similarity to the East African rift-plume interaction (Burke and Dewey, 1973;
845 Montelli et al., 2006; Yirgu et al., 2006). Since the Neo-Tethyan seafloor spreading history is
846 incomplete, it remains difficult to ascertain which continental blocks rifted from the Argo segment of
847 the Australian margin (Table 2). Rifting of East Java and West Sulawesi from New Guinea was
848 invoked as a preferred scenario in our base models in the Late Jurassic (Gibbons et al., 2015;
849 Zahirovic et al., 2014), with the possibility that micro-continental fragments along Sumatra (such as
850 the now-disputed Natal and Sikuleh fragments, Fig. 2) had an origin in the Argo Abyssal Plain,
851 following Audley-Charles et al. (1988), Metcalfe (1994) and Heine and Müller (2005). However,
852 recent zircon age spectra analyses from East Java suggesting strong affinities with the NW Australian
853 Shelf (Sevastjanova et al., 2015; Smyth et al., 2007), led Hall (2012) to argue that East Java was the
854 enigmatic "Argoland" fragment (Table 2). We present both a NW Australian shelf and a New Guinea
855 origin for Argoland in our alternative plate reconstruction scenarios, and evaluate their plate
856 kinematic and geodynamic consequences on the Neo-Tethyan tectonic evolution.
857
858 Table 2. Previously-interpreted continental fragments originating from northern Gondwana in the eastern Tethys in the
859 Late Jurassic.

| *Model* | *All continental fragments originating from northern Gondwana in the Late Jurassic eastern Tethys* | *Argoland fragment* |
|---|---|---|
| Audley-Charles et al. (1988) | South Tibet (Lhasa), West Burma, Malaya, Sumatra, East and West Borneo fragments, West Sulawesi | West Burma |
| Metcalfe (1994) | West Burma, Sikuleh, Natal, West Sulawesi, Mangkalihat, Banda Allochthons | West Burma |
| Heine and Müller (2005) | West Burma | West Burma |
| Hall (2012) | Southwest Borneo core, East Java, West Sulawesi | East Java and West Sulawesi |
| Zahirovic et al. (2014) Gibbons et al. (2015) | Sikuleh, Natal, East Java, Southeast Borneo, West Sulawesi | Sikuleh, Natal and other possible fragments that may be in the Mawgyi Nappe along West Burma |
| This Study | East Java, Eastern Borneo, Mangkalihat, West Sulawesi and Sepik (New Guinea) | East Java, Eastern Borneo, Mangkalihat and West Sulawesi |

The ~ 155 Ma onset of seafloor spreading in the Argo segment of the north Gondwana margin is consistent with Jurassic sedimentary rift-drift sequences (Pigram and Panggabean, 1984), and mafic rocks that are as old as 158 Ma on West Sulawesi (Polvé et al., 1997), likely representing the drift of the East Java and West Sulawesi continental fragments (Zahirovic et al., 2014). The early seafloor spreading history is preserved in the Argo Abyssal Plain, with the youngest marine magnetic anomaly of M10Ny (Gibbons et al., 2013) representing an age of 128.9 Ma, after which the seafloor spreading history is unconstrained. As discussed extensively in Zahirovic et al. (2014), and summarised below in Section 3.4, the East Java and West Sulawesi fragments may have collided with an intra-oceanic arc in the mid-Cretaceous (Wakita, 2000), and sutured to Sundaland by 80 Ma. However, the Neo-Tethyan full seafloor spreading velocity required by the ~ 115 Ma arc-continent collision approaches ~ 25 cm/yr between ~ 128 and 115 Ma when assuming a NW Australian shelf origin of East Java and

West Sulawesi (see Supplementary Fig. 1), which is likely to be an upper limit for plate velocities in the post-Pangea timeframe (Stampfli and Borel, 2002; Vérard et al., 2012; Zahirovic et al., 2015). An alternative explanation for the ~ 115 Ma peak in very high pressure (VHP) metamorphic rocks in the Luk Ulo-Meratus Suture Zone (Parkinson et al., 1998) (Fig. 2) includes the initiation of subduction of the Woyla/Barito back-arc basins, which reduces the synthetic seafloor spreading velocities to ~ 11 cm/yr (Figs. 10-11). We adopt the latter option that does not introduce a geodynamically implausible velocity spike in Tethyan plate velocities.

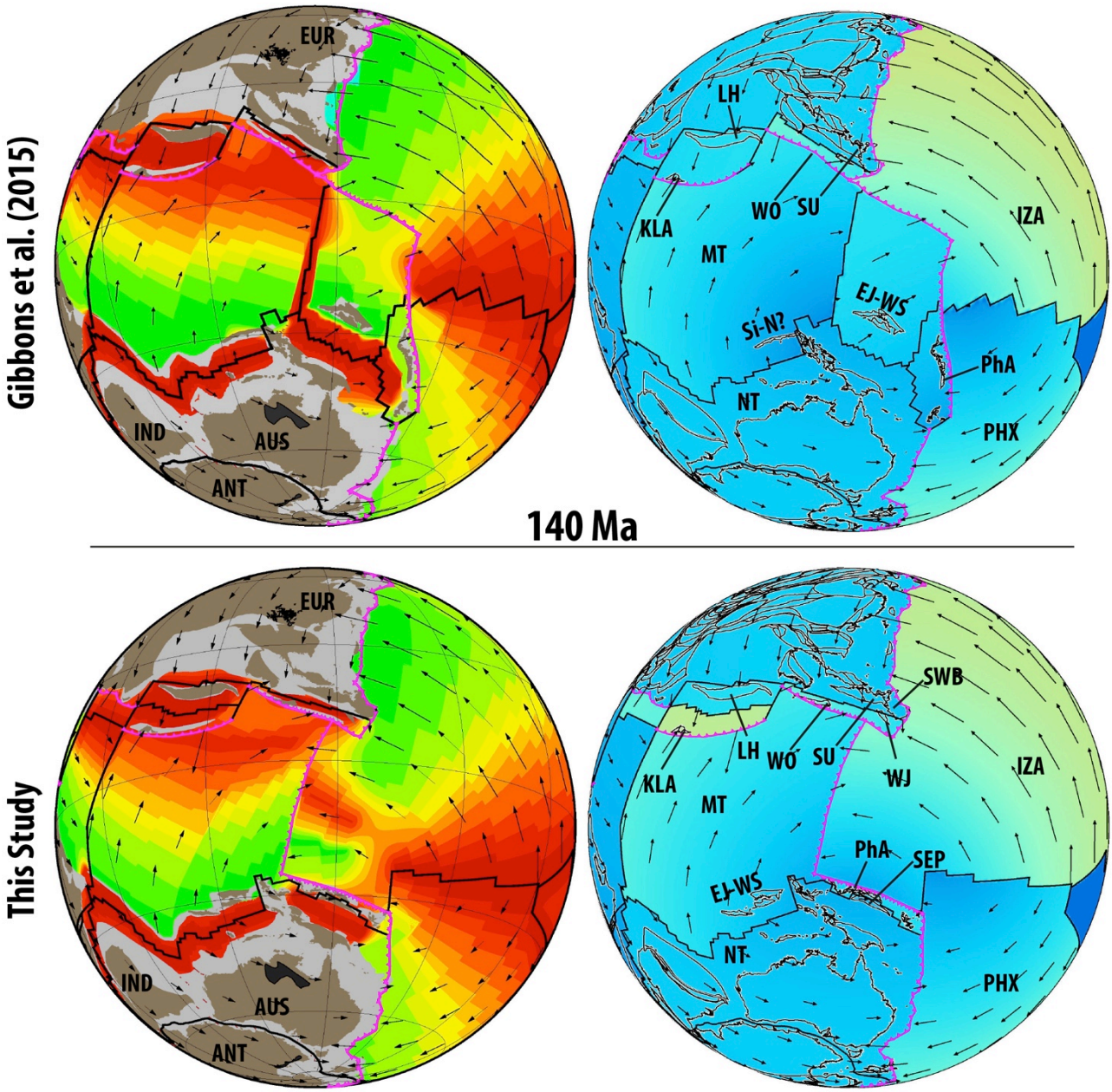

881 **Fig. 9.** Ongoing Meso-Tethyan subduction leads to the opening of the Kohistan-Ladakh (KLA) and
882 Woyla (WO) back-arc basins, as well as the Neo-Tethys (NT) along northern Gondwana. The
883 Philippine Archipelago (PhA) is detached from the Sepik Terrane (SEP) through a northward ridge
884 jump and continued rollback of the Izanagi slab.
885

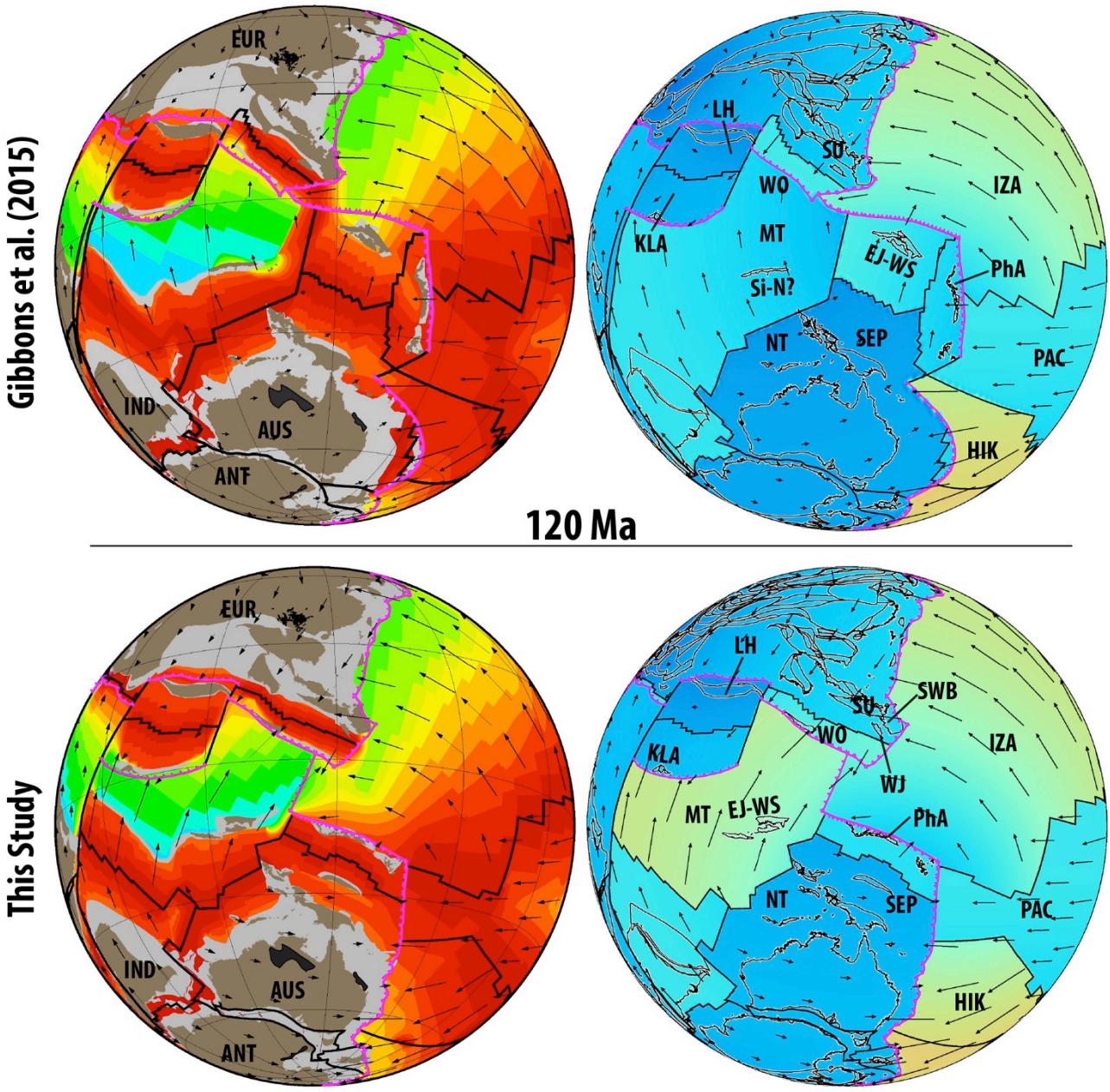


886

887 **Fig. 10.** In the models of Zahirovic et al. (2014) and Gibbons et al. (2015) the Neo-Tethyan ridge
888 system is abandoned by 120 Ma. In this study, seafloor spreading continues because of ongoing
889 subduction of the Meso-Tethyan Plate. Although the oldest preserved seafloor spreading constraints

for the Neo-Tethys are ~ 128 Ma in the Argo Abyssal Plain, we impose continued seafloor spreading in the Neo-Tethys that is driven by northward slab pull. HIK – Hikurangi Plate.

### 3.2 Active margin evolution in the Lhasa segment

The Late Jurassic is characterized by the asynchronous development of an active margin along southern Eurasia that was consuming the Meso-Tethyan ocean basin along a north-dipping subduction zone (Fig. 8). Along southern Lhasa, subduction-related calc-alkaline granites and granitoids ranging in age from ~ 170 to 137 Ma indicate the onset of north-dipping Meso-Tethyan Andean-style subduction (Zhang et al., 2012). The onset of subduction-related magmatism within the Kohistan Arc, which has no continental basement (Burg, 2011; Jagoutz and Schmidt, 2012), at ~ 154 Ma in the form of the Matum Das tonalite (Schaltegger et al., 2003) suggests the rollback of a Meso-Tethyan slab (e.g., Petterson and Windley, 1985; Pudsey, 1986) and the possible origin of Kohistan and Ladakh as fore-arc oceanic crust, following the generic model of forearc formation proposed by Flower and Dilek (2003) and Stern et al. (2012). Further east along the present-day suture zone, the interpreted intra-oceanic Zedong Terrane records latest Jurassic ages of subduction-related igneous suites including a dacite breccia dated as 161.0 ± 2.3 Ma, a number of samples with an age of ~ 156 Ma (andesite dyke, andesite breccia and quartz diorite), and an andesitic dyke with an age of 152.2 ± 3.3 Ma (McDermid et al., 2002). The Kohistan-Ladakh, Zedong and more-broadly Neo-Tethyan intra-oceanic subduction zone likely became established through continued southward slab rollback between ~ 150 and 120 Ma, which is marked by a magmatic hiatus in the Gangdese Batholith on Lhasa until ~ 110 Ma (Ji et al., 2009; Wen et al., 2008b). However, while the magmatic evolution of the Kohistan-Ladakh intra-oceanic arc is well-studied, its paleo-latitudinal position remains controversial and poorly constrained. Burg (2011) and Gibbons et al. (2015) place Kohistan on the equator at ~ 100 Ma (Fig. 11) based on the magnetisation of mid-Late Cretaceous red beds (Zaman

and Torii, 1999), suggesting a maximum southward extent for the Neo-Tethyan intra-oceanic arc. In addition, although Kohistan and Ladakh form the only significant preserved remnants of the Early Cretaceous intra-oceanic arc within the Yarlung-Tsangpo Suture Zone, additional ophiolites with intra-oceanic affinity are embedded in the suture zone east of Kohistan and Ladakh (Aitchison et al., 2000; Hébert et al., 2012).

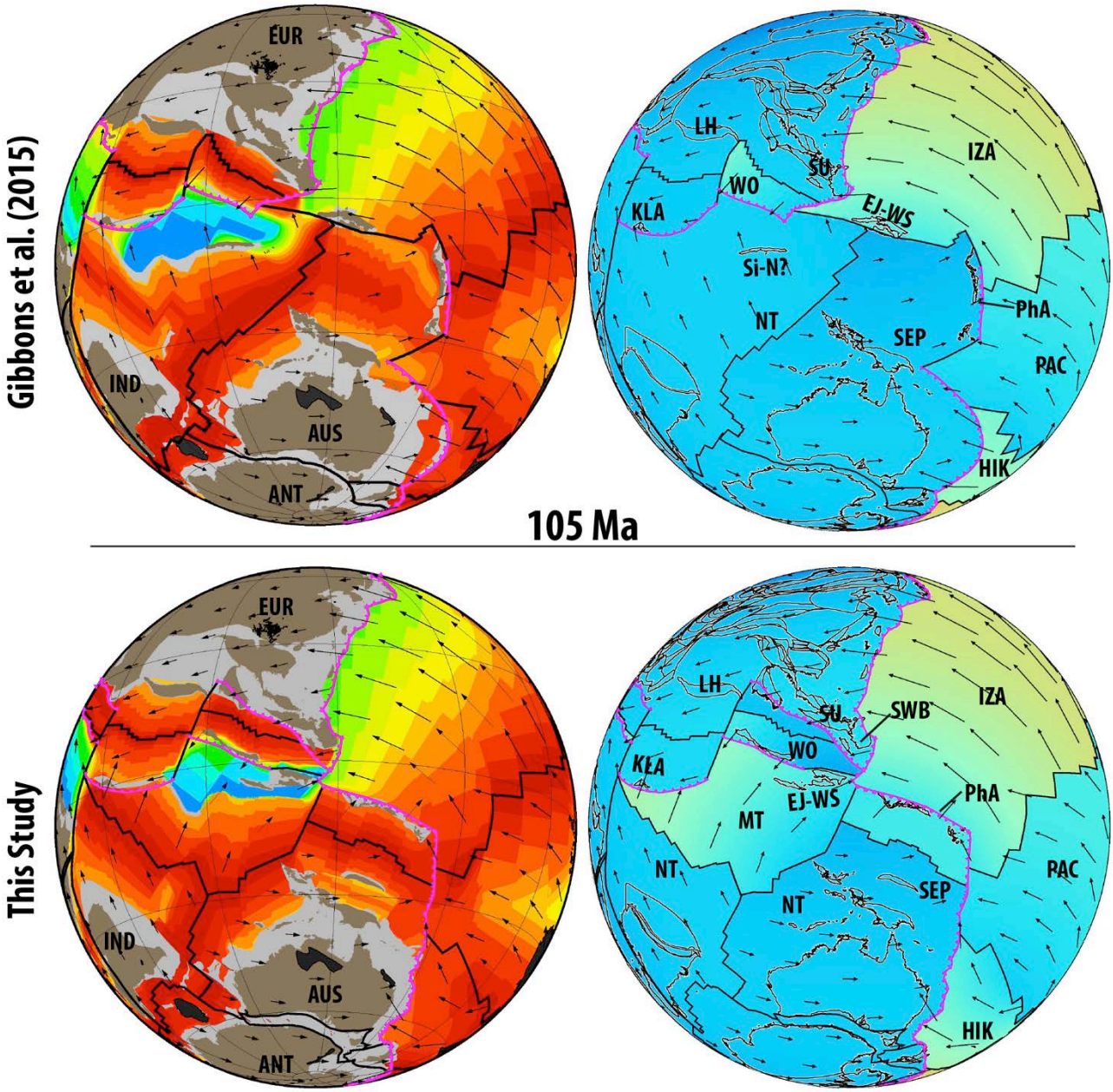


**Fig. 11.** The change in the motion of India from largely counterclockwise in the Early Cretaceous to largely northward, is recorded in fracture zone bends in the Wharton Basin at ~ 105-100 Ma (Matthews et al., 2012). In this study, the Neo-Tethyan ridge is consumed at the Kohistan-Ladakh

925 (KLA) intra-oceanic subduction zone from ~ 105 Ma, leading to a greater northward slab pull acting
926 on the Indian Plate (IND), which we interpret as causing the change in India Plate motion. The
927 collision of the East Java-West Sulawesi continental fragments possibly impeded subduction at the
928 Woyla Arc at ~ 105 Ma, and led to obduction of the Meratus ophiolite in the Cenomanian-Turonian
929 (~ 100-93 Ma) (Pubellier et al., 2004; Yuwono et al., 1988). The Kohistan-Ladakh and Woyla arcs
930 likely occupied near-equatorial latitudes by ~ 100 Ma, with both back-arc systems subducted
931 northward from ~ 115 Ma in the Sunda segment and from ~ 110 Ma along Lhasa, resulting in two
932 coeval north-dipping subduction zones in the Neo-Tethys (see Section 3.2).
933
934 The Aptian to Albian (~ 126-100 Ma) Yasin Group sedimentary sequence on the Kohistan-
935 Ladakh Arc is intercalated with syn-tectonic arc volcanics, and subsequent intrusions of diorites and
936 granodiorites (Pudsey et al., 1985; Rehman et al., 2011). A large portion of the magmatic products
937 were emplaced during a key timeframe between ~ 110 and 90 Ma (Petterson and Windley, 1985;
938 Rehman et al., 2011; Schärer et al., 1984), with significant magmatic accretion forming the Sapat
939 Complex on the Kohistan Arc between ~ 105 and 99 Ma (Bouilhol et al., 2011). This short-lived
940 "trenchward migration of the hot mantle source" (Bouilhol et al., 2011) may indicate the arrival of
941 the Neo-Tethyan mid-oceanic ridge with slab window formation, consistent with the ~ 95 Ma high-
942 temperature granulite metamorphism in the Jijal Complex and the peak metamorphic event in the
943 Kamila Amphibolite unit (Petterson, 2010). The demise of the Neo-Tethyan mid-oceanic ridge
944 between ~ 110 and 90 Ma along the Kohistan-Ladakh intra-oceanic arc (Fig. 11) likely had substantial
945 geodynamic implications for the region at the time, resulting in stronger northward slab pull acting
946 on the Indian Plate. Although the slab window likely temporarily impeded subduction, the
947 progressively increasing northward slab pull from ~ 105 Ma likely resulted in a major change in the
948 direction and speed of the Indian Plate, observable in the significant bends observed in the Wharton
949 Basin fracture zones (e.g., Wallaby-Zenith Fracture Zone) at ~ 105-100 Ma that required an ~ 50°
950 clockwise reorientation of the Indo-Australian spreading system (Matthews et al., 2012), and possibly

951 triggered a regional plate-reorganization event (Matthews et al., 2011). In addition, the onset of
952 northward slab pull on the Indian Plate from ~ 100 Ma may explain the paleomagnetic observations
953 of rifting within Greater India in the Late Cretaceous (van Hinsbergen et al., 2012).

954 The intersection of the Neo-Tethyan ridge with the Kohistan-Ladakh intra-oceanic subduction
955 zone, as modelled in this study, may have temporarily interrupted subduction due to the decrease of
956 negatively buoyant oceanic lithosphere entering the trench, with convergence accommodated along
957 the active continental Eurasian margin from ~ 110 Ma rather than along the intra-oceanic subduction
958 zone. The Gangdese Batholith recorded a major pulse of granitic magmatism from ~ 109 to 80 Ma
959 (Ji et al., 2009), indicating the resumption of Andean-style subduction along Lhasa that is
960 contemporaneous with intra-oceanic subduction along Kohistan-Ladakh, and hence signifies the
961 onset of two simultaneous north-dipping subduction zones in the Neo-Tethys from ~ 110 Ma.

962 The Late Cretaceous evolution of the Kohistan-Ladakh Arc has conflicting interpretations.
963 Conventional models suggest a Late Cretaceous collision and suturing of Kohistan-Ladakh to Eurasia
964 (Clift et al., 2002; Debon et al., 1987; Treloar et al., 1996), whereas more recent works, which have
965 incorporated detailed geochronology and structural interpretations of Kohistan, have concluded that
966 instead of suturing to Eurasia, the Late Cretaceous is punctuated by an arc rifting and splitting episode
967 by ~ 85 Ma (Bouilhol et al., 2011; Burg, 2011; Burg et al., 2006), which suggests Neo-Tethyan slab
968 rollback rather than collisional processes. The ~ 75-60 Ma magmatic gap in the Gangdese Batholith
969 (Chung et al., 2005; Wen et al., 2008b) may imply that the majority of India-Eurasia convergence
970 was accommodated by subduction along Kohistan-Ladakh rather than by subduction along Lhasa. A
971 scenario that precludes Kohistan-Ladakh collision with Eurasia in the Late Cretaceous requires that
972 an intra-oceanic arc first accreted onto Greater India (Chatterjee et al., 2013). A similar model
973 proposes that the Muslim Bagh Ophiolite represents the Kohistan-Ladakh forearc and was obducted
974 onto the leading edge of Greater India at ~ 65 Ma in near-equatorial latitudes, which resulted in the
975 cessation of calc-alkaline magmatism on Kohistan-Ladakh during ~ 65-61 Ma (Khan et al., 2009).
976 This scenario requires the accompanying suturing between Kohistan-Ladakh and Greater India along

977 the Indus Suture to occur earlier than the closure of Shyok Suture. Such a scenario is consistent with
978 the plate reconstructions presented in this study, in which Greater India reaches equatorial latitudes
979 at ~ 65 Ma. A recent stratigraphic analysis presented in Hu et al. (2015) suggests that the India-
980 Eurasia collision was underway by 59 ± 1 Ma, which we interpret as the initial arc-continent collision,
981 consistent with the tectonic evolution of the Kohistan-Ladakh Arc. The major slowdown in spreading
982 across the Central and Southeast Indian Ridges at ~ 52 Ma (Chron 23o, Cande et al., 2010) may
983 indicate the complete abandonment of the intra-oceanic subduction zone, and the completion of the
984 initial arc-continent collision between Greater India and the Neo-Tethyan intra-oceanic arc. Recent
985 geochemical analyses of granitoids from the Kohistan-Ladakh Arc indicate a major change in magma
986 chemistry (Nd and Hf isotopes) and the arrival of the Greater Indian continental margin into the
987 subduction zone by 50.2 ± 1.5 Ma (Bouilhol et al., 2013), which is consistent with the cessation of
988 intra-oceanic subduction by this time.
989 The continent-continent collision between Greater India and Eurasia likely occurred at
990 ~ 47 Ma, recorded in the marked slowdown of seafloor spreading at Chron 21o along the Southeast
991 Indian Ridge (Cande and Patriat, 2015) and the contemporaneous formation of an Indian Ocean
992 microplate near the Ninetyeast Ridge (Matthews et al., 2016). Suturing along the Shyok Suture Zone
993 between the two continents was likely complete by 40.4 ± 1.3 Ma (Bouilhol et al., 2013), which
994 accounts for the ~ 60-40 Ma Andean-style emplacement of the Linzizong volcanics in Lhasa (Chung
995 et al., 2005). The ~ 47-40 Ma continent-continent collision timing is consistent with an additional
996 slowdown and change in spreading direction along the Central and Southeast Indian Ridges and the
997 abandonment of the Wharton Ridge sometime between ~ 43 and 36 Ma (see discussion in Gibbons
998 et al., 2015).
999

1000 **3.3 Convergence along the West Burma and Sumatra margin segment**
1001

1002 Eastern Sumatra, as part of the Sibumasu ribbon terrane, docked with the Eurasian margin
1003 sometime in the Late Triassic to Early Jurassic (Metcalfe, 2011), and has since recorded Meso- and
1004 Neo-Tethyan subduction and accretion histories. The Woyla Terrane, which accreted to Sumatra in
1005 the Late Cretaceous (Morley, 2012a), plays a key role in elucidating the geodynamic setting of the
1006 Sumatran active margin since the Late Jurassic. However, the nature of the Woyla Terrane crust and
1007 the subduction polarity and history has given rise to a number of competing models for the tectonic
1008 evolution of Sumatra. The Jurassic to Cretaceous Woyla Group of sedimentary and volcanic units has
1009 previously been interpreted as an arc built on re-worked continental basement (Barber and Crow,
1010 2003; Cameron et al., 1980), largely due to the presence of a tin geochemical signature in the Sikuleh
1011 granitoids (Fig. 2) that may have been interpreted as analogous to the Southeast Asian tin belts that
1012 were built on continental crust (e.g., Bangka and Billiton Islands; Searle et al., 2012). Parts of the
1013 Woyla basement near Sikuleh, Natal and Bengkulu are composed of quartzite and phyllite (Acharyya,
1014 1998), and overprinted by widespread granitoid intrusions largely Late Cretaceous in age (Barber and
1015 Crow, 2003), leading some authors to interpret these micro-blocks as Gondwana-derived continental
1016 fragments (Görür and Sengör, 1992; Haile, 1979; Metcalfe, 1994; Metcalfe, 2002; Metcalfe and
1017 Irving, 1990). The paleomagnetic study of a Jurassic limestone sample by Haile (1979) suggests that
1018 the crust in the vicinity of Sikuleh (Locality H in Haile, 1979) was at 26°S in the Jurassic. This result
1019 was used by Metcalfe (1994) to suggest a Gondwana origin for the proposed micro-continental
1020 fragment.
1021 The continental nature of the Sikuleh part of the Woyla Terrane (Si, Fig. 2) is rejected by
1022 Barber and Crow (2003), who instead propose an intra-oceanic arc origin. The Woyla Group consists,
1023 at least in part, of accreted fragments that include seamounts, reef fragments, ophiolites and
1024 associated ocean floor sedimentary sequences (Barber and Crow, 2003; Wajzer et al., 1991), but no
1025 clear continental basement can be identified, much like the Kohistan-Ladakh Arc in the central Neo-
1026 Tethys. Paleontological constraints from a single foraminifera specimen within the Batang Natal
1027 Megabreccia provide a Late Triassic age (Wajzer et al., 1991), and suggest that the oceanic crust that

1028 was consumed in the Woyla intra-oceanic subduction system in the Cretaceous was at least Late
1029 Triassic in age, consistent with the age of Meso-Tethyan oceanic crust subducted along the Sumatra
1030 segment predicted by our reconstructions for the Cretaceous (Fig. 10). In addition, the accretion of
1031 highly disrupted lenses of oceanic crust and sedimentary sequences onto the Woyla Terrane is
1032 consistent with the observations of accreted oceanic plate stratigraphy further east in the Luk Ulo-
1033 Meratus Suture Zone between East Java-West Sulawesi and the core of Borneo (Wakita, 2000;
1034 Wakita and Metcalfe, 2005).
1035

1036 ***3.3.1 Development of the Woyla intra-oceanic arc***

1037

1038 The Woyla Terrane, largely represented by the Woyla Group of sedimentary sequences and
1039 intrusions, likely developed on an active intra-oceanic margin (with possible continental basement)
1040 in the Early Cretaceous (Figs. 9-11), separated from mainland Sumatra by a marginal sea (Rock et
1041 al., 1983; Wajzer et al., 1991). However, the origin of the Woyla Arc has recently been debated, with
1042 a model proposing a Gondwana origin for both the Woyla and the Kohistan-Ladakh Arc (Hall, 2012)
1043 as the result of continued rollback of a south-dipping subduction zone (Fig. 4b-c). Alternatively, the
1044 model of Zahirovic et al. (2014), and the one presented here, invoke a southern Eurasia origin of the
1045 Kohistan-Ladakh and Woyla intra-oceanic island arcs. The scenario invoking south-dipping
1046 subduction along northern Gondwana in the Late Jurassic could be corroborated by the preservation
1047 of contemporaneous arc rocks on Greater India (Tethyan Himalayas) or the NW Australian Shelf,
1048 which are not yet documented. The scenario invoking north-dipping Meso-Tethyan subduction to
1049 detach the Argoland continental fragments and open the Neo-Tethys in the latest Jurassic can be
1050 corroborated by the subduction history along Lhasa, West Burma (Myanmar) and Sundaland.
1051 Subduction is suggested to have initiated along the West Burma block at ~ 163-152 Ma by jadeite
1052 geochronology (Shi et al., 2008; Shi et al., 2014). This age is similar to that of the 154 Ma Matum
1053 Das tonalite within the Kohistan-Ladakh arc (Schaltegger et al., 2003) to the west. The formation of

1054 the Naga Ophiolite during ~ 156-150 Ma, based on Kimmeridgian-lower Tithonian cherts (Baxter et
1055 al., 2011), suggests a close temporal and geodynamic association between the Kohistan-Ladakh
1056 (Lhasa segment), Mawgyi (West Burma segment) and Woyla (Sumatra segment) intra-oceanic arcs
1057 along which Meso-Tethyan oceanic crust began subducting in the latest Jurassic.
1058

1059 ***3.3.2 Subduction of the Woyla back-arc basin***

1060

1061 The resumption of Andean-style subduction in the central Neo-Tethys along Lhasa is well-
1062 constrained to ~ 109 Ma, based on the onset of subduction-related magmatism in the Gangdese
1063 Batholith (Ji et al., 2009). However, the timings of subduction initiation along West Burma and
1064 Sumatra are less well constrained. An Albian (~ 113-100 Ma) unconformity on West Burma (Morley,
1065 2012a) may indicate compression related to subduction initiation, which is contemporaneous with
1066 observations in Lhasa, and the supra-subduction formation of the Andaman Ophiolite at 95 ± 2 Ma
1067 (Pedersen et al., 2010) may suggest the onset of rollback and extension in the overriding plate. Here
1068 we interpret the ~ 115 Ma peak in Ultra- and Very-High Pressure metamorphics in the Luk-Ulo Suture
1069 Zone (Figs. 10-12) (Parkinson et al., 1998) as indicators of subduction initiation of the Woyla back-
1070 arc basin to account for the Albian unconformity on West Burma. The 105 to 90 Ma dioritic and
1071 granodioritic intrusions into the Wuntho-Popa Arc (Mitchell et al., 2012), west of the Sagaing Fault,
1072 suggest continuity of the contemporaneous Lhasa subduction zone into the West Burma segment of
1073 the margin. However, subduction to consume the Woyla back-arc basin may (also) have been south-
1074 dipping as argued in Morley (2012a).

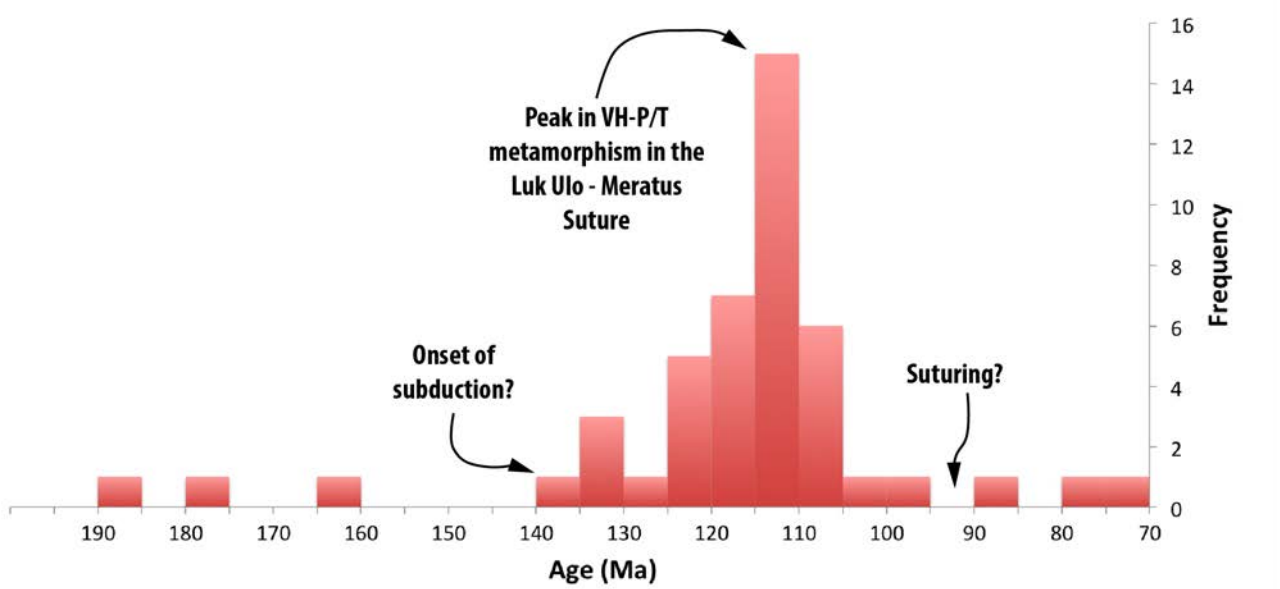


**Fig. 12.** Very High and Ultra High Pressure (VHP/UHP) metamorphic rocks in the Luk Ulo-Meratus suture on Java and Borneo (Fig. 2) record well-established subduction from at least ~ 140 Ma. A significant spike at ~ 115 Ma has been previously interpreted as a collision between East Java-West Sulawesi and the Woyla intra-oceanic arc (Gibbons et al., 2015; Zahirovic et al., 2014). However, in the refined plate reconstructions presented herein, the origin of East Java from the Argo Abyssal Plain would require excessive seafloor spreading rates, and instead we interpret the peak in VHP/UHP metamorphism to represent the onset of Woyla back-arc subduction along West Burma and Sundaland. Figure modified from Parkinson et al. (1998).

Although the Kohistan-Ladakh Arc is loosely constrained to near-equatorial paleo-latitudes during the mid-Cretaceous (Burg, 2011), no latitudinal constraints exist for the Woyla Arc. However, some constraints are available for the closure of the Woyla back-arc basin, and the collision of the intra-oceanic arc with Sumatra (Figs. 13-14). The Woyla Group is intruded by a number of Late Cretaceous igneous bodies, including the 84.7 ± 3.6 Ma (K-Ar) Batu Madingding diorite and the 78.4 ± 2.5 Ma (K-Ar) andesite in the southwest Batang Natal section (Wajzer et al., 1991), after which a significant magmatic gap is interpreted to represent collision of the Woyla Terrane with Sumatra. Hall (2012) argued that no subduction occurred on the Woyla/Sumatra segment of the Tethyan margin

between 90 and 45 Ma (Fig. 4C), largely due to the presence of a regional unconformity that was interpreted to signify the absence of subduction-related dynamic subsidence on the overriding plate (Clements et al., 2011). However, only an ~ 10-15 Myr magmatic gap associated with a hiatus in subduction between ~ 75 and 62 Ma (Fig. 15) can be accounted for in the volcanic record on Sumatra (McCourt et al., 1996; Zahirovic et al., 2014). However, some of these (~ 10 Myr) magmatic gaps may be due to sampling issues, and future work may reveal more continuous subduction histories. The choice to impose an ~ 45 Myr (Hall, 2012) rather than an ~ 10-15 Myr (Zahirovic et al., 2014) subduction hiatus has significant geodynamic implications for the region, where the continued northward motion of the Indian Plate needs to be accommodated by an oceanic transform that cuts across older oceanic lithosphere and pre-existing structural fabric in the reconstructions of Hall (2012) (Fig. 4C).

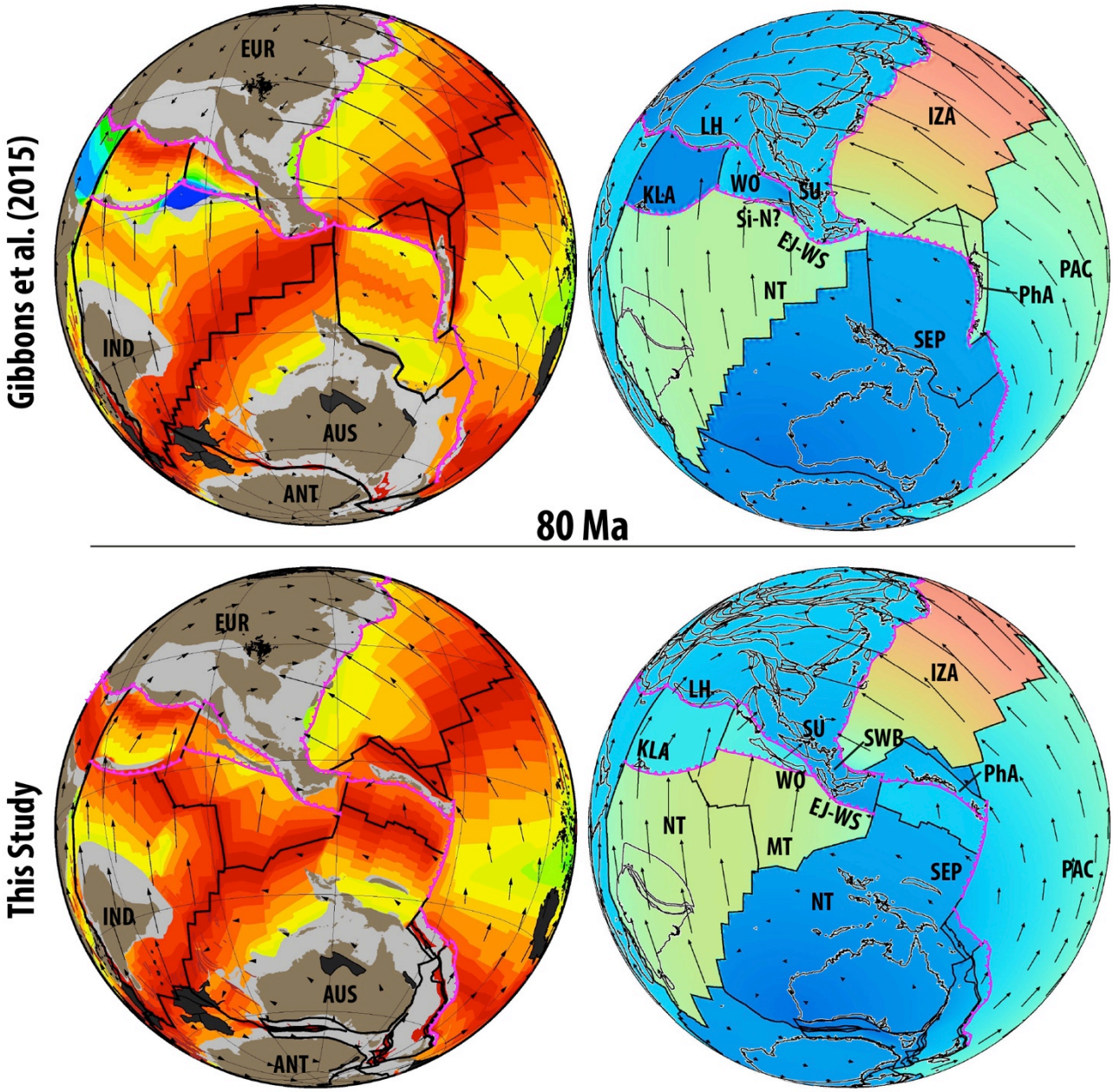


**Fig. 13.** India's northward motion accelerated from ~ 80 Ma. The subduction polarity likely reversed along the Philippine Arc and suturing of the East Java and West Sulawesi continental fragments to the Southwest Borneo Core was complete by this time. The Woyla Terrane was approaching the Sumatran margin by this time. Additional polygons in the lower panels for Australian-Antarctic and Lord Howe-Tasman Sea regions represent areas of deforming continental crust.

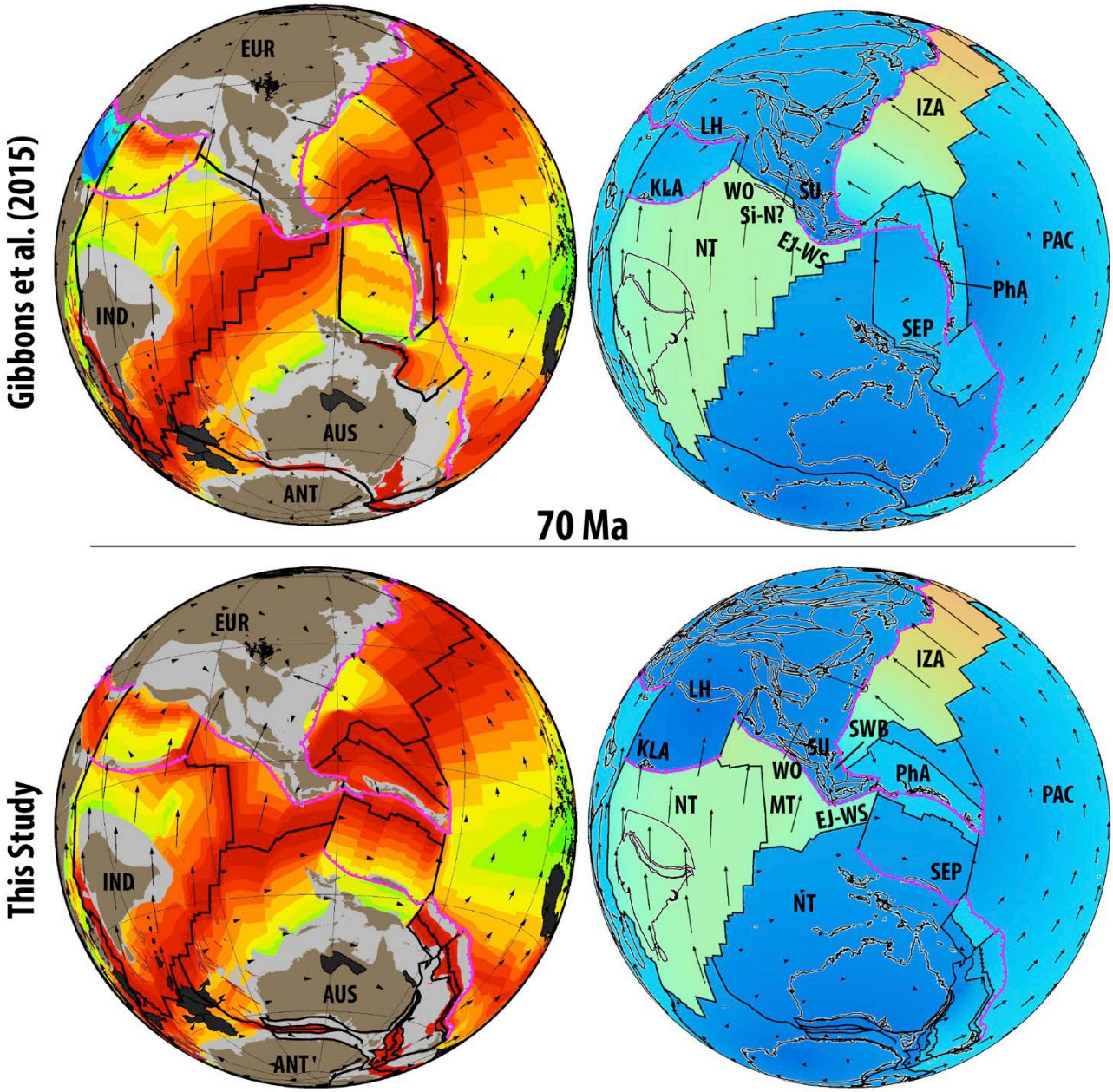


**Fig. 14.** The Woyla Arc collided with Sundaland (SU) by ~ 75 Ma, and impeded subduction in this segment of the margin for ~ 10 Myr. The Meso-Tethyan Plate was still likely being subducted along the Sunda Trench based on the refined plate reconstructions, with Wharton Ridge arrival near eastern Sundaland between ~ 70 and 60 Ma in both reconstructions. In this study, we reconstruct the subduction of the Sepik oceanic gateway from ~ 71 Ma based on the age of the Emo volcanics (Worthing and Crawford, 1996).

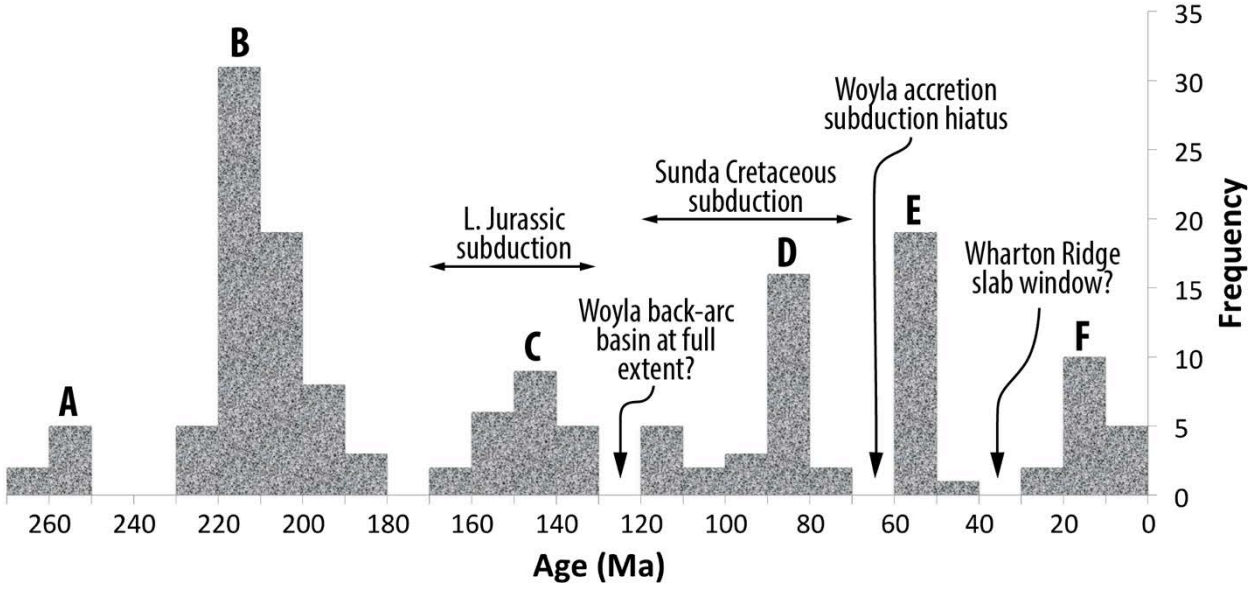


**Fig. 15.** A synthesis of arc volcanism on Sumatra, adapted from McCourt et al. (1996), highlights a number of short-lived magmatic hiatuses likely related to back-arc basin rifting and/or collisional processes that impeded subduction along the Sumatran continental margin.

The post-Cretaceous history of the Sumatran margin is less controversial, with magmatism related to the subduction of the Neo-Tethys and Indian oceans (McCourt et al., 1996), and widespread basin rifting and flooding occurring since Paleocene times on Sundaland (Doust and Sumner, 2007). One important geodynamic consideration for the Sumatra margin is the interaction of the (extinct) Wharton Ridge with the Java-Sunda trench, with the model of Whittaker et al. (2007) suggesting a long-lived slab window sweeping westward from eastern Sundaland (near Java) from ~ 75 Ma to the present. Such a scenario implies a time-dependent along-trench thermal anomaly affecting the Sundaland continent, and more importantly, the subduction of young oceanic crust (and hence thinner oceanic lithosphere) has important implications on the long-wavelength mantle-driven topography on the overriding plate (e.g., Flament et al., 2015, for Patagonian uplift associated with the Chile Triple Junction; Guillaume et al., 2009). The combination of a subduction hiatus in the Late Cretaceous, as well as the subduction of very young oceanic crust in the Eocene along the Java-Sunda trench would likely result in widespread regional dynamic uplift that has been proposed by Clements

et al. (2011) to account for a widespread Late Cretaceous to Paleocene regional unconformity across Sundaland, as explored in Zahirovic et al. (In Press).

## 3.4 Accretionary history of the Java and Borneo margin segment

A key region recording the evolution of Southeast Asia in the context of Eurasian, Tethyan and (proto-) Pacific convergence is the Sundaland continental promontory. The core of Sundaland is composed of north-eastern Sumatra, West Java and the Southwest Borneo block (Hall, 2012; Metcalfe, 1988; Metcalfe, 2011; Zahirovic et al., 2014). The promontory is largely Phanerozoic continental crust (Hall, 2011), with accreted intra-oceanic and allochthonous continental fragments – some, like East Java, carrying Archean zircon signatures (Smyth et al., 2007). The continental fragments making up Sundaland have largely Tethyan-Gondwanan affinities based on paleontological, stratigraphic and paleo-magnetic constraints, as reviewed in Metcalfe (2006).

### *3.4.1 Subduction and accretion history of southern Sundaland*

The onset of Late Jurassic subduction in the eastern Tethys is best represented by the ~ 180-165 Ma schists found within the Meratus Complex on the eastern periphery of the Southwest Borneo core, as well as the presence of Bajocian (~ 170 Ma) and younger radiolarians embedded in the Meratus Suture Zone (Wakita et al., 1998). Zircons shed into the Ciemas and Bayah Formations on West Java, have ages of 160 Ma and younger (Clements and Hall, 2007), and likely represent the onset of subduction along this margin. The Late Jurassic-Early Cretaceous age of subduction onset on this segment is consistent with the establishment of a major subduction system along southern Eurasia, spanning at least from western Lhasa to the easternmost Tethyan margin on eastern Sundaland (see previous sections for full chronology). A continuous record of very-high-pressure (VHP) metamorphic rocks (Fig. 12), including greenschists, blueschists, granulites, eclogites and

jadeite-bearing metamorphics from ~ 140 Ma in the Luk-Ulo and Meratus region of Sundaland (Parkinson et al., 1998) suggests a well-established subduction zone in the Early Cretaceous. The VHP metamorphic peak at ~ 115 Ma has previously been interpreted as an arc-continent collision of Gondwana-derived continental fragments (including East Java, West Sulawesi, Mangkalihat, and eastern Borneo) with the eastward continuation of the Woyla Arc (Zahirovic et al., 2014). However, in this study we prefer an interpretation of Woyla back-arc basin subduction initiation at this time to account for the UHP/VHP metamorphism, as discussed in earlier sections.

A significant spike in the zircon age spectra at ~ 100 Ma (Clements and Hall, 2007) may indicate the arrival of the East Java-West Sulawesi in the vicinity of Sundaland. The obduction of the Meratus Ophiolite in the Cenomanian/Turonian between ~ 100 and 93 Ma (Pubellier et al., 2004; Yuwono et al., 1988) is consistent with the Cenomanian radiolarians found in the Meratus Complex (Wakita et al., 1998). The final closure of the Barito Sea back-arc basin along southern Sundaland occurred by ~ 80 Ma based on the lack of volcanic-derived zircons in fore-arc sandstones (Clements and Hall, 2011; Wakita, 2000). A Late Cretaceous to Paleocene (~ 72 to 65 Ma) unconformity on southwest Sulawesi (Milsom, 2000) may indicate collisional (uplift/denudation) processes, a subduction hiatus, or a combination of both. A resumption of subduction likely occurred in the Paleocene (Yuwono et al., 1988), with ~ 65-58 Ma (K-Ar) subduction related rocks (Guntoro, 1999), a 63 Ma tuff reported on South Sulawesi (van Leeuwen, 1981), and continuous calc-alkaline and tholeiitic volcanism occurring between 51 and 17 Ma on the western and northern arm of Sulawesi (Elburg et al., 2003). Ongoing subduction and major deformation (Figs. 16-17), largely due to the arrival of the Australian continental margin, namely the Sula Spur (Figs. 18-19), started with the obduction of the East Sulawesi Ophiolite at ~ 20 Ma (Oligocene to Miocene) in a continent-continent collision setting (Bergman et al., 1996). The subsequent compressional deformation and widespread oroclinal bending of Sundaland are discussed at length in Hutchison (2010) and Zahirovic et al. (2014), and are summarised in the following sections.

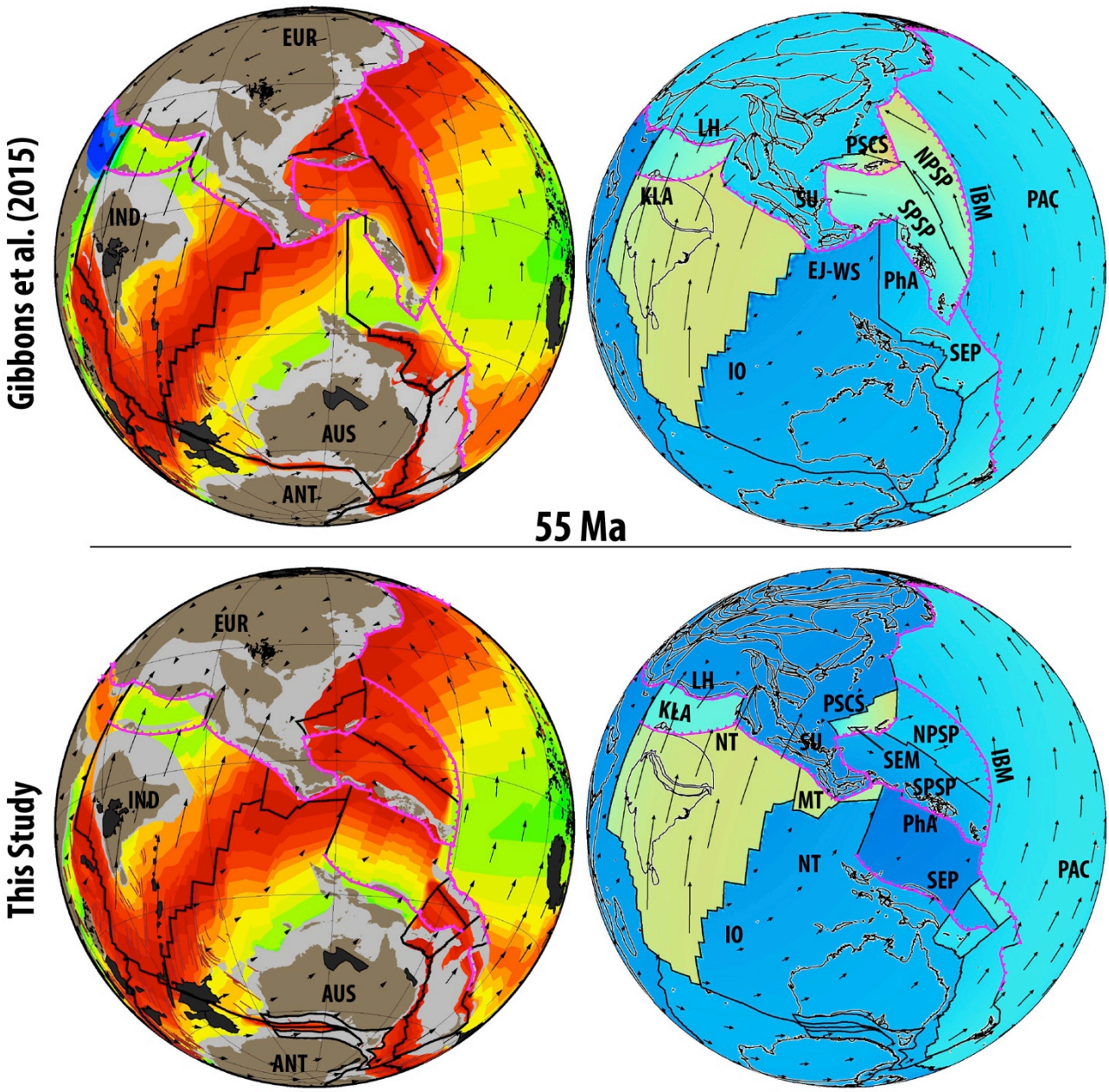


**Fig. 16.** The 55 Ma reconstruction marks the initial stages of contact between Greater India and the Kohistan-Ladakh Arc to close the Indus Suture Zone, leading to major changes in spreading rate and direction on the India-Antarctica ridge system. The rollback of the Izanagi slab opens the Proto South China Sea (PSCS) from ~ 60 Ma in a Tyrrhenian-style back-arc system. Subduction is initiated at ~ 55 Ma along the Izu-Bonin-Marina Arc (IBM) to consume Pacific (PAC) oceanic crust. IO – Indian Ocean, NPSP – North Philippine Sea Plate, SPSP – South Philippine Sea Plate, SEM – Semitau Block.

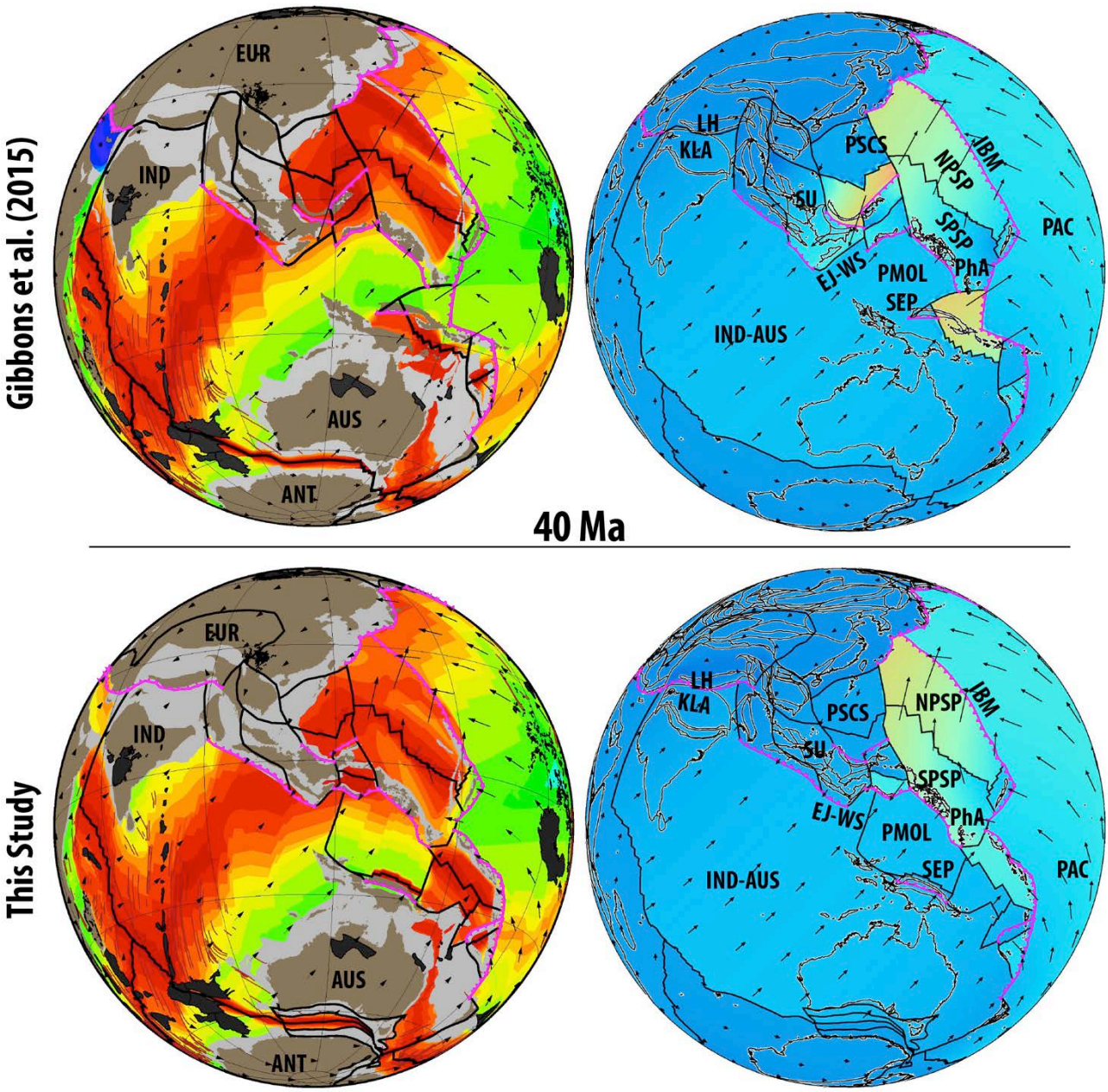


**Fig. 17.** Continent-continent collision between India and Eurasia likely initiated by ~ 47 Ma, leading to final closure of the Yarlung-Tansgpo and Shyok suture zones (see Fig. 1). The rollback of the Izanagi slab opens the Proto South China Sea and transfers the Semitau and Mindoro continental fragments from the South China margin onto northern Borneo, leading to a mid-Eocene collision. The Sepik oceanic gateway is almost consumed along a north-dipping subduction zone, north of which the Proto Molucca Plate (PMOL) is consumed contemporaneously along the Philippine Arc.

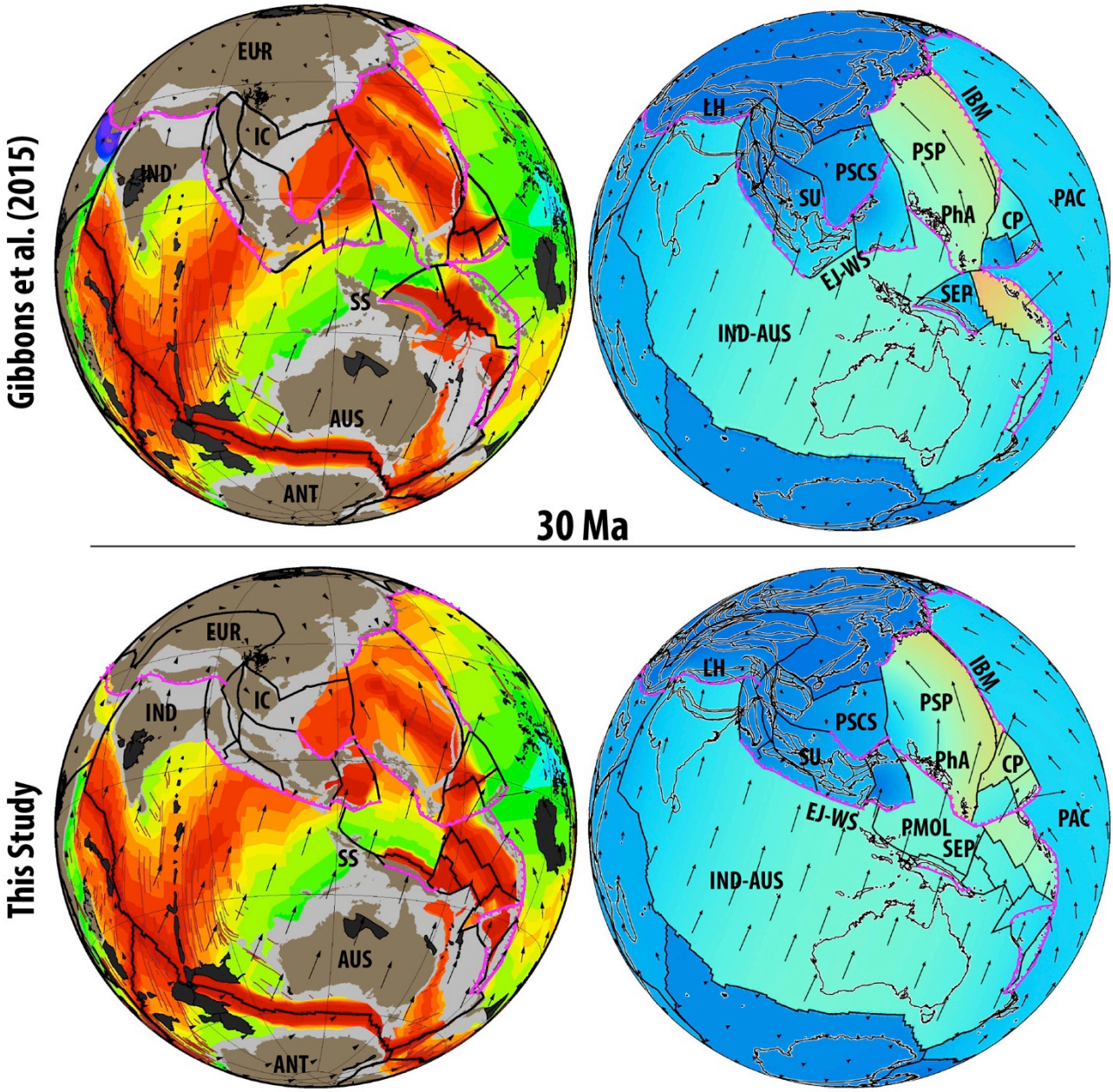


1207

1208 **Fig. 18.** India's continued, although slowed, northward advance results in the clockwise rotation and

1209 lateral extrusion of Indochina (IC), leading to the first stages of oroclinal bending in western

1210 Sundaland. The Sepik Terrane docks with the New Guinea margin, and the Sula Spur (SS) continental

1211 promontory on the northern Australian margin approaches Sundaland. CP – Caroline Plate, PSP –

1212 Philippine Sea Plate.

1213

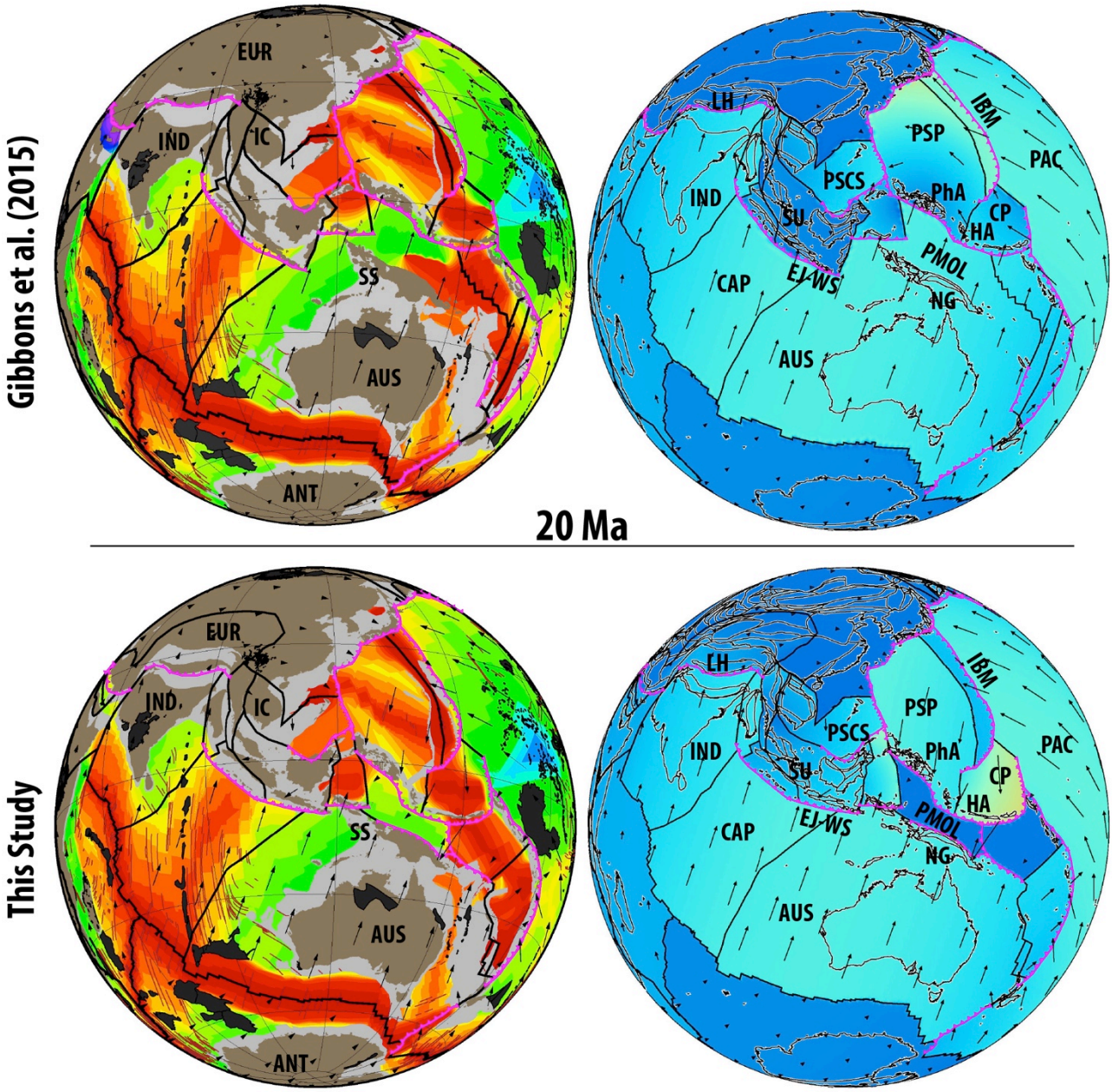


**Fig. 19.** The extrusion of Indochina due to India's northward motion, together with the collision between Sula Spur and West Sulawesi results in the oroclinal bending of Sundaland, resulting in major counterclockwise rotation of Borneo relative to Sumatra and the Malay Peninsula. South-dipping subduction initiates by ~ 20 Ma to account for the Maramuni Arc volcanics on New Guinea, with coeval north-dipping subduction of the Proto Molucca Plate (PMOL) accommodating southward motion of the Caroline Plate (CP) and the Halmahera Arc (HA).

### *3.4.2 Northern Sundaland collisions*

The geological record on the Sundaland continental promontory captures the geodynamic interaction between the Tethyan and proto-Pacific oceanic domains, and holds clues as to how the present-day complexity of plate boundaries developed. Most notably, an ongoing topic of interest relates to how the east Asian margin transitioned from purely Andean-style subduction (Fig. 20) in the Late Cretaceous (Shi and Li, 2012), to one that is presently dominated by a labyrinthine network of intra-oceanic active margins connected by splayed transforms, ridge segments and diffuse plate boundaries (Bird, 2003). Although much of the proto-Pacific plates has been recycled into the mantle, the preserved flanks of the seafloor spreading history have been used to restore the lost plates, assuming seafloor spreading symmetry (Seton et al., 2012). However, the location and evolution of subduction zones are difficult to constrain, with the only clues coming from paleomagnetic constraints, arc volcanics and present-day mantle structure (Hall and Spakman, 2002; Miller et al., 2006; Queano et al., 2007; Zhao et al., 2007).

Although a key component of the intra-oceanic system is the Philippine Sea Plate, which is discussed in Section 3.5.1, the transition from Andean-style to intra-oceanic subduction north of Sundaland is most likely controlled by back-arc basin opening processes in the Late Cretaceous (Morley, 2012a). In the model proposed in Zahirovic et al. (2014), and adopted here, the emplacement of the Fukien-Reinan massif (Fig. 20) from Andean-style subduction ceases in the Late Cretaceous (Jahn et al., 1976), and was replaced with extension and back-arc basin opening (Li, 2000) due to rollback of the Izanagi slab (Figs. 13-14, 16). Such a scenario is consistent with the onset of Late Cretaceous tectonic subsidence in East Asian basins (Yang et al., 2004), as well as the crustal and biogeographic affinity between continental fragments wedged in northern Borneo and the Philippine Archipelago, namely the Semitau and Mindoro blocks, and their likely origin on the South China continental margin (Fig. 20) in the Late Cretaceous (Zahirovic et al., 2014). The rollback induced extension in the overriding plate (Schellart and Lister, 2005) likely progressed to back-arc basin

opening, following the analogue of the Tyrrhenian back-arc system in the Mediterranean that detached and carried continental blocks to eventually collide as allochthons with a distant margin (Doglioni, 1991; Jolivet et al., 1999; Rehault et al., 1987). In the case of the Proto South China Sea, the Semitau and Mindoro fragments were likely detached from the East Asian margin by ~ 65 Ma, based on the onset of tectonic subsidence (Yang et al., 2004) and the ~ 59 Ma emplacement of supra-subduction zone ophiolites on Mindoro (Yumul et al., 2009). The continued rollback transferred Semitau and Mindoro southward, resulting in an Eocene collision with the northern Borneo margin to produce the Sarawak Orogeny (Cullen, 2010; Fyhn et al., 2010; Hutchison, 1996; Hutchison, 2004), after which southward subduction consumed the Proto South China Sea to emplace widespread volcanism on northern Borneo (Soeria-Atmadja et al., 1999).

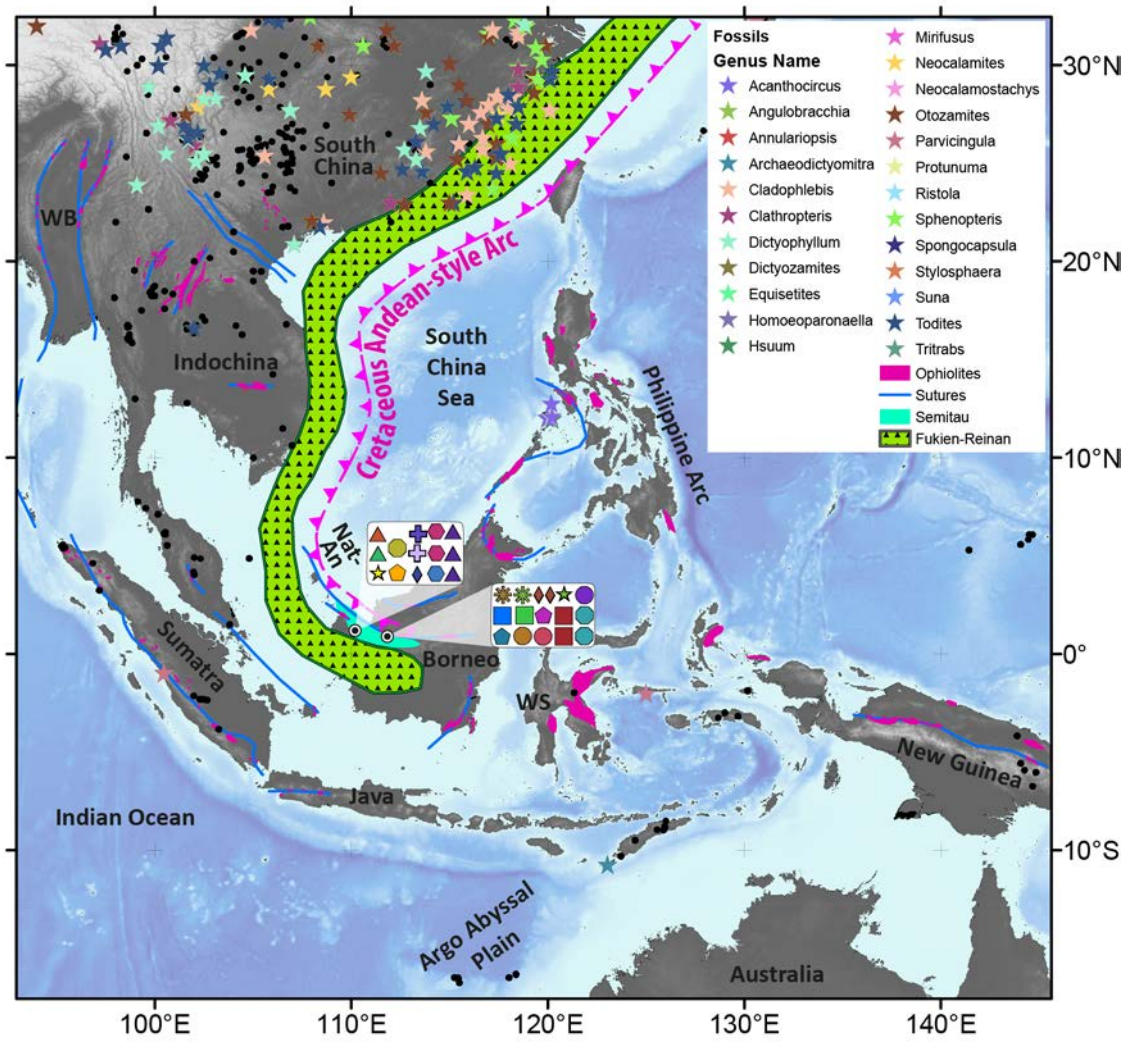

**Fig. 20.** Triassic and Jurassic fossil occurrences from the global Paleobiology Database (now Fossilworks) from Semitau (northern Borneo), represented by coloured symbols. The same fossils are also found elsewhere in Asia, with the strongest biogeographic affinity with mainland South China. The curved Fukien-Reinan massif (green hatched region) represents the Cretaceous Andean-style east Asian margin, which was replaced with an intra-oceanic setting in the Late Cretaceous. The curvature of the Andean-style magmatic arc also supports strong oroclinal bending of Sundaland in post-Cretaceous times. Nat-An – Natuna–Anambas Arc, WB – West Burma, WS – West Sulawesi. Figure adapted from Zahirovic et al. (2014).

The slab pull from south-dipping Proto South China Sea subduction along northern Borneo, along with the clockwise (CW) extrusion of Indochina resulting from the India-Eurasia collision (Fuller et al., 1991; Tapponnier et al., 1982), may have led to significant adjustments in the plate boundary forces acting on Sundaland. The ~ 32 Ma onset of seafloor spreading along the South China margin (Fig. 18) detached the Dangerous Grounds-Reed Bank continental blocks to open the South China Sea (Lee and Lawver, 1994; Lee and Lawver, 1995), with collision of the continental fragments with northern Borneo and South Palawan at ~ 15 Ma resulting in ophiolite obduction and the Sabah Orogeny (Hutchison, 2004; Hutchison et al., 2000), as well as choking the north Borneo subduction system and shutting down seafloor spreading in the South China Sea (Briais et al., 1993). This southward collision was wedged between the India-Eurasia collision from ~ 47 Ma (see Section 3.2) and the collision of the Australian northern margin with eastern Sundaland from ~ 25 Ma (Bergman et al., 1996; Hall, 2002). This arrangement of plate boundaries, and the driving forces, presumably had significant consequences for the rotational history of Borneo and the deformation of Sundaland.

### *3.4.3 Sundaland oroclinal bending*

The large counterclockwise (CCW) rotation of Borneo, relative to stable Sundaland, in the Cenozoic has drawn a range of interpretations and led to a number of competing models (see discussion in Zahirovic et al. (2014)). Each model of Borneo rotation has consequences for the deformation history on Sundaland (in particular, the basins of the Sunda Shelf and Java Sea), as well as understanding the mechanism that led to the 90° CCW rotation of Borneo relative to Sundaland in the Mesozoic, including up to 50° CCW rotation since 25 Ma (Fuller et al., 1999). In the absence of large transform faults, such as the Red River Fault bounding northern Indochina, within the Java Sea or the Sunda Shelf, Hutchison (2010) proposed a model of oroclinal bending for the rotation of Borneo as a mechanism to explain the deformation of the Sundaland continental promontory.

Hutchison (2010) synthesised the paleomagnetic evidence, as well as observations of curved lineaments observed in the gravity anomalies of Sundaland and the curvature of the Natuna and Anambas Cretaceous paleo-arc (Fig. 20) to infer that wholesale bending of Sundaland accommodated the CW rotation of Indochina and the CCW rotation of Borneo (Fuller et al., 1999; Fuller et al., 1991). The curved lineaments (Fig. 21) are most likely to be successive generations of ancient volcanic arcs (Hutchison, 2010), with the most obvious example being the curved arc belonging to the Middle to Late Triassic tin belt granites on Bangka and Billiton islands, as well as the previously-mentioned Natuna-Anambas Cretaceous Arc. Zahirovic et al. (2014) expanded on the work of Hutchison (2010) and used filtered Bouguer anomalies (Balmino et al., 2012) to extract geometrical constraints on the oroclinal bending (Fig. 21), and constructed a kinematic oroclinal bending model that accounts up to ~ 78° CCW rotation of Borneo since ~ 50 Ma.

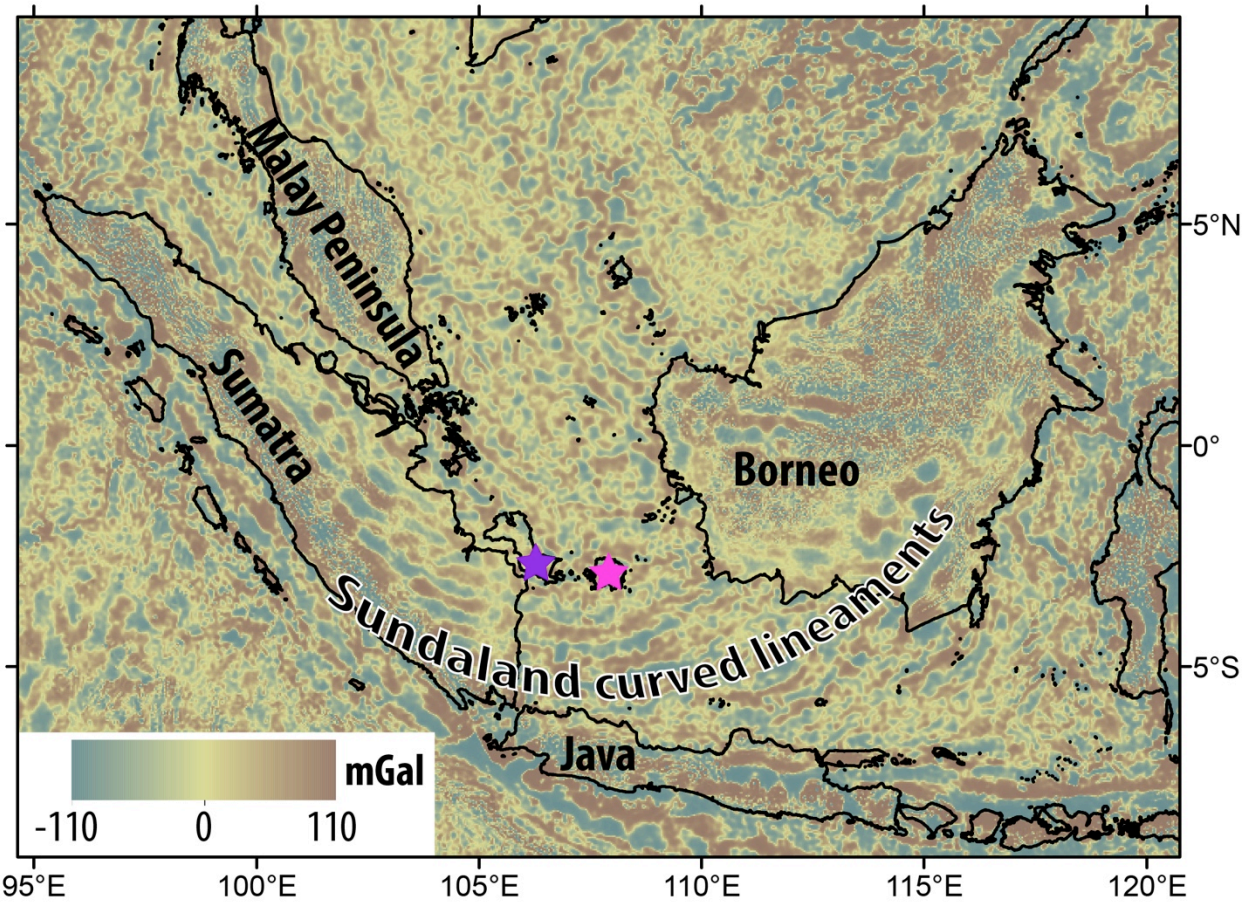


**Fig. 21.** The band-pass-filtered (150 to 10 km) Bouguer gravity anomalies from the 1 min World Gravity Map (Balmino et al., 2012) highlights the large-scale structures and the curved lineaments on Sundaland, resulting from oroclinal bending as proposed by Hutchison (2010). Bangka Island – purple, Belitung (Billiton) Island – pink.

One important distinction between the oroclinal bending of Sundaland and classical models of oroclinal bending largely relates to the tightness of the oroclinal folds and the deformation experienced by the continental crust (Carey, 1955; Eldredge et al., 1985). In the case of Sundaland, the hinge of the orocline is likely to be in the Sunda Shelf west of Borneo, with a wide region of bending rather than tight oroclinal bends that are typically reported for Kazakhstan (Abrajevitch et al., 2008) and the Mediterranean (Rosenbaum, 2014). Although the boundaries of the Sundaland continental promontory experienced compression during oroclinal bending, the Java Sea and Sunda Shelf were dominated by extension from Eocene times to the mid-Miocene, after which a major phase

of basin inversion dominated the tectonic regime of Sundaland to the present (Doust and Sumner, 2007; Pubellier and Morley, 2014).

## 3.5 New Guinea and the Philippines

### *3.5.1 Origin and evolution of the Philippine Archipelago*

Tectonic reconstructions of the transfer of Gondwana-derived terranes following the breakup of Pangea are limited by the lack of preserved seafloor, but are typically supplemented with high-quality and well-constrained onshore geological data that helps reconstruct the synthetic seafloor spreading histories. However, the region east of Sundaland, which includes the Philippines and New Guinea are considerably more complicated, as they straddle the Tethyan and (proto-) Pacific tectonic domains, resulting in a complex interaction dominated by back-arc basin formation processes and multiple phases of collision, obduction and subduction that consumed them.

One early synthesis of the tectonic evolution of the post-Eocene West Pacific was carried out by Jolivet et al. (1989), who modelled the plate motions in six stages (56, 43, 32, 20, 12 and 3 Ma), and importantly, provided finite rotation poles that define their time-dependent plate circuit. In the reconstructions of Jolivet et al. (1989), and subsequent models (Hall et al., 1995a; Lee and Lawver, 1995; Pubellier et al., 2003; Queano et al., 2007; Zahirovic et al., 2014), the Philippine Sea Plate develops in near-equatorial southern latitudes during the Eocene (Hall et al., 1995a; Hall et al., 1995b; Richter and Ali, 2015), and is isolated from the surrounding plate circuits by a network of plate boundaries (including subduction zones and transforms) for much of the time. This tectonic isolation, and lack of preserved seafloor spreading linking the Philippine Sea Plate directly to the Pacific, Eurasian or Australian plates lead to difficulties in reconstructing the absolute and relative plate motions of this region that links the Pacific with the Indian Ocean. However, the seafloor spreading history within the Philippine Sea Plate itself has been well-documented, including the opening of the

West Philippine Basin between ~ 55 and 33 Ma (see Hilde and Chao-Shing (1984), Deschamps and Lallemand (2002), and references therein) and the back-arc opening of the Shikoku and Parece Vela back-arc basins between ~ 29 and 15 Ma from Philippine Sea Plate rotation (Sdrolias et al., 2004) and Izu-Bonin-Mariana trench rollback (Kobayashi, 2004).

Although the seafloor spreading history of the Philippine Sea Plate is confined to post-Eocene times, the Philippine Arc has recorded a much longer history of subduction, with the earliest supra-subduction zone (SSZ) rocks from the Late Jurassic. The SSZ ophiolites from the Philippine Arc have ages of 156.3 ± 2.0 Ma and 150.9 ± 3.3 Ma (Lagonoy Ophiolite), and 142 ± 4 Ma (Gag Island, Halmahera) from the synthesis of Encarnación (2004). They are discussed at length in Zahirovic et al. (2014). Recent work by Deng et al. (2015) reported mid-Cretaceous, 126 ±3 Ma and 119 ± 2 Ma (U-Pb), SSZ volcanics from Cebu Island. These ages are consistent with the minimum 99.9 ± 7.0 Ma (Ar-Ar) age of the Calaguas Ophiolite (Geary et al., 1988; Geary and Kay, 1989), and the 100 ± 4 Ma arc rocks reported from Obi Island on Halmahera (Hall et al., 1995b), suggesting continuous Early Cretaceous subduction along the Philippine Arc. To reconcile the likely southern hemisphere origin of the Philippine Arc and the Late Jurassic-Early Cretaceous temporal similarity with north Gondwana rifting events, Zahirovic et al. (2014) proposed a SSZ origin in the vicinity of New Guinea, recently independently suggested by Deng et al. (2015). The multiple generations of ophiolites may suggest a tectonic scenario similar to the current multi-generation opening of back-arcs along the Izu-Bonin-Mariana system, and may explain the origin of the Daito and Oki-Daito ridges as paleo-arc features in the north West Philippine Basin.

### *3.5.2 Nature of the New Guinea margin since the Late Jurassic*

To accommodate the northern Gondwana rifting episode in the Late Jurassic, Zahirovic et al. (2014) placed the East Java-West Sulawesi continental fragments along New Guinea as the simplest end-member of transferring blocks north towards Sundaland, but acknowledged that an Argo Abyssal

Plain origin (NW Australian shelf) would also be possible due to the lack of preserved seafloor spreading histories to constrain a pre-drift fit. In this study, we implement the Argo origin end-member scenario, which is consistent with the zircon age spectra linking East Java to the NW Australian shelf (Sevastjanova et al., 2015; Smyth et al., 2007). The 158-137 Ma ages of mafic rocks, some of which are associated with pillow basalts, on West Sulawesi (Polvé et al., 1997) are consistent with the oldest oceanic crust (155 ± 3.4 Ma) in the Argo Abyssal Plain on the NW Australian Shelf (Gradstein and Ludden, 1992). By shifting these continental fragments west along northern Gondwana, the New Guinea margin can accommodate the source of the Philippine Archipelago to have formed along its margin. The benefit of such a scenario is that it accounts for the origin of (likely) Jurassic age SSZ ophiolites within the Central Ophiolite Belt in New Guinea (Monnier et al., 2000). However, the Late Jurassic-Early Cretaceous (~ 157 ± 16 Ma) and Late Cretaceous (66 ± 1.6 Ma) are unpublished ages from Permana (1998), reported in Pubellier et al. (2003), and require further corroboration. What is known is that at least part of the New Guinea margin was an active margin in Early Cretaceous times, as indicated by the Early Cretaceous volcanism and the Kondaku Tuffs (Dow, 1977; Rickwood, 1954), and likely represents the continuation of the long-lived east Gondwana active margin.

To what extent the Late Jurassic-Early Cretaceous active margin extended west into the Indonesian portion of New Guinea remains poorly constrained. In the east, the protolith of the Bena Bena metamorphics is partly Late Triassic (221 Ma) in age, and is intruded by Jurassic granite of 172 Ma in age (Davies, 2012). In the west, the Bird's Head region experienced granitoid emplacement in the Early Jurassic with one sample yielding an age of 197 ± 3 Ma (K-Ar) (Pieters et al., 1983) and the 210 ± 25 Ma Mangole volcanics on Banggai-Sula (Charlton, 2001), with a similar age of 205 ± 5 Ma reported further east in the P'nyang-1 exploration well in Papua New Guinea (Valenti, 1993). These results suggest that the trench along western New Guinea may have undergone rollback by the Late Jurassic to explain Early Cretaceous volcanics confined only to eastern New Guinea. Such a scenario is also consistent with the sedimentary history that records syn-rift sedimentation in the

1399 Early-Middle Jurassic, followed by a post-breakup unconformity and the formation of a diachronous
1400 passive margin along much of New Guinea (Pigram and Panggabean, 1984), with the exception of
1401 continued Early Cretaceous arc volcanism in the east.

1402 Although the Early-Middle Jurassic rift-drift sequence is well preserved on New Guinea, few
1403 constraints exist to identify which (if any) continental terranes rifted from this margin (Hill and Hall,
1404 2003; Pigram and Symonds, 1991). Apart from the East Java and West Sulawesi blocks (Zahirovic
1405 et al., 2014), parts of the Sepik Terrane may represent a para-allochthon that detached from the margin
1406 in the Jurassic, as invoked in this study, to open a somewhat-narrow oceanic basin and form the Late
1407 Jurassic SSZ ophiolites (Permana, 1998; Pubellier et al., 2003) exposed along the Central Ophiolite
1408 Belt in New Guinea (Fig. 3). Even though the Sepik Terrane is the largest accreted block on the New
1409 Guinea margin, the composite nature of the Sepik crust – with both continental and intra-oceanic arc
1410 fragments (Klootwijk et al., 2003) – leads to an enigmatic tectonic evolution. The New Guinea margin
1411 experienced at least two collisional phases; one in the late Eocene (Hall, 2002) to mid-Oligocene
1412 (Crowhurst et al., 1996; Pigram and Symonds, 1991), and another major collision responsible for
1413 compressional deformation in the Mobile Belt during the late Miocene (Hall, 2002; Hill and Hall,
1414 2003; Hill and Raza, 1999). However, the collisional history of the Sepik Terrane remains
1415 controversial in terms of whether the terrane first collided with one or more intra-oceanic arcs and
1416 subsequently welded to New Guinea, or whether the converse is true.

1417 Although the size of the oceanic basin that separated the Sepik Terrane from mainland New
1418 Guinea remains uncertain, the longevity of the oceanic basin can be inferred from subduction-related
1419 metamorphics that are distributed along the Central (Irian) Ophiolite Belt (Fig. 3), and eastward into
1420 the April Ultramafics and the Marum Ophiolite. The ~ 68 Ma high-temperature metabasites and
1421 ~ 44 Ma blueschists in the West Papuan Ophiolite (Weyland Overthrust) indicate that subduction of
1422 the Sepik oceanic basin was underway (Davies, 2012), which is consistent with ~ 45 to 40 Ma
1423 glaucophane (K-Ar) and 28 to 25 Ma (K-Ar) phengite ages (Baldwin et al., 2012) in the April
1424 Ultramafics. The Balantak Ophiolite on the East and Southeast Sulawesi Arm records ages of ~ 96-

32 Ma (Monnier et al., 1995), with a paleo-latitudinal constraint of 17 ± 4°S at 80 Ma (Mubroto et al., 1994) suggesting that these ophiolites formed somewhere between Sundaland and the New Guinea margin. Such a scenario is consistent with north-dipping subduction of the Sepik oceanic basin, which may have generated supra-subduction zone ophiolites that were subsequently obducted onto Sulawesi. The Maastrichtian (~ 71 to 66 Ma, stratigraphic correlation and dating using foraminifera) Emo volcanics (Worthing and Crawford, 1996) were likely emplaced in a back-arc setting from north-dipping subduction along the Sepik Terrane, with final docking likely taking place by ~ 30 Ma (Findlay, 2003; Zahirovic et al., 2014), based on the 35 to 31 Ma (Ar-Ar) amphibolite age of the Emo metamorphics (Worthing and Crawford, 1996) and the cooling histories of exhumed blocks (Crowhurst et al., 1996).

Following the docking of the Sepik composite terrane, south-dipping subduction was likely established (Figs. 19, 22) to account for the ~ 18 to 8 Ma Maramuni Arc volcanism (Hill and Hall, 2003; Page, 1976), followed by post-collisional volcanism to at least ~ 1 Ma (Holm et al., 2014; van Dongen et al., 2010). The approaching Halmahera Arc, attached to the southern portion of the Caroline Plate, likely collided with the northern New Guinea margin by ~ 14 Ma (Figs. 22-23), leading to a major compressional phase in the Mobile Belt, that has been inferred from apatite fission track geochronology (Hill and Raza, 1999; Kendrick, 2000). Although the New Guinea margin is a key component of the Australian, Pacific and Eurasian convergence zone, more work is required to resolve competing tectonic scenarios for this margin (van Ufford and Cloos, 2005). However, additional insights can be made from interpretations of mantle structure from seismic tomography, as well as testing end-member scenarios using coupled plate kinematic and numerical mantle convection modelling of the New Guinea margin.

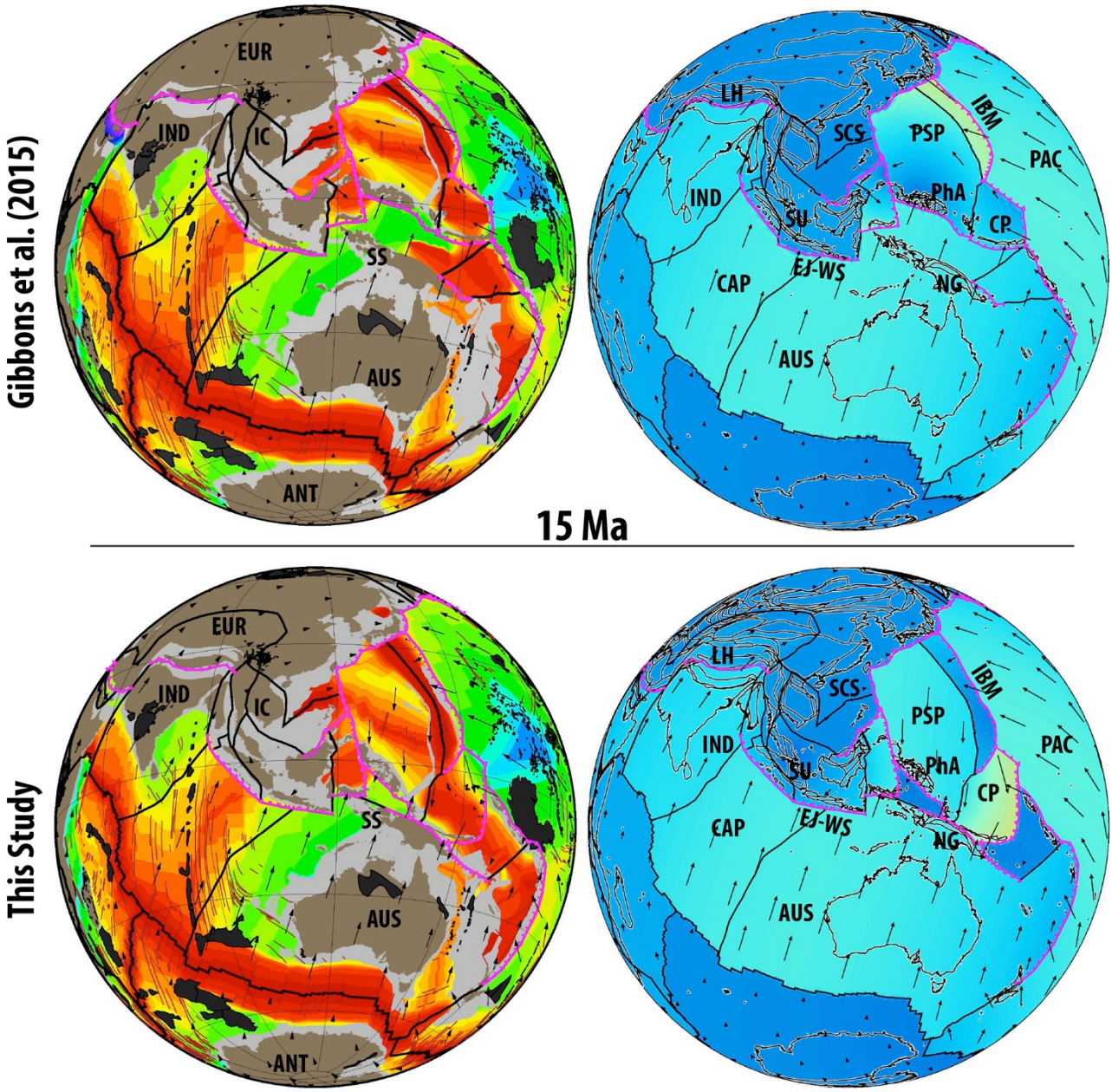


**Fig. 22.** The 15 Ma timestep records the transition to compressional tectonics on Sundaland and New Guinea. The arrival of the Dangerous Grounds-Reed Bank continental fragment shuts down Proto South China Sea subduction along Borneo, and results in ophiolite obduction in Palawan and orogenesis on Borneo. In the refined reconstructions, the Halmahera Arc collides with New Guinea at ~ 15 Ma to result in major compression in the New Guinea Mobile Belt.

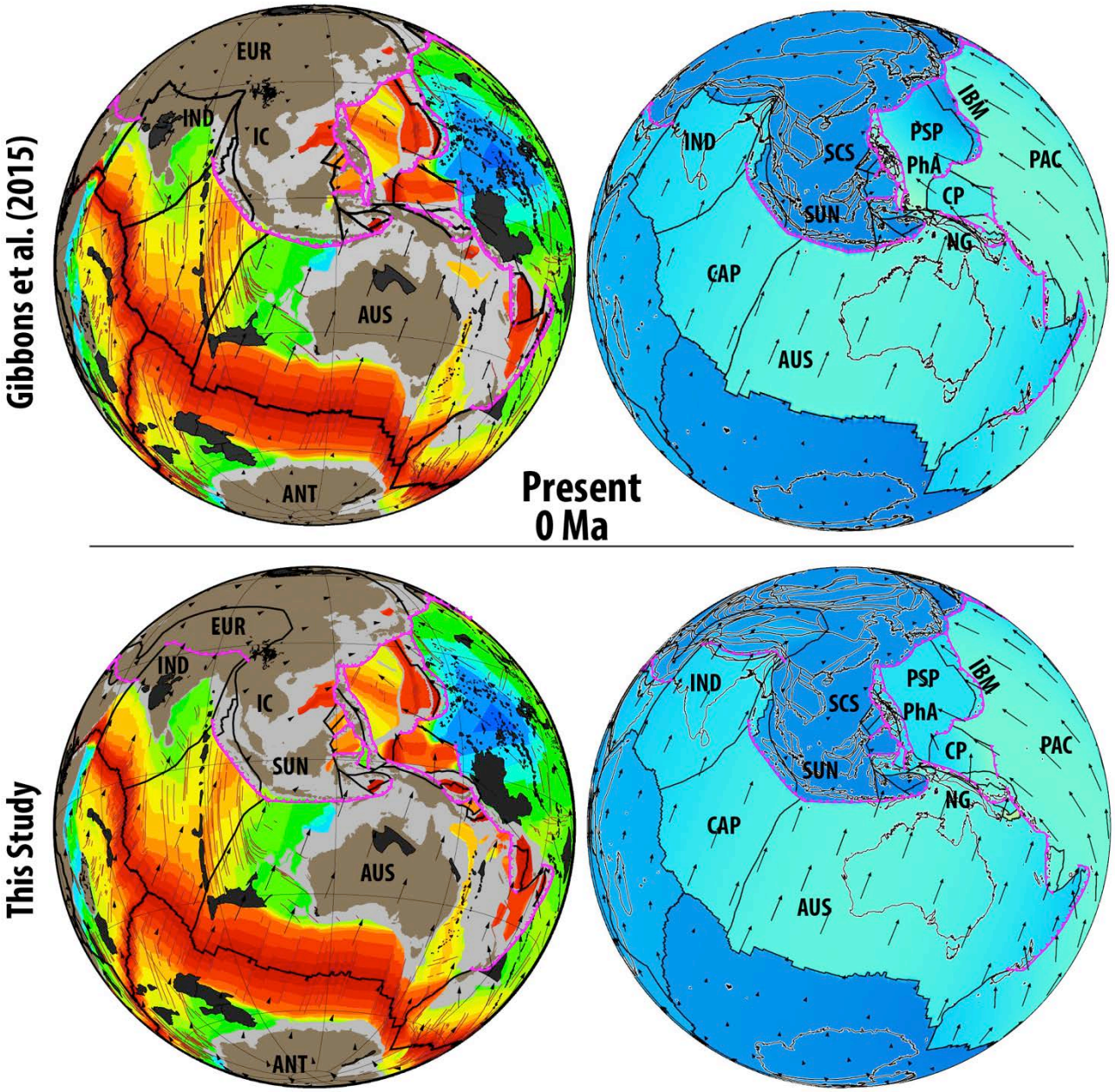


1453

1454 **Fig. 23.** The present-day tectonic configuration of Southeast Asia is the result of long-lived Indo-
1455 Australian, Eurasian and Pacific convergence accommodated by the subduction of Tethyan ocean
1456 basins and back-arcs. The northward motion of India is significantly slower than in the early Eocene,
1457 with intra-plate diffuse deformation in the Capricorn (CAP) Plate since ~ 20 Ma.

1458 **4 Insights from age-coded slabs in seismic tomography**

1459

In light of the complex tectonic evolution of Southeast Asia and the Tethyan-Pacific oceanic linkages, we interpret high velocity seismic anomalies from the P-wave model of Li et al. (2008) to obtain insights into the subduction history (Fig. 24). Although assuming constant and vertical slab sinking is a simplification, it is arguably a reasonable assumption for the late Cenozoic where large lateral slab advection would be limited, as indicated by previous estimates of less than ~ 1-2 cm/yr of mid-mantle lateral flow in the Tethyan realm (Becker and Faccenna, 2011; Zahirovic et al., 2012). We compare the plate reconstructions with age-coded depth slices of high velocity seismic anomalies, applying a sinking rate of 2 cm/yr in the lower mantle, and end-member estimates of 3 and 8 cm/yr in the upper mantle (see Methods).

The plate reconstructions in our base model (Zahirovic et al., 2014) were calibrated for the Philippine Sea Plate and Sundaland using a similar method (assuming sinking rates of 3 and 1.2 cm/yr in the upper and lower mantle, respectively). However, in the refined reconstructions, we do not modify the Sundaland oroclinal bending model, but modify the position of the Philippine Sea Plate since ~ 30 Ma to ensure collision of the Halmahera Arc with New Guinea at ~ 15 Ma, to account for the onset of widespread compression in the New Guinea Mobile Belt (Hill and Hall, 2003). Consequently, the match between Sundaland subduction zones and age-coded slabs from tomography is not surprising. Modifications to fit the Philippine Sea Plate to surface geology since ~ 30 Ma, rather than seismic tomography, present a case study to test whether both geological and seismic tomographic constraints can be accommodated simultaneously.

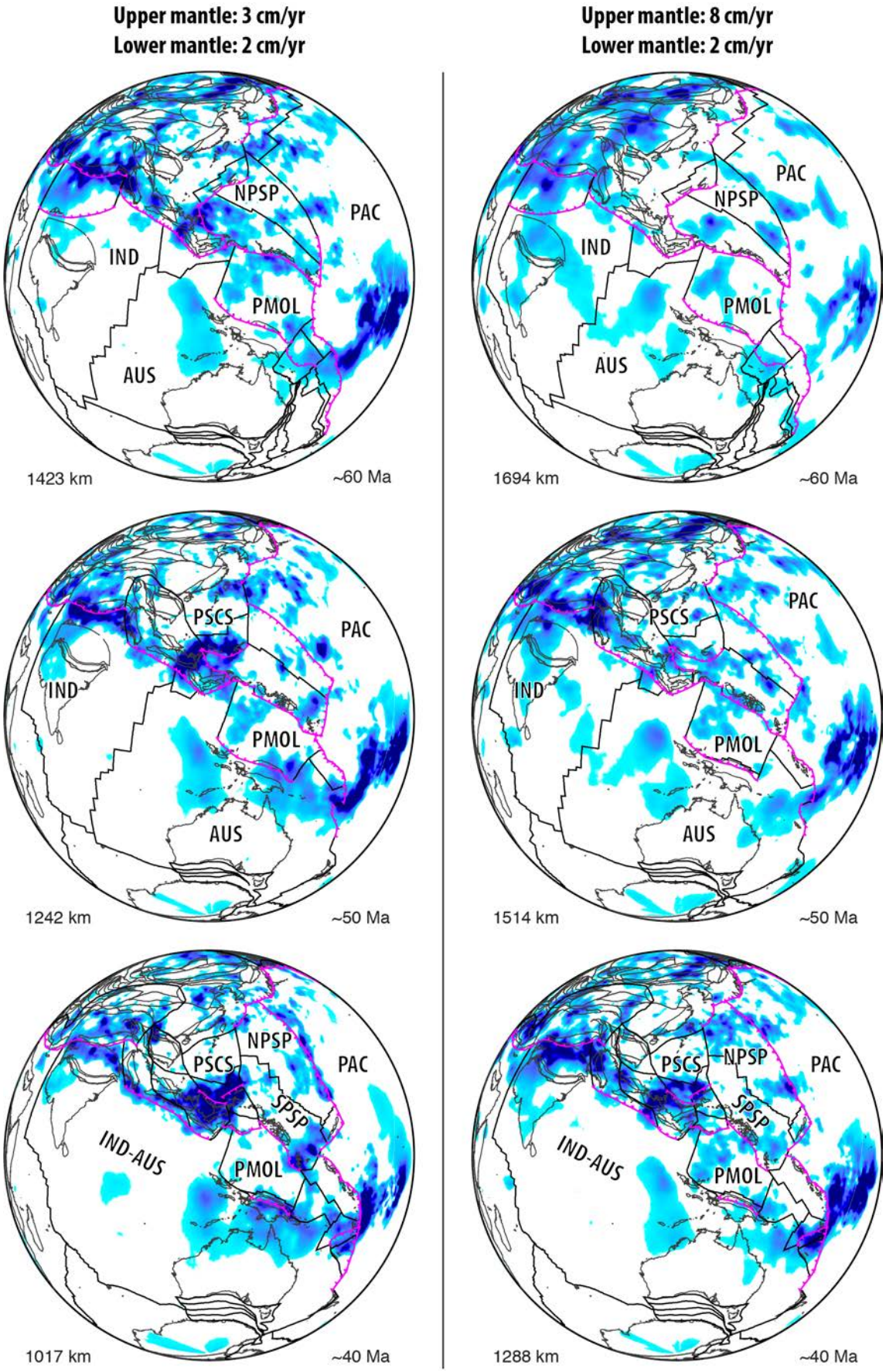


1480

1481 **Fig. 24**. Fast seismic velocity anomalies from the Li et al. (2008) P-wave seismic tomography model

1482 compared to our refined plate reconstructions. Ages are attributed to depths assuming that the average

1483 vertical sinking rate of slabs is ~ 2 cm/yr in the lower mantle, and 3 cm/yr (left) and 8 cm/yr (right)
1484 in the upper mantle. Additional polygons in Australian-Antarctic and Lord Howe-Tasman Sea regions
1485 represent areas of deforming continental crust. See Supplementary Animations 5 and 6.

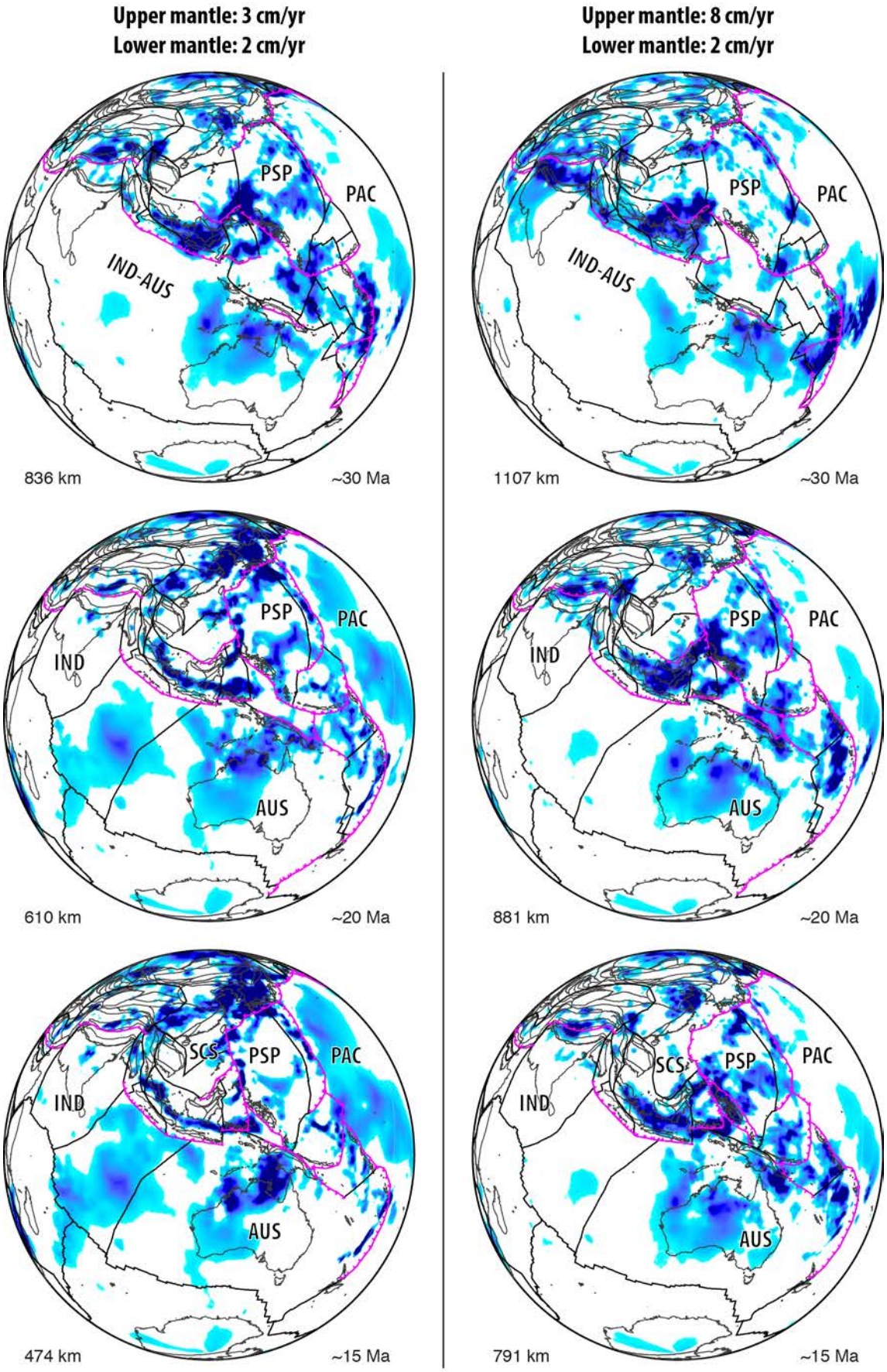
Upper mantle: 3 cm/yr
Lower mantle: 2 cm/yr
Upper mantle: 8 cm/yr
Lower mantle: 2 cm/yr
PSP
PAC
IND-AUS
836 km
~30 Ma
1107 km
~30 Ma
IND
AUS
610 km
~20 Ma
881 km
~20 Ma
SCS
474 km
~15 Ma
791 km
~15 Ma
0.0
0.1
0.2
0.3
0.4
0.5
Seismic Velocity Anomaly (%)

1486

**Fig. 24.** (continued)

At ~ 60 Ma (Fig. 24), the scenario invoking a slower sinking rate in the upper mantle better reproduces the Sunda slab, as well as the subduction of the Proto Molucca Plate (PMOL) beneath the Philippine Arc and the rollback-induced opening of the Proto South China Sea. The match with the Sunda and Philippine slabs is not surprising, as a slower sinking rate was also used to calibrate the position of these blocks in our base plate motion model (Zahirovic et al., 2014). Interestingly, the gap in the Sunda slab along Sumatra in both sinking rate end-members, coinciding with the modelled location of the Wharton Ridge, supports the slab window scenario proposed by Whittaker et al. (2007). Both slab sinking scenarios reproduce the Andean-style subduction along southern Eurasia consuming the Kohistan-Ladakh and Woyla back-arc basins, as implemented in the reconstructions based on the near-equatorial latitudes from paleomagnetic estimates. At ~ 50 Ma, the slower sinking rate matches the oroclinal bending of Sundaland and subduction of the Proto South China Sea, which is again expected due to calibration of the reconstructions with tomography. However, the match to subduction of the Sepik oceanic basin north of New Guinea is not imposed, and suggests that the large E-W slab presently beneath Australia is likely sourced from this subduction system (Schellart and Spakman, 2015).

The 40 and 30 Ma timesteps in the age-coded seismic tomography depth slices support waning subduction in the India-Eurasia segment of the active margin, and active subduction along northern Borneo (Fig. 24). The ~ 20 and 15 Ma reconstructions (Fig. 19 and 21) highlight the requirement of south-dipping subduction along New Guinea to account for the Maramuni volcanics (Fig. 24), as well as contemporaneous north-dipping subduction along the Halmahera Arc, which is terminated after ~ 15 Ma following the arc-continent collision on northern New Guinea. The collision of Dangerous Grounds-Reed Bank with northern Borneo at ~ 15 Ma also choked the north Borneo subduction zone, and likely resulted in Proto South China Sea slab breakoff. The ~ 15 Ma reconstruction using the

faster sinking rate, and corresponding to a 791 km depth slice, shows a discrete slab volume along northern Borneo that we interpret as the Proto South China Sea slab (Fig. 24).

The seismic tomographic interpretation highlights that the refinement of the New Guinea margin (namely the Maramuni subduction zone) and the adjustment to the Philippine Sea Plate (namely the position of the Halmahera Arc) since ~ 30 Ma can accommodate both the geological and the tomographic constraints. Neither sinking rate scenarios produce consistent matches throughout the plate reconstruction timeframe, likely due to the complex time-varying slab sinking rates and regional interactions of slabs in a spherical mantle shell. However, the assumption of vertical sinking of slabs is likely to be an acceptable estimate of trench locations in the Cenozoic for slabs that are still attached to the subducting plate, or slabs that have experienced little stagnation or folding in the mantle transition zone. The numerical computations described in the following section provide a more consistent approach to tracking slabs in the mantle resulting from the complex subduction history in the Tethys, east and Southeast Asia, and New Guinea.

# 5 Numerical modelling results

## 5.1 Large-scale post-Jurassic mantle evolution of the Tethyan tectonic domain

We present the first synthesis of post-Jurassic Tethyan plate reconstructions and geodynamics in a 4D (space and time) global context. We ran five cases of coupled plate kinematic and geodynamic numerical experiments, mainly to test end-member plate reconstructions, and present 3D snapshots of two experiments that compare the Zahirovic et al. (2014) model with refinements for the Neo-Tethys, Philippine Sea Plate and New Guinea presented in this study (Fig. 25). Although the mantle convection models are initiated at 230 Ma during the time of Pangea stability, we present only the post ~ 160 Ma timeframe applicable to the refined plate reconstructions. At ~ 160 Ma, the dominant feature of the mantle is the circum-Pangea subduction girdle, as well as the southern Eurasian active

margin consuming Meso-Tethyan oceanic lithosphere (Fig. 25A). The tectonic scenario presented invokes the northward continuation of East Gondwana subduction along New Guinea and connecting to the East Asian subduction of the Izanagi Plate. By ~ 140 Ma the rollback of the Lhasa trench opens the Kohistan-Ladakh back-arc basin, with a slower opening and southward position of ~ 10°N in our base model by 100 Ma (Zahirovic et al., 2014), compared with the equatorial position implemented in this study following Burg (2011) and Gibbons et al. (2015).

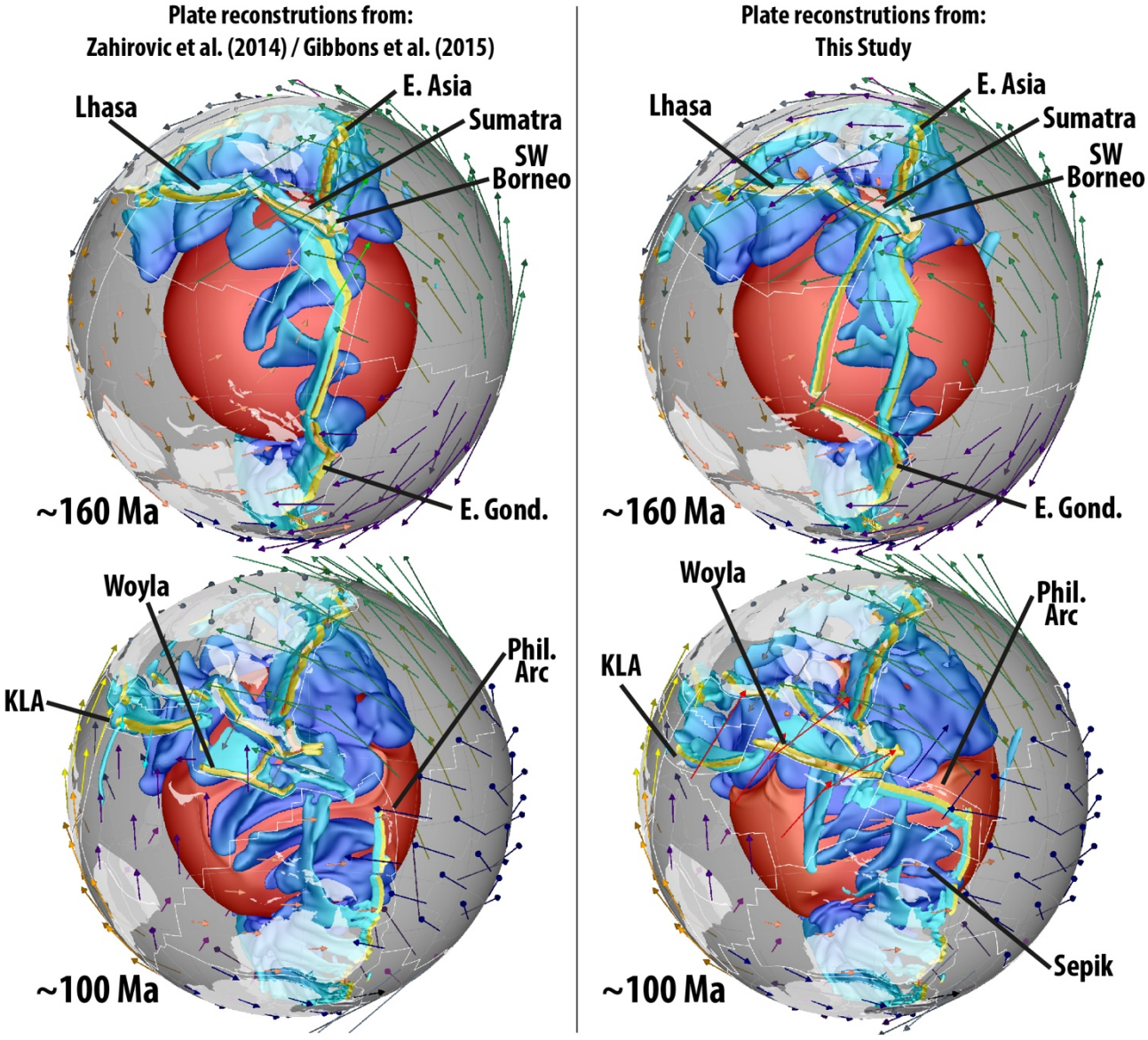


**Fig. 25a.** Snapshots of mantle structure including sinking slab volumes (blue) and thermochemical upwellings (red) from the core-mantle boundary are visualised in GPlates using the mantle temperature predictions from the CitcomS numerical experiments of mantle flow depicting Case 4 (left) and 5 (right). The snapshots compare the large-scale mantle evolution in the latest Jurassic and

Early Cretaceous from Tethyan subduction along Lhasa and the Kohistan-Ladakh Arc (KLA), as well as recycling of proto-Pacific lithosphere along the East Asian, East Gondwana and Philippine Arc subduction zones. Plate boundaries (white), velocities (coloured arrows) and reconstructed present-day coastlines (translucent white) are plotted. Subduction zones are yellow regions, and slab colouring is a function of depth from light blue (shallow slabs) to darker blue (deep slabs). These snapshots highlight the global nature of our numerical experiments, with complex interactions of slabs as they sink in the mantle shell. The experiments allow us to track the sinking trajectory (vertical and lateral) of the slabs to identify their source from the present-day mantle prediction, which are compared to the mantle structure imaged using P- and S-wave seismic tomographic techniques. Central co-ordinate is 10°S, 115°E.

As our modelling domain is spherical, and because the flow is constrained to follow surface velocities that include net rotation of the lithosphere, lateral mantle flow may influence the trajectory of sinking slabs. As subducting slabs sink in the mantle, the core-mantle boundary becomes draped with older slabs that sweep the hotter material into the large-scale Pacific and African upwellings (Bower et al., 2013; McNamara and Zhong, 2005) (Fig. 25). In addition, mantle flow advects slabs laterally, with notable southward (and somewhat westward) translation of the Paleo-Tethyan slabs, and eastward advection of the east Asian slabs (Fig. 25). India's collision with the Kohistan-Ladakh Arc ceases intra-oceanic subduction by ~ 50 Ma in our model, resulting in the Andean-style subduction of the Kohistan-Ladakh back-arc basin along southern Lhasa (Fig. 25B). The ~ 47 Ma continent-continent collision temporarily shuts down subduction, causing a slab break-off event, followed by ongoing subduction of the Greater Indian mantle lithosphere (Capitanio et al., 2010). Australia's northward motion results in the northern margin, including New Guinea, overriding the Southeast Asian slab graveyard from ~ 30 Ma following the docking of Sepik, and the initiation of south-dipping Maramuni subduction from ~ 20 Ma.

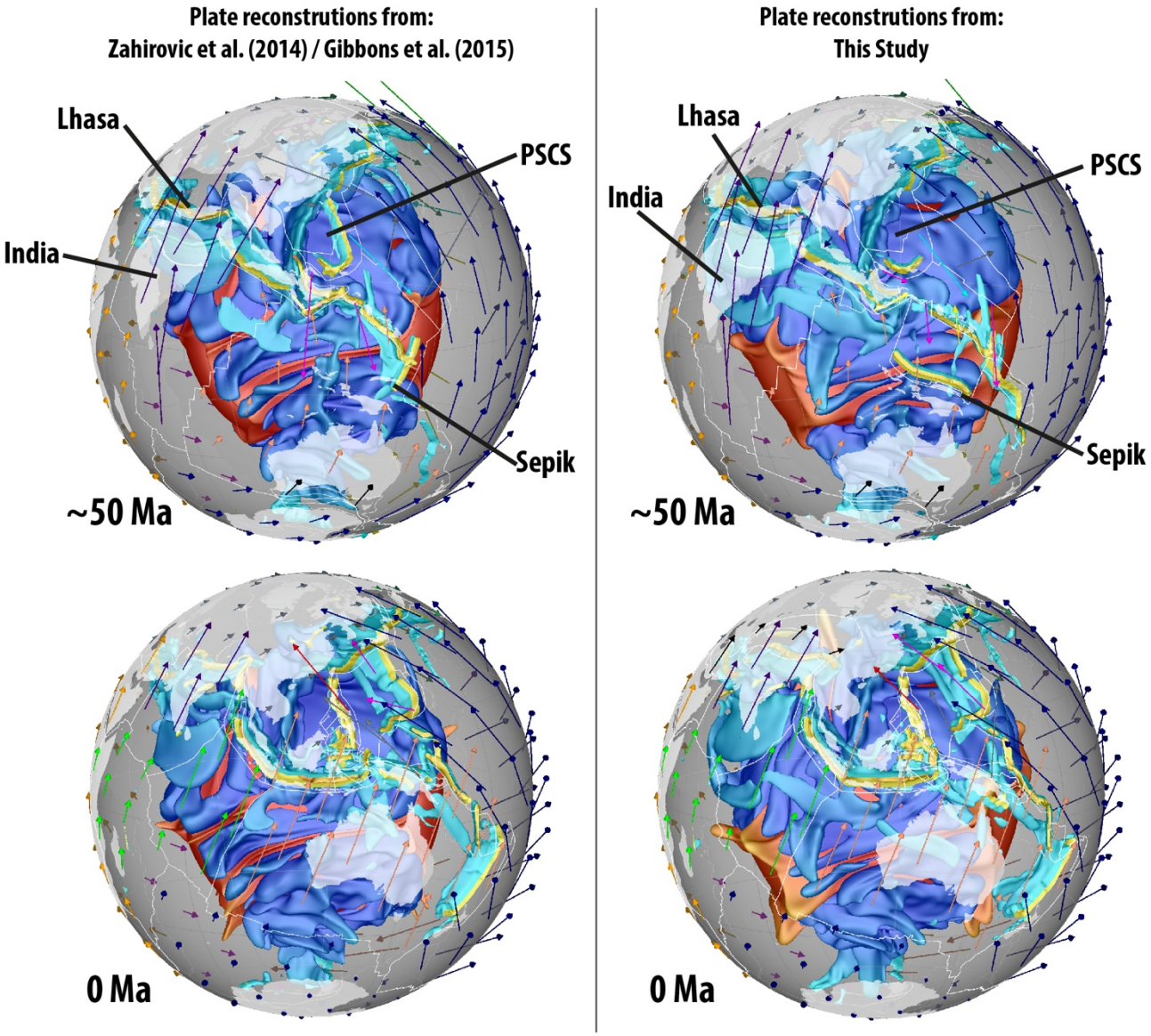


**Fig. 25b.** Coupled plate reconstructions and mantle flow models in the Eocene and present-day, highlighting the draping of subducted slabs along the core-mantle boundary and the self-organization of the African and Pacific large-scale upwellings as a result of post-Pangea subduction. These models are interrogated regionally using vertical profiles in Figs. 26-29. Centre co-ordinate is 10°S, 115°E. See Supplementary Animation 7 that is consistent with right panels.

The large-scale evolution of slab sinking and lateral advection, as well as the evolution of the large-scale upwellings, can be depicted in 3D hemispherical views of the mantle, while regional cross-sections of the numerical experiments provide a more detailed approach to interrogating the

1583 spatio-temporal geodynamic evolution of key subduction zones from post-Jurassic plate
1584 reconstructions.
1585

1586 **5.2 Regional interpretations of mantle evolution**

1587

1588 To capture the detailed evolution of subduction, vertical cross-sections of the mantle are
1589 presented in a plate frame of reference (i.e., fixed to the overriding plate, Figs. 26-29). Such time-
1590 dependent sections help understand the sinking trajectory of subducted slabs, as well as interpreting
1591 sinking rates and lateral mantle flow resulting from the post-Jurassic plate reconstructions. For the
1592 geological reasoning underpinning the reconstructions, please refer to Section 3 and Table 3.

1593 ***5.2.1 India-Eurasia convergence***

1594

1595 The India-Eurasia segment is best represented by a largely north-south profile at present-day
1596 that is reconstructed with Lhasa (Fig. 26). At ~ 160 Ma, the Paleo-Tethyan slab has detached and is
1597 sinking through mid-mantle depths at ~ 1.5 cm/yr (Fig. 26A, H), while the Meso-Tethys is being
1598 actively consumed northward beneath Lhasa in both plate reconstruction scenarios. Both tectonic
1599 scenarios include southward slab rollback and the establishment of a Kohistan-Ladakh (Tethyan)
1600 back-arc basin, reaching to ~ 10°N in the base model (Zahirovic et al., 2014) and the equator at
1601 ~ 100 Ma in this study (Fig. 26C, J). Using the base reconstructions, the Meso-Tethyan slab only
1602 penetrates the mantle transition zone at ~ 100 Ma and begins sinking into the lower mantle by ~ 90 Ma
1603 (Fig. 26, Supplementary Animation 7). In the refined reconstructions the slab enters the mantle
1604 transition zone by ~ 120 Ma, and enters the lower mantle by ~ 110 Ma. This reflects greater
1605 convergence rates due to the combined effect of greater slab rollback in the refined reconstructions,
1606 as well as continued seafloor spreading north of India during this timeframe. In the base
1607 reconstructions, the seafloor spreading north of India is abandoned by ~ 120 Ma, leading to lower
1608 convergence rates across the Kohistan-Ladakh Tethyan trench (Fig. 10). This results in the subduction

1609 of larger volumes of older, and therefore thicker, oceanic lithosphere, while in the refined
1610 reconstructions subducted volumes along the Kohistan-Ladakh Arc system in the Early to mid-
1611 Cretaceous are smaller because the oceanic lithosphere associated with the Neo-Tethyan seafloor
1612 spreading north of India by ~ 100 Ma is younger and thinner (Fig. 26J). Once the Tethyan slab has
1613 entered the lower mantle, the sinking rate in the refined reconstruction is only ~ 1.4 cm/yr (between
1614 100 and 89 Ma), while it is ~ 2.5 cm/yr in the base reconstructions (between 89 and 79 Ma) likely
1615 due to the larger subducted volumes.

1616 The intersection of the Neo-Tethyan mid-oceanic ridge with the Kohistan-Ladakh subduction
1617 zone in the mid-Cretaceous would likely lead to slab breakoff and the formation of a slab window.
1618 However, our model does not capture the complexity of a subduction hiatus that would be associated
1619 with a slab window along Kohistan-Ladakh in the mid-Cretaceous. Perhaps due to the arrival of
1620 buoyant oceanic crust at the intra-oceanic subduction system, north-dipping subduction becomes
1621 established along Lhasa and begins to consume the Kohistan-Ladakh back-arc basin, eventually
1622 resulting in two Late Cretaceous north-dipping subduction zones in the Neo-Tethys (see Section 3.2).
1623 The mid-ocean ridge from the Kohistan-Ladakh back-arc is subducted in the Late Cretaceous in both
1624 reconstruction scenarios, with no interruption in subduction assumed in the base reconstructions. In
1625 the alternative reconstructions we impose a subduction hiatus along Lhasa from 80 to 65 Ma, which
1626 leads to slab breakoff. This slab window may be linked to adakitic volcanism at ~ 80 Ma (Wen et al.,
1627 2008a), followed by an ~ 75-60 Ma magmatic gap, in the Gangdese Batholith (Chung et al., 2005; Ji
1628 et al., 2009; Wen et al., 2008b).

1629 In both reconstruction scenarios, Greater India collides with Kohistan-Ladakh by ~ 50 Ma,
1630 inducing Neo-Tethyan slab break-off at ~ 5-10°N. Since the Kohistan-Ladakh Arc is at equatorial
1631 latitudes in the refined reconstructions in the mid-Cretaceous, one may expect the collision with India
1632 to occur by ~ 60 Ma. As the magmatic chemistry change is much later, at 52 Ma (Bouilhol et al.,
1633 2013), the model includes some advance of the intra-oceanic subduction system between ~ 60 and 52
1634 Ma. In the base reconstructions, the Kohistan-Ladakh Arc is closer to Eurasia at pre-collision times,

meaning that relatively little trench advance is required. However, in both instances, the Tethyan slab is anchored in the lower mantle, leading to India overriding the sinking slabs. Andean-style subduction of the Kohistan-Ladakh back-arc along southern Lhasa is temporarily shut off by the ~ 47-40 Ma continent-continent collision, after which subduction of Greater India (continental) mantle lithosphere continues to present-day in the refined reconstructions. The Meso- and Neo-Tethyan slabs are predicted at present to be approximately at mid-mantle depths (~ 1000 to 2000 km), with a latitudinal range of ~ 0 to 35°N, using the base model plate reconstructions (Fig. 30, IND-EUR). More generally, the base plate reconstruction in modelled Case 4 reproduces a number of discrete slabs at mid-mantle depths, with a large latitudinal range, which is consistent with the interpretations of the mantle structure by van der Voo et al. (1999b) (Fig. 5).

Although the numerical model that uses the refined reconstructions presented in this study has the same radial viscosity profile, the Meso- and Neo-Tethyan slabs are predicted to be shallower at ~ 800 to 1500 km depths, as opposed to ~ 1000 to 2000 km depths predicted using the base reconstructions (Fig. 26G, N). This is likely due to the subduction of smaller volumes of younger Tethyan oceanic lithosphere north of India in the Cretaceous, resulting in less negative buoyancy. In addition, the required trench advance also results in folding of the Tethyan slab at the mantle transition zone, leading to generally shallower penetration into the lower mantle. In the post-collision timeframe, the Tethyan slab sinks at a rate of ~ 0.65 cm/yr (from 38 to 0 Ma) using the base reconstructions, and ~ 0.25 cm/yr (from 39 to 0 Ma) using the refined reconstructions where the slab is almost stagnant at ~ 1000 km depth (Supplementary Animation 7). The time-varying sinking rates in the lower mantle highlight the role active subduction has in adding negatively buoyant slab volumes into the mantle, and the role of thermal diffusion of slabs in reducing negative buoyancy of subducted lithosphere. A slightly deeper depth range (~ 1000 to 2000 km) provides a better match to the equivalent P- and S-wave tomography slice (Fig. 30, IND-EUR), as is obtained with the base plate reconstructions (Gibbons et al., 2015; Zahirovic et al., 2014), with the potential that slabs may extend further south of the equator based on the S-wave model.

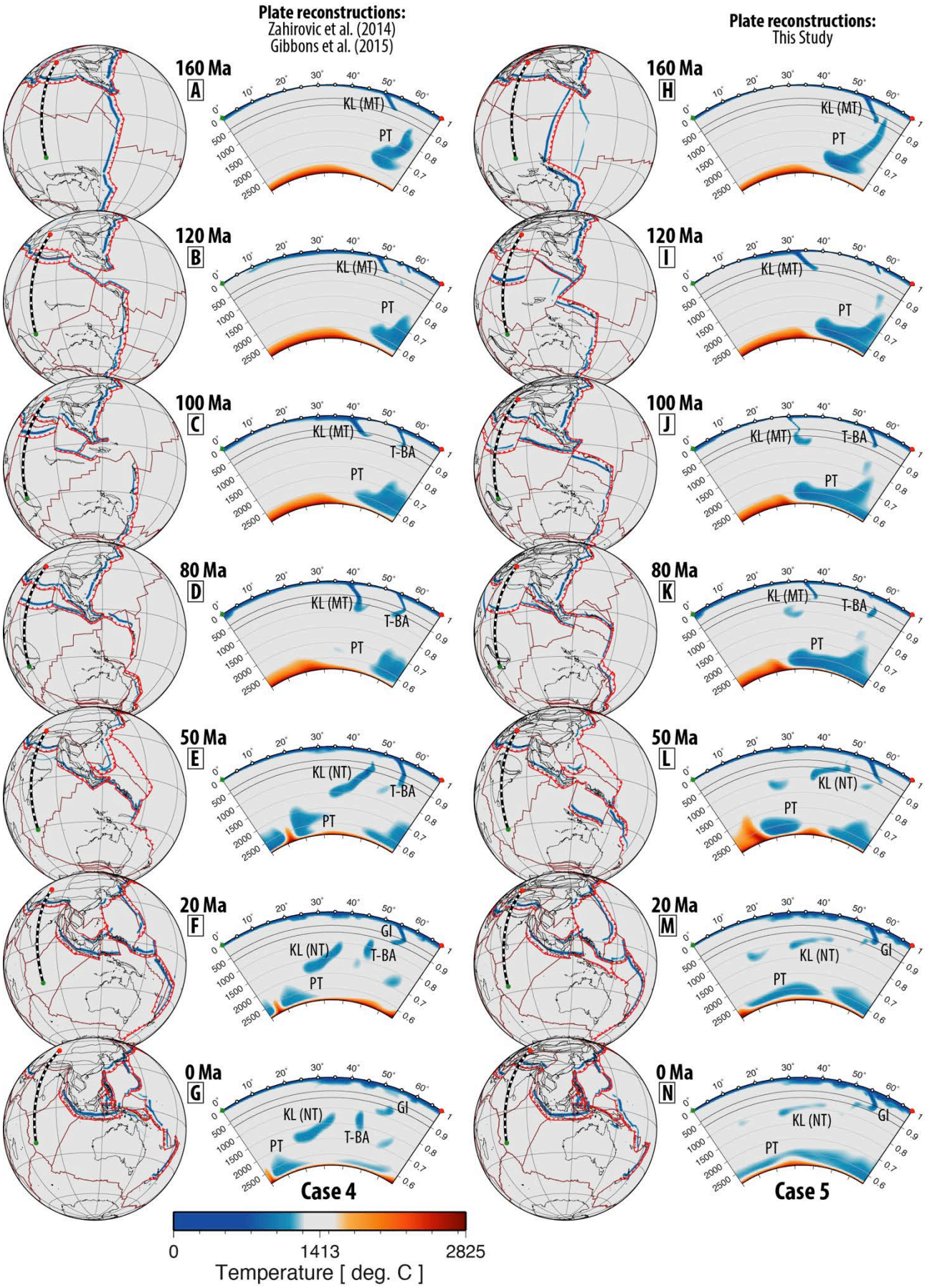
Plate reconstructions:
Zahirovic et al. (2014)
Gibbons et al. (2015)
Plate reconstructions:
This Study
160 Ma
A
120 Ma
B
100 Ma
C
80 Ma
D
50 Ma
E
20 Ma
F
0 Ma
G
160 Ma
H
120 Ma
I
100 Ma
J
80 Ma
K
50 Ma
L
20 Ma
M
0 Ma
N
KL (MT)
KL (NT)
PT
T-BA
GI
Case 4
Case 5
0
1413
2825
Temperature [ deg. C ]

1661

**Fig. 26.** Time-dependent evolution of the India-Eurasia convergence zone, with a representative vertical slice reconstructed with Lhasa to capture the evolution of the Kohistan-Ladakh (KL) and Tethyan (T-BA) intra-oceanic subduction zones modelled in Zahirovic et al. (2014) and Gibbons et al. (2015) (left), and compared to the subduction histories implied in the revised plate reconstructions presented in this study (right). The cross-sections depict the temperature field from the numerical mantle flow models, and the globes show the position of the vertical slices through time, the plate reconstruction and the predicted mantle temperature field at ~ 400 km depth. The background mantle temperature is ~ 1413°C, and the small tick marks on the temperature scale represent temperature intervals of 250°C. Great circle angular distance along the vertical profile is shown on the x-axis. The left y-axis represents depth in kilometres, and on the right represents non-dimensional Earth radius. The plate reconstructions are plotted in an orthographic projection with centre co-ordinate of 15°S, 115°E. GI – Greater India (continental) mantle lithosphere, MT – Meso-Tethys slab, NT – Neo-Tethys slab, PT – Paleo-Tethys slab. See Supplementary Animation 8.

### *5.2.2 Woyla and Sumatra active margin evolution*

The Sumatra segment of the Sunda margin accommodates northward subduction of the Meso-Tethys in the Late Jurassic, with rollback of the slab opening the Woyla back-arc to near-equatorial latitudes (Fig. 27), similar to the development of the Kohistan-Ladakh Arc further to the west. In the base reconstructions, the rollback imposed is faster and the maximum southward extent of subduction is ~ 0-10°S (Fig. 11). This leads to a smaller volume of subducted slabs folded in the mantle transition zone. Although the base reconstruction maintains convergence across the Woyla subduction zone, there is significant trench advance between ~ 100 and 75 Ma, leading to a similar smearing effect of slabs in the transition zone. Although trench advance occurs at present-day along the Izu-Bonin-Mariana Trench (Becker et al., 2015; Carlson and Mortera-Gutiérrez, 1990; Mathews, 2014), the

1687 modelled values in our base reconstructions are likely excessive, with a more geodynamically
1688 reasonable evolution of trench migration in the refined reconstructions.
1689
1690 Subduction continues along Sumatra to consume the Woyla back-arc basin, and is interrupted
1691 for ~ 10 Myr between accretion of the Woyla Arc onto the Sumatran margin between ~ 75 and 65
1692 Ma in the base reconstructions. Due to the convergence required between the Tethyan-Indian Ocean
1693 and Eurasia, we impose a shorter ~ 5 Myr hiatus in subduction between 75 and 70 Ma to induce slab
1694 breakoff that may have occurred due to Woyla Terrane accretion. Our assumption of slab breakoff is
1695 simplistic and based on the magmatic gap, and more realistic slab breakoff timings of 5-10 Myr after
1696 collision (Li et al., 2013; van Hunen and Allen, 2011) will need to be considered in future refinements
1697 of the model in this region.
1698 In both tectonic reconstructions, subduction at the Sunda Trench is initiated at ~ 70-65 Ma,
1699 and persists to present-day. The slab is predicted to have penetrated the lower mantle by ~ 50 Ma,
1700 after which the collision of India with Eurasia, and subsequent rotation of Indochina and much of
1701 Sundaland from ~ 30 Ma leads to a kink in the slab in the mantle transition zone (410 to 660 km,
1702 Fig. 27G, N). Although the kink results from the constant slab dip imposed in the slab assimilation,
1703 this slab kink is imaged by the P- and S-wave seismic tomography models analysed here, and also
1704 recently discussed in Hall and Spakman (2015). The numerical experiments of mantle flow also
1705 reproduce the latitudinal range of the subducted slab (Fig. 30, SUM), as well as a gap in the slab at
1706 depths greater than ~ 1500 km, consistent with earlier interpretations of the Sunda slab (Widiyantoro
1707 and van der Hilst, 1996). The mantle convection models predict the Woyla/Meso-Tethys slab at
1708 ~ 1500 to 2000 km depths at ~ 10°S along the Sumatran vertical slice (Fig. 30, SUM), and ~ 20°S
1709 along the Java-Borneo Sundaland slice (Fig. 30, SUN), which is likely to be equivalent to fast seismic
1710 velocities in P- and S-wave tomography models at ~ 1500-2000 and ~ 1200-1600 km depth along the
1711 Sumatran and Java-Borneo vertical slices, respectively.

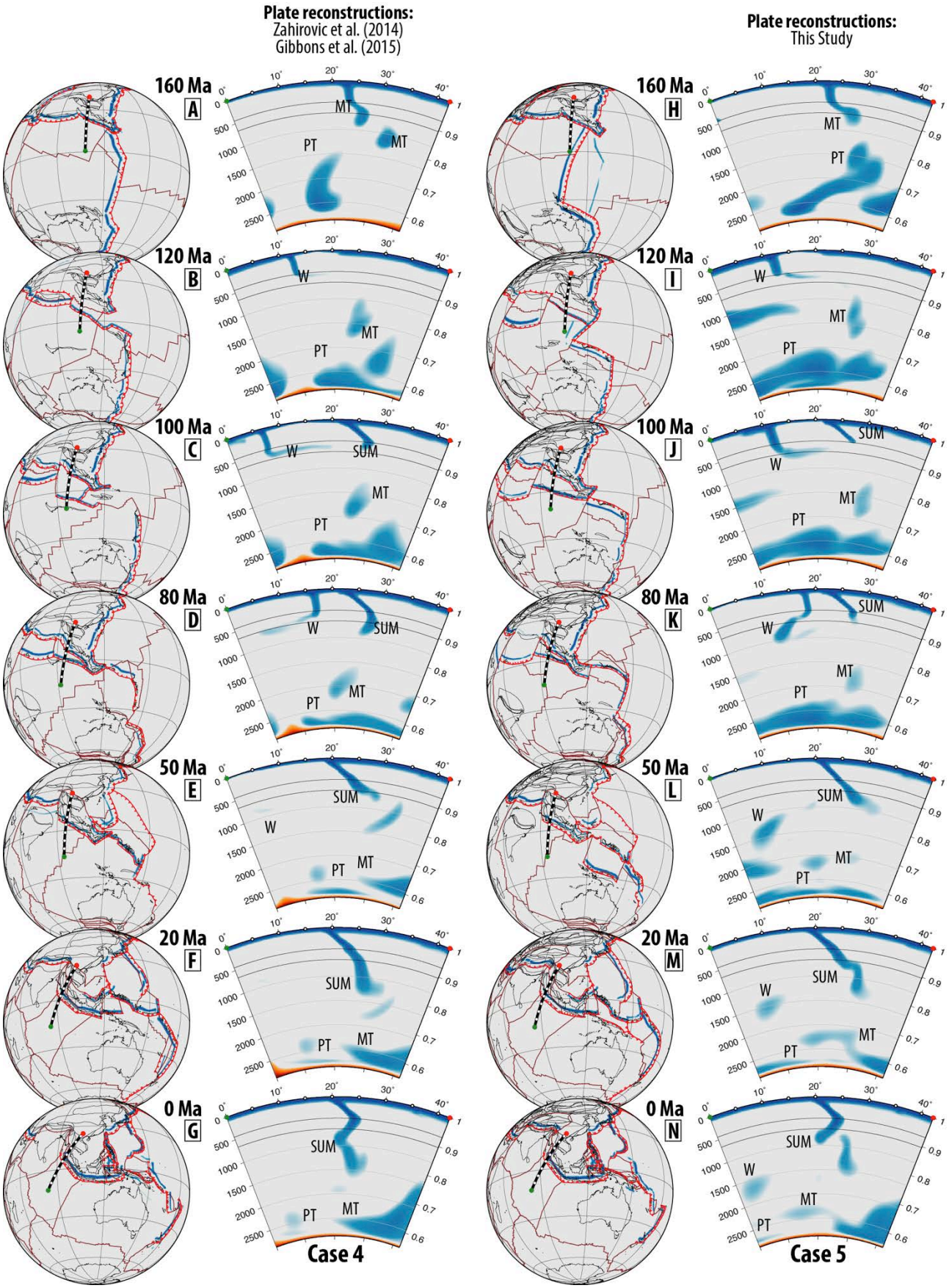


**Fig. 27.** Reconstructed vertical profiles across northwest Sumatra highlighting the evolution of the Woyla intra-oceanic and Sunda subduction zones through time, with both numerical experiments

predicting a significant kink in the Sumatran portion of the Sunda slab (SUM) when the slab dip is held constant during the clockwise rotation and extrusion of Indochina. MT – Meso-Tethys slab, NT – Neo-Tethys slab, PT – Paleo-Tethys slab, W – Woyla slab. See Supplementary Animation 9.

### *5.2.3 Java and Borneo subduction history*

Similar to the Sumatra margin, the Java segment of the Sunda Trench accommodates subduction of the Meso-Tethys and the Woyla back-arc basin during the Cretaceous (Fig. 28). However, as this segment represents the Sundaland continental promontory, south-dipping subduction of the Izanagi Plate is contemporaneous to the Tethyan subduction history. As a result, the mid- and lower mantle slabs are likely to be a mixture of Pacific- and Tethyan-derived slabs. The accretion of the Woyla Arc temporarily shuts off subduction in this segment in the Late Cretaceous at ~ 70 Ma in the base reconstructions (Fig. 28B, H), followed by the accretion of the Semitau continental fragment and Proto South China Sea Arc onto northern Borneo at ~ 45 Ma in both reconstruction scenarios (Fig. 28C, I). The late Eocene is dominated by renewed north-dipping Sunda subduction and south-dipping subduction of the Proto South China Sea. Although the Sunda subduction continues to the present-day, the Proto South China Sea subduction is interrupted at ~ 15 Ma with the docking of the Dangerous Grounds-Reed Bank continental fragment along northern Borneo, which leads to the abandonment of South China Sea seafloor spreading. The refined reconstructions imply a longer-lived Meso-Tethyan Plate that is completely consumed by ~ 45 Ma, leading to much younger oceanic crust and thinner oceanic lithosphere subducted at the Sunda Trench than in the base reconstructions. This leads to the subduction of smaller slab volumes between ~ 60 and 30 Ma for the refined reconstructions that predict a smaller and shallower slab that penetrates to ~ 1200 km depth at present. In contrast, the base reconstructions lead to a larger Sunda slab at depths of ~ 1500 km (Fig. 30, SUN), which is consistent with the interpretations of P- and S-wave seismic tomography models. The kink in the slab observed in the Sumatra segment (Fig. 30, SUM) is much

1741 less pronounced in the Java region (Fig. 30, SUN), especially when compared to the results using our
1742 base plate reconstruction. A gap in the slab is also reproduced for depths greater than ~ 1500 km,
1743 with older Tethyan and Izanagi slab fragments reproduced near the core-mantle boundary when
1744 comparing to the S-wave seismic tomography (Fig. 30, SUN). The Proto South China Sea slab is
1745 predicted at ~ 600-1000 km depths, while P- and S-wave tomographic images indicate a slab
1746 stagnating at the base of the 410-660 km mantle transition zone.
1747

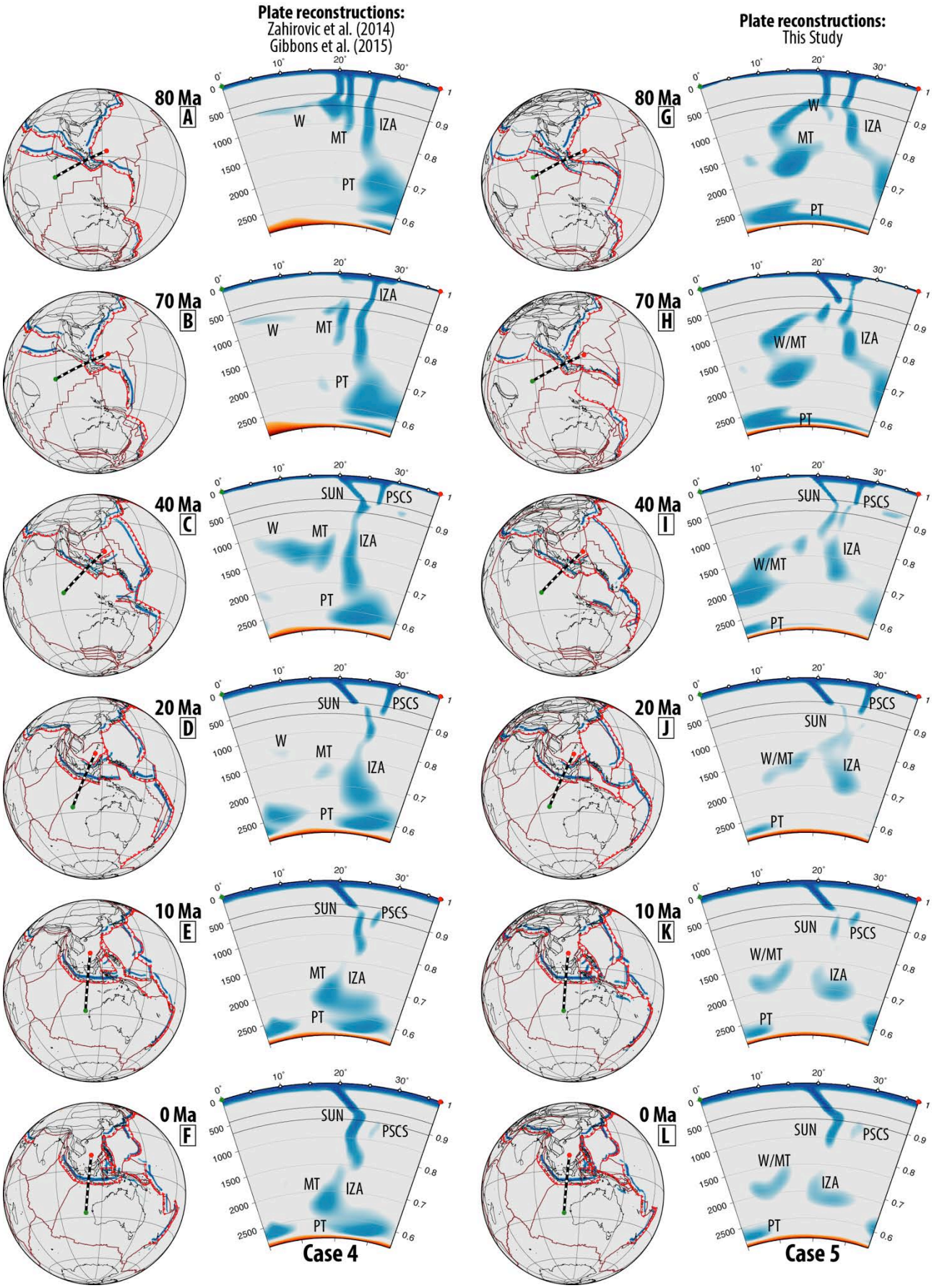


1748

1749 **Fig. 28.** Reconstructed vertical slice through eastern Sundaland, capturing the subduction of the

1750 Meso- and Neo-Tethyan, as well Indian Ocean, basins. The Sunda slab is predicted to reach a

maximum depth of ~ 1500 km along southern Sundaland in the base reconstructions, and ~ 1200 km in the refined reconstructions, while a small Proto South China Sea slab is predicted just beneath the 660 km upper-lower mantle transition. See Supplementary Animation 10.

### *5.2.4 New Guinea margin evolution*

Further east along the New Guinea Tethyan segment, the Early Cretaceous Sepik oceanic basin is consumed at a north-dipping subduction zone from ~ 40 Ma (Fig. 29B) in the base model reconstructions, while in our refined model subduction starts earlier at ~ 71 Ma (Fig. 29G) to account for the ~ 71 to 66 Ma Emo volcanics (Worthing and Crawford, 1996) that likely formed in the back-arc of this subduction system. North-dipping subduction along the Sepik Terrane is interrupted at ~ 30 Ma in both plate reconstruction scenarios, based on the timing of docking of the composite terrane at the New Guinea margin. We impose slab breakoff during the collision, leading to a slab that is entrained in the upper part of the lower mantle (660-1000 km depths) for both reconstruction scenarios. In the base model, north-dipping subduction is then accommodated along the Halmahera Arc, which forms the southern boundary of the Caroline Plate, and is accreted to the New Guinea margin diachronously from west to east by ~ 5 Ma. In the refined reconstructions, a south-dipping subduction zone is implemented (Fig. 29J) to account for the ~ 18 to 8 Ma Maramuni Arc volcanics (Hill and Hall, 2003; Page, 1976), as well as simultaneous north-dipping subduction along the Halmahera Arc. Both subduction zones are abandoned progressively from ~ 15 Ma, resulting from the collision of the Halmahera-Caroline Arc with the New Guinea margin.

The numerical experiments of mantle flow assimilating the base plate motion model predict two slabs at depths between ~ 500 and 1000 km (Fig. 30, PNG), with the southernmost slab at ~ 20°S belonging to the Sepik oceanic basin, and the northern slab at 0 to 5°S resulting from the subduction of the Solomon Sea along the Halmahera Arc. With the addition of the Maramuni subduction zone in the refined plate reconstructions (~ 20 to 10 Ma, Fig. 29), an additional slab is predicted at slightly

deeper depths of ~ 900 to 1500 km at ~ 15°S. The Sepik oceanic basin slab is predicted to be further south in the refined plate reconstruction scenario, at depths of ~ 700 to 1000 km and latitude of ~ 30°S (Fig. 30, PNG). This difference in latitude is largely due to the earlier onset of Sepik oceanic gateway subduction at ~ 71 Ma in the refined reconstructions, leading to the slab entering the lower mantle at more southerly latitudes, as opposed to the younger age of ~ 40 Ma subduction onset using the base reconstructions (Fig. 29B). The refined plate reconstructions result in a much better fit with the mantle structure than the base model, with the ~ 30°S position of the Sepik oceanic gateway slab corresponding to the fast seismic anomaly interpreted beneath Lake Eyre in eastern Australia, recently interpreted in Schellart and Spakman (2015). However, a slab at ~ 1300 to 1800 km depths at present-day (PNG, Fig. 30), and latitudes between ~ 10°S and the equator, is not accounted for in either model of mantle flow – suggesting that the (pre-) Cretaceous plate reconstruction needs additional refinement.

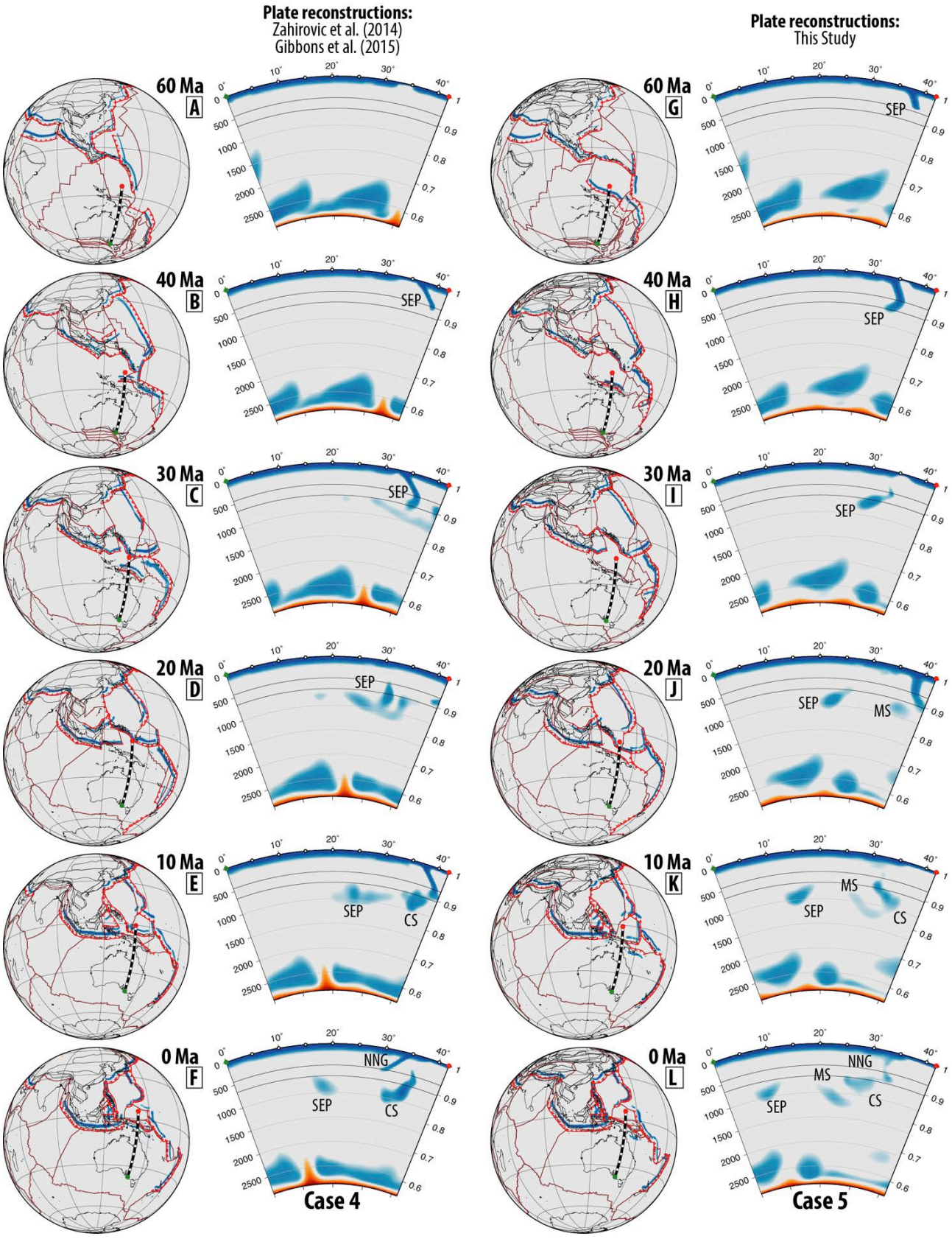


**Fig. 29.** Reconstructed representative profile through Australia and New Guinea, highlighting that the revised plate reconstructions account for additional slab volumes above mid-mantle depths. The southernmost slab is related to the subduction of the Sepik oceanic gateway (SEP) between ~ 71 and

30 Ma, while Maramuni subduction (MS) has taken place since ~ 20 Ma, coeval with north-dipping subduction along the Halmahera Arc to produce the Caroline/Proto Molucca slab (CS). See Supplementary Animation 11.

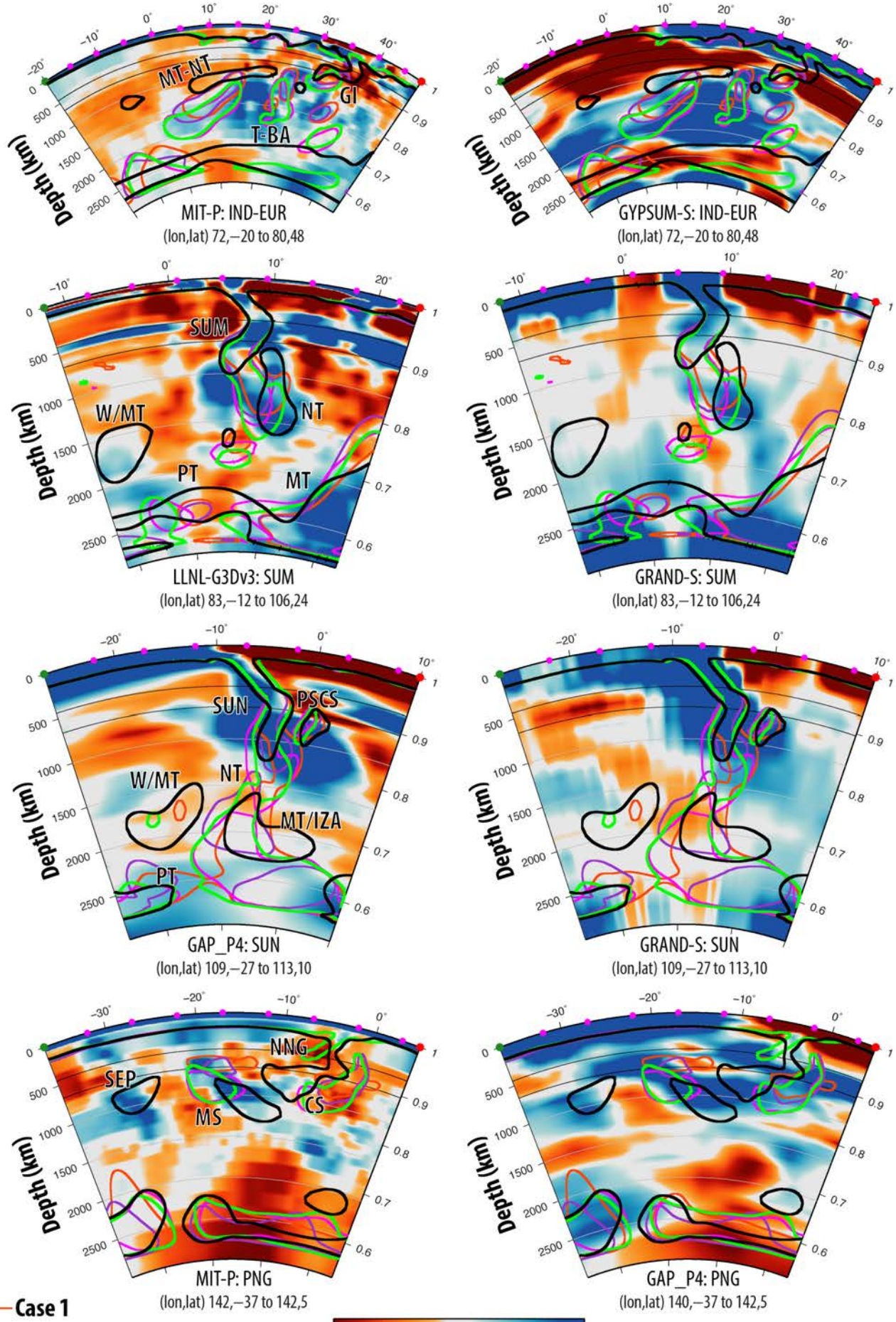
MT-NT
GI
T-BA
Depth (km)
MIT-P: IND-EUR
(lon,lat) 72,−20 to 80,48
GYPSUM-S: IND-EUR
(lon,lat) 72,−20 to 80,48
SUM
W/MT
NT
PT
MT
LLNL-G3Dv3: SUM
(lon,lat) 83,−12 to 106,24
GRAND-S: SUM
(lon,lat) 83,−12 to 106,24
SUN
PSCS
W/MT
NT
MT/IZA
PT
GAP_P4: SUN
(lon,lat) 109,−27 to 113,10
GRAND-S: SUN
(lon,lat) 109,−27 to 113,10
NNG
SEP
MS
CS
MIT-P: PNG
(lon,lat) 142,−37 to 142,5
GAP_P4: PNG
(lon,lat) 140,−37 to 142,5
Case 1
Case 2
Case 4
Case 3
Case 5
−0.5
0.0
0.5
Seismic Velocity Anomaly (%)

1798

**Fig. 30.** Present-day mantle structure along vertical slices through India (IND-EUR), northwest Sumatra (SUM), eastern Sundaland (SUN) and Australia-New Guinea (PNG) using P- and S-wave seismic tomography models, superimposed with the predicted slabs (coloured lines) from five computations of mantle flow. Case 1 to 4 uses the Zahirovic et al. (2014) plate reconstruction, but varies the radial viscosity profile of the mantle. Case 5 uses the plate reconstruction presented in this study, and the preferred viscosity structure used in Case 4. Slabs from the numerical models are defined as regions 10% colder than the background mantle temperature. The P-wave seismic tomographic models used are the MIT-P (Li et al., 2008), GAP_P4 (Obayashi et al., 2013) and LLNL-G3Dv3 (Simmons et al., 2015). The S-wave seismic tomographic models GYPSUM-S (Simmons et al., 2010) and GRAND-S (Grand, 2002) are also presented. The x-axis of the vertical section represents latitude. Table 4 lists the differences between Cases 1 to 5. The start and end coordinates for each profile are included on each cross-section, and plotted geographically in Figs. 26-29 and Supplementary Fig. 2.

## 6 Discussion

We have demonstrated the strength of using coupled plate tectonic reconstructions and numerical models of mantle flow to test competing kinematic scenarios in the absence of preserved seafloor spreading histories. In addition, the global nature of the models removes the edge effects associated with Cartesian box models of mantle convection, and allows us to track the origin and trajectory of sinking slabs, and therefore their sinking rates, which can then be compared to the mantle structure interpreted from P- and S-wave seismic tomography models (Fig. 30).

### 6.1 Intra-oceanic subduction in the Meso- and Neo-Tethys

In the India-Eurasia segment of the Tethyan margin, a number of important geodynamic implications arise from the Neo-Tethyan seafloor spreading history and the evolution of intra-oceanic subduction zones along southern Eurasia. Although early plate reconstructions of the Tethys incorporated intra-oceanic subduction and an initial collision between Greater India and the Kohistan-Ladakh Arc at or before ~ 53 Ma (Patriat and Achache, 1984), this two-stage India-Eurasia collision scenario was abandoned based on subsequent work that argued that Kohistan and Ladakh first collided with Eurasia in the Late Cretaceous along the Shyok Suture Zone (Clift et al., 2002; Debon et al., 1987; Treloar et al., 1996). However, recent work requires near-equatorial position of the Kohistan-Ladakh Arc in the Late Cretaceous (Burg, 2011; Chatterjee et al., 2013; Zaman et al., 2013; Zaman and Torii, 1999), and an initial arc-continent collision between Greater India and the Neo-Tethyan intra-oceanic arc sometime between ~ 60 and 50 Ma (Aitchison et al., 2007; Bouilhol et al., 2013; Khan et al., 2009). Our results favour an ~ 60 Ma arc-continent collision if the near-equatorial paleo-latitudes of Kohistan-Ladakh are robust, as a younger collision requires more significant advance of the Kohistan-Ladakh intra-oceanic trench before Greater India enters the subduction zone, terminating the subduction of oceanic lithosphere. The Kohistan-Ladakh back-arc basin was then subducted along southern Lhasa at an Andean-style margin, with final Shyok suturing occurring by 40 Ma (Bouilhol et al., 2013; Gibbons et al., 2015; Zahirovic et al., 2014).

The geodynamic implications of a well-established intra-oceanic system in the Neo-Tethys, suggest a scenario that is much like the present-day Izu-Bonin-Mariana Arc in the west Pacific. The paleo-latitudinal position of the intra-oceanic arc largely determines the timing of Neo-Tethyan ridge subduction, as well as the plate driving forces acting on the Indian Plate. In our reconstruction, the Neo-Tethyan mid-oceanic ridge is consumed at the Kohistan-Ladakh subduction zone from ~ 105 Ma (Figs. 11 and 26c,j). Subduction of the southern Neo-Tethyan flank of the spreading system from ~ 100 Ma would have been associated with progressively strengthening northward slab pull, to which we attribute the change towards largely northward convergence with Eurasia that is best represented

1848 by the ~ 110-90 Ma fracture zone bends in the Wharton Basin (Gibbons et al., 2015; Matthews et al.,
1849 2011; Matthews et al., 2012).

1850 The role of two coeval north-dipping subduction zones in the Neo-Tethys (Fig. 26) was
1851 suggested to have contributed to the ~ 80 Ma acceleration of India in Gibbons et al. (2015), which
1852 has recently been proposed as a mechanism for India's rapid northward advance using numerical
1853 techniques quantifying plate driving forces in Jagoutz et al. (2015). Although the arrival of the
1854 Reunion Plume head south of India at ~ 65 Ma possibly played a role in India's acceleration (Cande
1855 and Stegman, 2011; van Hinsbergen et al., 2011), the effects were likely short-lived (~ 5-10 Myr),
1856 and post-date by 15 Myr the initial acceleration of India from ~ 80 Ma. India's northward acceleration
1857 resulting from greater slab pull (and slab suction) may have induced stronger large-scale mantle return
1858 flow, possibly triggering the ascent of the Reunion Plume from the margin of the lower mantle
1859 African super-swell (Fig. 25). The recent data compilations of the surface geology, as well as new
1860 plate reconstructions and numerical approaches, suggest that a two-stage collision between India and
1861 Eurasia is more likely than a single continent-continent collision, and that the Tethyan tectonic
1862 evolution was punctuated by generations of back-arc basins and intra-oceanic subduction systems
1863 more similar to the present-day West Pacific, than a simpler long-lived Andean-style margin.
1864

1865 **6.2 Southeast Asia and New Guinea**

1866

1867 Southeast Asia, and in particular Sundaland and New Guinea, played an important role in the
1868 convergence history of Australia, Eurasia and the Pacific. In this study we have shown that our plate
1869 reconstructions are compatible, at least to the first-order, with fast seismic anomalies imaged by
1870 seismic tomography. In particular, the numerical methods suggest that the extrusion and clockwise
1871 rotation of Indochina from ~ 30 Ma are likely responsible for the Sunda slab kink beneath west
1872 Sumatra. The models reproduce the depth of the Sunda slab beneath Sumatra and Borneo, which
1873 supports subduction initiation from ~ 65 Ma, rather than from ~ 45 Ma (Hall, 2012). If the 1600 km

1874 deep Sunda slab represents subduction since 45 Ma (Hall and Spakman, 2015), then an average
1875 whole-mantle sinking rate of 3.5 cm/yr is required, while our post-65 Ma subduction history would
1876 require average sinking rates of 2.5 cm/yr, which is more consistent with previous studies of sinking
1877 rates in numerical models (Butterworth et al., 2014; Steinberger et al., 2012). The constraints from
1878 the subduction-related volcanic history of Sumatra (McCourt et al., 1996) result in a predicted slab
1879 that is consistent with P- and S-wave tomography models. This highlights that segmentation of the
1880 Neo-Tethyan and Indian Ocean plates across pre-existing structural fabric (Hall, 2012) is not required
1881 to account for the subduction history recorded on the Sumatra-Java Sundaland margin. Although Hall
1882 and Spakman (2015) invoke a leaky transform in the Neo-Tethys at ~ 90°E (Fig. 4C) to explain a
1883 possible ~ 90-45 Ma subduction hiatus, the mantle discontinuity linked to this interpretation is much
1884 further east at 110°E. There is a clearer discontinuity in slab structure east of ~ 120°E (Fig. 24), which
1885 represents the complex subduction history of New Guinea that is possibly linked to the evolution of
1886 the Philippine Sea Plate and the Pacific, rather than Sundaland.
1887 The relatively small slabs predicted at ~ 600 to 1000 km depth beneath northern Borneo in our
1888 models roughly correspond to the interpreted Proto South China Sea slab (Zahirovic et al., 2014)
1889 imaged in seismic tomography at shallower depths in the mantle transition zone (~ 410 to 660 km).
1890 This suggests that Proto South China Sea subduction along northern Borneo may have started later
1891 than 45 Ma, which would be consistent with a shallower slab, and perhaps linked to an ~ 32 Ma onset
1892 in seafloor spreading of the South China Sea (Briais et al., 1993). However, a major phase of
1893 volcanism along northern Borneo from ~ 50 Ma (Soeria-Atmadja et al., 1999) might instead indicate
1894 earlier subduction initiation. In this case, stagnation of the Proto South China Sea slab in the mantle
1895 transition zone could play an important role in the depth mismatch between our numerical
1896 experiments and the seismic tomographic constraints. Recent backward-advection modelling by
1897 Yang et al. (2016) suggests that the large volume of subducted slab beneath Sundaland stagnated in
1898 the mantle transition zone before ~ 30 Ma, and entered the lower mantle as a slab avalanche in the
1899 Miocene from ~ 20 Ma. This work highlights the time-varying slab sinking rates in the region, but

more importantly, demonstrates that a slab avalanche resulted in dynamic subsidence of Sundaland and flooding (Yang et al., 2016) that was asynchronous with global eustasy (Haq et al., 1987). In addition, the slab avalanche was likely responsible for Miocene basin inversions (Doust and Sumner, 2007) by propagating stresses acting on the lithosphere. Since Proto South China Sea subduction ceased at ~ 15 Ma, recorded by cessation of seafloor spreading in the South China Sea (Briais et al., 1993), it is therefore likely that the Proto South China Sea slab is in the upper mantle or transition zone when considering the role of slab stagnation in this region. This interpretation is in contrast with that of Hall and Spakman (2015) who argued for a lower mantle (~ 1200 km deep) position of the Proto South China Sea slab.

Further east on New Guinea, the complexity of the surface geology has led to competing plate tectonic reconstruction scenarios (van Ufford and Cloos, 2005), some of which are discussed in this study. Our plate reconstructions and numerical experiments of mantle flow require Sepik oceanic gateway subduction in the Late Cretaceous, likely from ~ 70 Ma, which accounts for the present-day slab at mid-mantle depths at ~ 30°S beneath Lake Eyre in northern South Australia, consistent with recent interpretations (Schellart and Spakman, 2015). However, the slab predicted in our mantle flow model is smaller, which raises the possibility that the Sepik oceanic basin was larger than modelled in our plate reconstructions. The refinement to the plate reconstructions and inclusion of south-dipping Maramuni Arc subduction along New Guinea from ~ 20 to 6 Ma, with coeval north-dipping subduction along the Halmahera Arc, improves the fit between predicted slab distributions and the mantle structure inferred from seismic tomography. We interpret the presently-inactive Trobriand Trough as the Maramuni Arc subduction zone (active ~ 18 to 8 Ma). The Maramuni subduction may have caused the dynamic subsidence and progressive flooding inferred for the northern Australian shelf since the Oligocene (DiCaprio et al., 2009; DiCaprio et al., 2011; Sandiford, 2007; Spasojevic and Gurnis, 2012). Although our results reproduce the Sepik and Maramuni slabs, more work is required to account for a consistently-imaged near-equatorial slab at ~ 1500 km depths that is not reproduced by either of the plate reconstruction scenarios presented in this study. Further work using

numerical techniques is required to improve the understanding of the complex tectonic linkage between Southeast Asia and the Pacific through New Guinea.

### 6.3 Relevance to global plate reconstructions and geodynamics

Our coupled plate kinematic and numerical geodynamic approach has wider implications for understanding the long-term evolution of the plate-mantle system. One important outcome is that numerical models testing alternative plate reconstruction scenarios that are compared to mantle structure from seismic tomography should consider the regional and global plate tectonic evolution. The evolution of Neo-Tethyan intra-oceanic subduction along the Kohistan-Ladakh and Woyla arc systems also has wider geodynamic implications. Although we implemented subduction initiation at the passive margin of the back-arc systems, a more complicated geodynamic mechanism may be required, such as the inversion of a mid-oceanic ridge to become a subduction zone in order to accommodate convergence and explain ophiolite obduction (Hébert et al., 2012; Shemenda, 1993). Due to the paucity of data constraining the nature and location of subduction initiation of the Woyla back-arc basin, a south-dipping subduction zone as proposed by Morley (2012a) will also require testing in future work. However, India's Late Cretaceous northward acceleration from two coeval and coupled north-dipping subduction zones (Jagoutz et al., 2015) may also require two north-dipping subduction zones in the Woyla segment of the Neo-Tethyan active margin, which highlights the prevalence of intra-oceanic subduction in the Neo-Tethys.

## 7 Conclusions

This study shows the power of considering the coupled plate-mantle system to study the geodynamics of the Tethyan tectonic domain that is dominated by long-term Eurasian, Indo-Australian and Pacific convergence following Pangea breakup. The reconstructions, used as boundary

conditions in mantle flow numerical experiments, consider intra-oceanic subduction along the entire south Eurasian active margin from ~ 160 Ma in the Neo-Tethys. We suggest that the Neo-Tethyan ridge was likely consumed along the Kohistan-Ladakh intra-oceanic arc from ~ 105 Ma, followed by northward subduction of the Indian Plate that significantly modified India's plate motion direction. For Sundaland, a tectonic scenario with Woyla Arc accretion at ~ 75-70 Ma, followed by an ~ 10 Myr subduction hiatus, and renewed subduction along the south Sundaland margin by ~ 60 Ma places the Sunda slab at the same depth as in P- and S-wave seismic tomography models. In addition, our results suggest that a slab beneath northern Borneo, which is likely stagnant in the mantle transition zone, could be a remnant of the Proto South China Sea. Further east along New Guinea, the plate reconstructions coupled to geodynamic experiments are consistent with north-dipping subduction along the Halmahera Arc coeval with the ~ 20 Ma onset of south-dipping Maramuni subduction along New Guinea. The Late Cretaceous (~ 71 Ma) onset of Sepik oceanic basin subduction, followed by the docking of the Sepik composite terrane to New Guinea by ~ 30 Ma, produces a mid-mantle slab imaged in tomography beneath Lake Eyre in Australia, as discussed in Schellart and Spakman (2015), due to the combination of southward mantle flow and Australia's northward advance towards the Southeast Asian slab burial grounds.

We present testable and reproducible plate reconstructions with regional refinements and improvements to the understanding of post-Jurassic eastern Tethyan geodynamics. The reconstructions may form the basis of future work to better understand the tectonics of the Tethyan domain, and could also be used to study oceanic circulation, long-term climate change and biogeographic dispersal pathways. In addition, our work highlights the need for testing competing plate reconstruction scenarios using numerical modelling approaches in a global and geodynamic framework.

**Acknowledgements**

S.Z., N.F. and R.D.M. were supported by ARC grant IH130200012, K.J.M. and R.D.M. were supported by ARC grant DP130101946, K.C.H. was supported by Oil Search Limited, M.S. was supported by ARC grant FT130101564 and M.G. was supported by Statoil ASA and by the NSF through EAR-1161046 and EAR-1247022. This research was undertaken with the assistance of resources from the National Computational Infrastructure (NCI), which is supported by the Australian Government. We are grateful to John Cannon, Michael Chin, Robin Watson, Mark Turner, James Boyden and James Clark for their help in developing the open-source community plate reconstruction software GPlates, as well as relevant workflows. We thank Michael G. Tetley for providing technical support and workflow enhancement that improved the management of seafloor isochrons and other GPlates-related geometries, and Tobias Pfaffelmoser for help with implementing the GPlates 3D functionality. We are also grateful to Luke Mahoney for helpful discussions that improved the manuscript. We thank the Editor, Robert Holm and Bernhard Steinberger for constructive reviews. This work was conducted within the industry linkage and collaborative framework of the Basin GENeSIS Industrial Transformation Research Hub. The full supplement can be downloaded from ftp://ftp.earthbyte.org/Data_Collections/Zahirovic_etal_ESR_EasternTethys_Supplement.zip.

## References

Abrajevitch, A., van der Voo, R., Bazhenov, M.L., Levashova, N.M. and McCausland, P.J.A., 2008. The role of the Kazakhstan orocline in the late Paleozoic amalgamation of Eurasia. Tectonophysics, 455(1): 61-76.

Acharyya, S.K., 1998. Break-up of the greater Indo-Australian continent and accretion of blocks framing south and east Asia. Journal of Geodynamics, 26(1): 149-170.

Aitchison, J.C., Ali, J.R. and Davis, A.M., 2007. When and where did India and Asia collide? Journal of Geophysical Research, 112(B05423): 1-19.

Aitchison, J.C., Davis, A.M., Liu, J., Luo, H., Malpas, J.G., McDermid, I.R.C., Wu, H., Ziabrev, S.V. and Zhou, M., 2000. Remnants of a Cretaceous intra-oceanic subduction system within the Yarlung-Zangbo suture (southern Tibet). Earth and Planetary Science Letters, 183(1-2): 231-244.

Alisic, L., Gurnis, M., Stadler, G., Burstedde, C. and Ghattas, O., 2012. Multi‐scale dynamics and rheology of mantle flow with plates. Journal of Geophysical Research: Solid Earth 117(B10).

Alisic, L., Gurnis, M., Stadler, G., Burstedde, C., Wilcox, L.C. and Ghattas, O., 2010. Slab stress and strain rate as constraints on global mantle flow. Geophysical Research Letters, 37(22).

Amante, C., Eakins, B.W. and Boulder, C., 2009. ETOPO1 1 arc-minute global relief model: Procedures, data sources and analysis. NOAA Technical Memorandum.
Audley-Charles, M.G., 1966. Mesozoic palaeogeography of Australasia. Palaeogeography, Palaeoclimatology, Palaeoecology, 2: 1-25.
Audley-Charles, M.G., 1988. Evolution of the southern margin of Tethys (North Australian region) from early Permian to late Cretaceous. Geological Society, London, Special Publications, 37(1): 79-100.
Audley-Charles, M.G., Ballantyne, P.D. and Hall, R., 1988. Mesozoic-Cenozoic Rift-Drift Sequence of Asian Fragments from Gondwanaland. Tectonophysics, 155(1-4): 317-330.
Baldwin, S.L., Fitzgerald, P.G. and Webb, E.W., 2012. Tectonics of the New Guinea Region. Annu. Rev. Earth Planet. Sci., 40: 495-520.
Balmino, G., Vales, N., Bonvalot, S. and Briais, A., 2012. Spherical harmonic modelling to ultra-high degree of Bouguer and isostatic anomalies. Journal of Geodesy, 86(7): 499-520.
Barber, A.J. and Crow, M.J., 2003. An evaluation of plate tectonic models for the development of Sumatra. Gondwana Research, 6(1): 1-28.
Baumann, T.S. and Kaus, B.J.P., 2015. Geodynamic inversion to constrain the non-linear rheology of the lithosphere. Geophysical Journal International, 202(2): 1289-1316.
Baxter, A.T., Aitchison, J.C., Zyabrev, S.V. and Ali, J.R., 2011. Upper Jurassic radiolarians from the Naga ophiolite, Nagaland, northeast India. Gondwana Research, 20(2): 638-644.
Becker, T., Schaeffer, A., Lebedev, S. and Conrad, C., 2015. Toward a generalized plate motion reference frame. Geophysical Research Letters, 42(9): 3188-3196.
Becker, T.W., 2006. On the effect of temperature and strain-rate dependent viscosity on global mantle flow, net rotation, and plate-driving forces. Geophysical Journal International, 167(2): 943-957.
Becker, T.W. and Faccenna, C., 2011. Mantle conveyor beneath the Tethyan collisional belt. Earth and Planetary Science Letters, 310(3,Äì4): 453-461.
Bergman, S.C., Coffield, D.Q., Talbot, J.P. and Garrard, R.A., 1996. Tertiary tectonic and magmatic evolution of western Sulawesi and the Makassar Strait, Indonesia: evidence for a Miocene continent-continent collision. Geological Society, London, Special Publications, 106(1): 391-429.
Besse, J. and Courtillot, V., 1988. Paleogeographic maps of the continents bordering the Indian Ocean since the Early Jurassic. Journal of Geophysical Research: Solid Earth (1978–2012), 93(B10): 11791-11808.
Bijwaard, H. and Spakman, W., 2000. Non-linear global P-wave tomography by iterated linearized inversion. Geophysical Journal International, 141(1): 71-82.
Bijwaard, H., Spakman, W. and Engdahl, E., 1998. Closing the gap between regional and global travel time tomography. Journal of Geophysical Research, 103(B12): 30055.
Bird, P., 2003. An updated digital model of plate boundaries. Geochemistry, Geophysics, Geosystems, 4(3): 1-52.
Bouilhol, P., Jagoutz, O., Hanchar, J.M. and Dudas, F.O., 2013. Dating the India–Eurasia collision through arc magmatic records. Earth and Planetary Science Letters, 366: 163-175.
Bouilhol, P., Schaltegger, U., Chiaradia, M., Ovtcharova, M., Stracke, A., Burg, J.-P. and Dawood, H., 2011. Timing of juvenile arc crust formation and evolution in the Sapat Complex (Kohistan–Pakistan). Chemical Geology, 280(3): 243-256.
Bower, D., Gurnis, M. and Seton, M., 2013. Lower mantle structure from paleogeographically constrained dynamic Earth models. Geochemistry, Geophysics, Geosystems, 14(1): 44-63.
Bower, D.J., Gurnis, M. and Flament, N., 2015. Assimilating lithosphere and slab history in 4-D dynamic Earth models. Physics of the Earth and Planetary Interiors, 238: 8-22.
Boyden, J., Müller, R., Gurnis, M., Torsvik, T., Clark, J., Turner, M., Ivey-Law, H., Watson, R. and Cannon, J., 2011. Next-generation plate-tectonic reconstructions using GPlates. In: G. Keller and C. Baru (Editors), Geoinformatics: Cyberinfrastructure for the Solid Earth Sciences. Cambridge University Press, Cambridge, UK, pp. 95-114.

2062 Briais, A., Patriat, P. and Tapponnier, P., 1993. Updated interpretation of magnetic anomalies and
2063 seafloor spreading stages in the South China Sea: implications for the Tertiary tectonics of
2064 Southeast Asia. Journal of Geophysical Research, 98(B4): 6299-6328.
2065 Brown, G.F., 1951. Geologic reconnaissance of the mineral deposits of Thailand. US Government
2066 Printing Office.
2067 Bunge, H.-P., Hagelberg, C. and Travis, B., 2003. Mantle circulation models with variational data
2068 assimilation: inferring past mantle flow and structure from plate motion histories and
2069 seismic tomography. Geophysical Journal International, 152(2): 280-301.
2070 Bunge, H.-P., Richards, M. and Baumgardner, J., 2002. Mantle–circulation models with sequential
2071 data assimilation: inferring present–day mantle structure from plate–motion histories.
2072 Philosophical Transactions of the Royal Society of London A: Mathematical, Physical and
2073 Engineering Sciences, 360(1800): 2545-2567.
2074 Burg, J.P., 2011. The Asia–Kohistan–India Collision: Review and Discussion. In: D. Brown and P.
2075 Ryan (Editors), Arc-Continent Collision. Frontiers in Earth Sciences. Springer-Verlag
2076 Berlin, pp. 279-309.
2077 Burg, J.P., Jagoutz, O., Dawood, H. and Hussain, S.S., 2006. Precollision tilt of crustal blocks in
2078 rifted island arcs: structural evidence from the Kohistan Arc. Tectonics, 25(5).
2079 Burke, K. and Dewey, J., 1973. Plume-generated triple junctions: key indicators in applying plate
2080 tectonics to old rocks. The Journal of Geology: 406-433.
2081 Burrett, C., Duhid, N., Berry, R. and Varne, R., 1991. Asian and south-western Pacific continental
2082 terranes derived from Gondwana, and their biogeographic significance. Australian
2083 Systematic Botany, 4(1): 13-24.
2084 Butterworth, N., Talsma, A., Müller, R., Seton, M., Bunge, H.-P., Schuberth, B., Shephard, G. and
2085 Heine, C., 2014. Geological, tomographic, kinematic and geodynamic constraints on the
2086 dynamics of sinking slabs. Journal of Geodynamics, 73: 1-13.
2087 Cameron, N.R., Clarke, M.C.G., Aldiss, D.T., Aspden, J.A. and Djunuddin, A., 1980. The
2088 geological evolution of northern Sumatra.
2089 Cande, S.C. and Patriat, P., 2015. The anticorrelated velocities of Africa and India in the Late
2090 Cretaceous and early Cenozoic. Geophysical Journal International, 200(1): 227-243.
2091 Cande, S.C., Patriat, P. and Dyment, J., 2010. Motion between the Indian, Antarctic and African
2092 plates in the early Cenozoic. Geophysical Journal International(183): 127-149.
2093 Cande, S.C. and Stegman, D.R., 2011. Indian and African plate motions driven by the push force of
2094 the Reunion plume head. Nature, 475(7354): 47-52.
2095 Capitanio, F.A., Morra, G., Goes, S., Weinberg, R.F. and Moresi, L., 2010. India–Asia convergence
2096 driven by the subduction of the Greater Indian continent. Nature Geoscience, 3(2): 136-139.
2097 Carey, S.W., 1955. The orocline concept in geotectonics-Part I, Papers and proceedings of the
2098 Royal Society of Tasmania, pp. 255-288.
2099 Carlson, R. and Mortera-Gutiérrez, C., 1990. Subduction hinge migration along the Izu-Bonin-
2100 Mariana arc. Tectonophysics, 181(1-4): 331-344.
2101 Charlton, T.R., 2001. Permo-Triassic evolution of Gondwanan eastern Indonesia, and the final
2102 Mesozoic separation of SE Asia from Australia. Journal of Asian Earth Sciences, 19(5):
2103 595-617.
2104 Chatterjee, S., Goswami, A. and Scotese, C.R., 2013. The longest voyage: tectonic, magmatic, and
2105 paleoclimatic evolution of the Indian plate during its northward flight from Gondwana to
2106 Asia. Gondwana Research, 23(1): 238-267.
2107 Chung, S.L., Chu, M.F., Zhang, Y., Xie, Y., Lo, C.H., Lee, T.Y., Lan, C.Y., Li, X., Zhang, Q. and
2108 Wang, Y., 2005. Tibetan tectonic evolution inferred from spatial and temporal variations in
2109 post-collisional magmatism. Earth-Science Reviews, 68(3-4): 173-196.
2110 Clements, B., Burgess, P.M., Hall, R. and Cottam, M.A., 2011. Subsidence and uplift by slab-
2111 related mantle dynamics: a driving mechanism for the Late Cretaceous and Cenozoic
2112 evolution of continental SE Asia? Geological Society, London, Special Publications, 355(1):
2113 37-51.

Clements, B. and Hall, R., 2007. Cretaceous to Late Miocene stratigraphic and tectonic evolution of West Java. Indonesian Petroleum Association Proceedings, 31(IPA07-G-037): 1-18.
Clements, B. and Hall, R., 2011. A record of continental collision and regional sediment flux for the Cretaceous and Palaeogene core of SE Asia: implications for early Cenozoic palaeogeography. Journal of the Geological Society, 168: 1187-1200.
Clift, P.D., Hannigan, R., Blusztajn, J. and Draut, A.E., 2002. Geochemical evolution of the Dras–Kohistan Arc during collision with Eurasia: evidence from the Ladakh Himalaya, India. Island Arc, 11(4): 255-273.
Conrad, C.P. and Gurnis, M., 2003. Seismic tomography, surface uplift, and the breakup of Gondwanaland: Integrating mantle convection backwards in time. Geochemistry, Geophysics, Geosystems, 4(3).
Conrad, C.P. and Lithgow‐Bertelloni, C., 2004. The temporal evolution of plate driving forces: Importance of "slab suction" versus "slab pull" during the Cenozoic. Journal of Geophysical Research: Solid Earth, 109(B10).
Crowhurst, P.V., Hill, K.C., Foster, D.A. and Bennett, A., 1996. Thermochronological and geochemical constraints on the tectonic evolution of northern Papua New Guinea. Geological Society Special Publications, 106(Tectonic Evolution of Southeast Asia): 525-537.
Cullen, A.B., 2010. Transverse segmentation of the Baram-Balabac Basin, NW Borneo: refining the model of Borneo's tectonic evolution. Petroleum Geoscience, 16(1): 3-29.
Daly, M.C., Cooper, M.A., Wilson, I., Smith, D.G. and Hooper, B.G.D., 1991. Cenozoic plate tectonics and basin evolution in Indonesia. Marine and Petroleum Geology, 8(1): 2-21.
Davies, H.L., 2012. The geology of New Guinea-the cordilleran margin of the Australian continent. Episodes, 35(1): 87-102.
de Bruyn, M., Stelbrink, B., Morley, R.J., Hall, R., Carvalho, G.R., Cannon, C.H., van den Bergh, G., Meijaard, E., Metcalfe, I. and Boitani, L., 2014. Borneo and Indochina are major evolutionary hotspots for Southeast Asian biodiversity. Systematic biology, 63(6): 879-901.
Debayle, E. and Ricard, Y., 2013. Seismic observations of large-scale deformation at the bottom of fast-moving plates. Earth and Planetary Science Letters, 376: 165-177.
Debon, F., Le Fort, P., Dautel, D., Sonet, J. and Zimmermann, J.L., 1987. Granites of western Karakorum and northern Kohistan (Pakistan): a composite Mid-Cretaceous to upper Cenozoic magmatism. Lithos, 20(1): 19-40.
Deng, J., Yang, X., Zhang, Z.-F. and Santosh, M., 2015. Early Cretaceous arc volcanic suite in Cebu Island, Central Philippines and its implications on paleo-Pacific plate subduction: Constraints from geochemistry, zircon U–Pb geochronology and Lu–Hf isotopes. Lithos, 230: 166-179.
Deschamps, A. and Lallemand, S., 2002. The West Philippine Basin: An Eocene to early Oligocene back arc basin opened between two opposed subduction zones. Journal of Geophysical Research: Solid Earth (1978–2012), 107(B12): EPM 1-1-EPM 1-24.
DiCaprio, L., Gurnis, M. and Müller, R.D., 2009. Long-wavelength tilting of the Australian continent since the Late Cretaceous. Earth and Planetary Science Letters, 278(3-4): 175-185.
DiCaprio, L., Gurnis, M., Müller, R.D. and Tan, E., 2011. Mantle dynamics of continentwide Cenozoic subsidence and tilting of Australia. Lithosphere: L140. 1v1.
Doglioni, C., 1991. A proposal for the kinematic modelling of W‐dipping subductions‐possible applications to the Tyrrhenian‐Apennines system. Terra Nova, 3(4): 423-434.
Domeier, M. and Torsvik, T.H., 2014. Plate tectonics in the late Paleozoic. Geoscience Frontiers, 5(3): 303-350.
Doust, H. and Sumner, H.S., 2007. Petroleum systems in rift basins–a collective approach inSoutheast Asian basins. Petroleum Geoscience, 13(2): 127-144.
Dow, D.B., 1977. A geological synthesis of Papua New Guinea, 201. Bureau of Mineral Resources, Australian Government Publishing Service.

Elburg, M., van Leeuwen, T. and Foden, J., 2003. Spatial and temporal isotopic domains of contrasting igneous suites in Western and Northern Sulawesi, Indonesia. Chemical Geology, 199(3): 243-276.
Eldredge, S., Bachtadse, V. and van der Voo, R., 1985. Paleomagnetism and the orocline hypothesis. Tectonophysics, 119(1): 153-179.
Encarnación, J., 2004. Multiple ophiolite generation preserved in the northern Philippines and the growth of an island arc complex. Tectonophysics, 392(1): 103-130.
Faccenna, C., Becker, T.W., Lallemand, S. and Steinberger, B., 2012. On the role of slab pull in the Cenozoic motion of the Pacific plate. Geophysical Research Letters, 39(3).
Fairbridge, R.W., 1963. The Indian Ocean and the status of Gondwanaland. Progress in Oceanography, 3: 83-136.
Findlay, R.H., 2003. Collision tectonics of northern Papua New Guinea: key field relationships demand a new model. Geological Society of America Special Papers, 372: 291-307.
Fitch, T.J., 1972. Plate convergence, transcurrent faults, and internal deformation adjacent to southeast Asia and the western Pacific. Journal of Geophysical Research, 77(23): 4432-4460.
Fjeldskaar, W., Lindholm, C., Dehls, J.F. and Fjeldskaar, I., 2000. Postglacial uplift, neotectonics and seismicity in Fennoscandia. Quaternary Science Reviews, 19(14-15): 1413-1422.
Flament, N., Gurnis, M., Müller, R.D., Bower, D.J. and Husson, L., 2015. Influence of subduction history on South American topography. Earth and Planetary Science Letters, 430: 9-18.
Flament, N., Gurnis, M., Williams, S., Seton, M., Skogseid, J., Heine, C. and Müller, R.D., 2014. Topographic asymmetry of the South Atlantic from global models of mantle flow and lithospheric stretching. Earth and Planetary Science Letters, 387: 107-119.
Flower, M.F.J. and Dilek, Y., 2003. Arc-trench rollback and forearc accretion: 1. A collision-induced mantle flow model for Tethyan ophiolites. Geological Society, London, Special Publications, 218(1): 21-41.
Forsyth, D. and Uyeda, S., 1975. On the relative importance of the driving forces of plate motion. Geophysical Journal International, 43(1): 163-200.
Forte, A.M. and Mitrovica, J.X., 1996. New inferences of mantle viscosity from joint inversion of long‐wavelength mantle convection and post‐glacial rebound data. Geophysical Research Letters, 23(10): 1147-1150.
Foulger, G.R., Panza, G.F., Artemieva, I.M., Bastow, I.D., Cammarano, F., Evans, J.R., Hamilton, W.B., Julian, B.R., Lustrino, M. and Thybo, H., 2013. Caveats on tomographic images. Terra Nova, 25(4): 259-281.
Fuller, M., Ali, J.R., Moss, S.J., Frost, G.M., Richter, B. and Mahfi, A., 1999. Paleomagnetism of Borneo. Journal of Asian Earth Sciences, 17(1-2): 3-24.
Fuller, M., Haston, R., Lin, J.-L., Richter, B., Schmidtke, E. and Almasco, J., 1991. Tertiary paleomagnetism of regions around the South China Sea. Journal of Southeast Asian Earth Sciences, 6(3): 161-184.
Fyhn, M.B.W., Pedersen, S.A.S., Boldreel, L.O., Nielsen, L.H., Green, P.F., Dien, P.T., Huyen, L.T. and Frei, D., 2010. Palaeocene–early Eocene inversion of the Phuquoc–Kampot Som Basin: SE Asian deformation associated with the suturing of Luconia. Journal of the Geological Society, 167(2): 281-295.
Gaina, C. and Müller, R.D., 2007. Cenozoic tectonic and depth/age evolution of the Indonesian gateway and associated back-arc basins. Earth-Science Reviews, 83(3-4): 177-203.
Gasperini, P. and Sabadini, R., 1989. Lateral heterogeneities in mantle viscosity and post glacial rebound. Geophysical Journal International, 98(3): 413-428.
Geary, E.E., Harrison, T.M. and Heizler, M., 1988. Diverse ages and origins of basement complexes, Luzon, Philippines. Geology, 16(4): 341-344.
Geary, E.E. and Kay, R.W., 1989. Identification of an Early Cretaceous ophiolite in the Camarines Norte-Calaguas Islands basement complex, eastern Luzon, Philippines. Tectonophysics, 168(1): 109-126.

Gee, J.S. and Kent, D.V., 2007. Source of oceanic magnetic anomalies and the geomagnetic polarity time scale. Treatise on Geophysics, Vol. 5: Geomagnetism: 455-507.
Ghose, R., Yoshioka, S. and Oike, K., 1990. Three-dimensional numerical simulation of the subduction dynamics in the Sunda arc region, Southeast Asia. Tectonophysics, 181(1): 223-255.
Gibbons, A., Zahirovic, S., Müller, R.D., Whittaker, J. and Yatheesh, V., 2015. A tectonic model reconciling evidence for the collisions between India, Eurasia and intra-oceanic arcs of the central-eastern Tethys. Gondwana Research FOCUS, 28(2): 451-492.
Gibbons, A.D., Barckhausen, U., van den Bogaard, P., Hoernle, K., Werner, R., Whittaker, J.M. and Müller, R.D., 2012. Constraining the Jurassic extent of Greater India: Tectonic evolution of the West Australian margin. Geochemistry Geophysics Geosystems, 13(5): 25.
Gibbons, A.D., Whittaker, J.M. and Müller, R.D., 2013. The breakup of East Gondwana: Assimilating constraints from Cretaceous ocean basins around India into a best‐fit tectonic model. Journal of Geophysical Research: Solid Earth, 13(5).
Glišović, P. and Forte, A.M., 2014. Reconstructing the Cenozoic evolution of the mantle: Implications for mantle plume dynamics under the Pacific and Indian plates. Earth and Planetary Science Letters, 390: 146-156.
Goldfarb, R.J., Taylor, R.D., Collins, G.S., Goryachev, N.A. and Orlandini, O.F., 2014. Phanerozoic continental growth and gold metallogeny of Asia. Gondwana Research, 25(1): 48-102.
Görür, N. and Sengör, A.M.C., 1992. Paleogeography and tectonic evolution of the eastern Tethysides: implications for the northwest Australian margin breakup history, Proceedings of the Ocean Drilling Program, Scientific Results, pp. 83-106.
Gourlan, A.T., Meynadier, L. and Allègre, C.J., 2008. Tectonically driven changes in the Indian Ocean circulation over the last 25 Ma: Neodymium isotope evidence. Earth and Planetary Science Letters, 267(1): 353-364.
Gradstein, F.M. and Ludden, J.N., 1992. Radiometric age determinations for basement from Sites 765 and 766, Argo Abyssal Plain and northwestern Australian margin, Proceedings of the ocean drilling program, Scientific Results, pp. 557-559.
Grand, S.P., 2002. Mantle shear-wave tomography and the fate of subducted slabs. Philosophical Transactions of the Royal Society of London. Series A: Mathematical, Physical and Engineering Sciences, 360(1800): 2475.
Guillaume, B., Martinod, J., Husson, L., Roddaz, M. and Riquelme, R., 2009. Neogene uplift of central eastern Patagonia: Dynamic response to active spreading ridge subduction? Tectonics, 28(2).
Guntoro, A., 1999. The formation of the Makassar Strait and the separation between SE Kalimantan and SW Sulawesi. Journal of Asian Earth Sciences 17: 79-98.
Gurnis, M., Hall, C. and Lavier, L., 2004. Evolving force balance during incipient subduction. Geochemistry, Geophysics, Geosystems, 5: -.
Gurnis, M., Turner, M., Zahirovic, S., DiCaprio, L., Spasojevic, S., Müller, R.D., Boyden, J., Seton, M., Manea, V.C. and Bower, D.J., 2012. Plate Tectonic Reconstructions with Continuously Closing Plates. Computers & Geosciences, 38(1): 35-42.
Hafkenscheid, E., Wortel, M.J.R. and Spakman, W., 2006. Subduction history of the Tethyan region derived from seismic tomography and tectonic reconstructions. Journal of Geophysical Research-Solid Earth, 111(B8): B08401.
Hager, B.H., 1984. Subducted slabs and the geoid: constraints on mantle rheology and flow. Journal of Geophysical Research, 89(B7): 6003-6015.
Hager, B.H. and O'Connell, R.J., 1981. A simple global model of plate dynamics and mantle convection. Journal of Geophysical Research: Solid Earth (1978–2012), 86(B6): 4843-4867.
Haile, N.S., 1979. Palaeomagnetic evidence for rotation and northward drift of Sumatra. Journal of the Geological Society, 136(5): 541-546.

Haile, N.S., McElhinny, M.W. and McDougall, I., 1977. Palaeomagnetic data and radiometric ages from the Cretaceous of West Kalimantan (Borneo), and their significance in interpreting regional structure. Journal of the Geological Society, 133(2): 133-144.
Halbouty, M.T., King, R.E., Klemme, H.D., Dott, S., R H and Meyerhoff, A.A., 1970. World's Giant Oil and Gas Fields, Geologic Factors Affecting Their Formation, and Basin Classification: Part II: Factors Affecting Formation of Giant Oil and Gas Fields, and Basin Classification, M 14: Geology of Giant Petroleum Fields, pp. 528-555.
Hall, C.E., Gurnis, M., Sdrolias, M., Lavier, L.L. and Müller, R.D., 2003. Catastrophic initiation of subduction following forced convergence across fracture zones. Earth and Planetary Science Letters, 212(1): 15-30.
Hall, R., 1996. Reconstructing Cenozoic SE Asia. Geological Society, London, Special Publications, 106(1): 153-184.
Hall, R., 2002. Cenozoic geological and plate tectonic evolution of SE Asia and the SW Pacific: computer-based reconstructions, model and animations. Journal of Asian Earth Sciences, 20(4): 353-431.
Hall, R., 2011. Australia–SE Asia collision: plate tectonics and crustal flow. Geological Society, London, Special Publications, 355(1): 75-109.
Hall, R., 2012. Late Jurassic–Cenozoic reconstructions of the Indonesian region and the Indian Ocean. Tectonophysics, 570-571: 1-41.
Hall, R., Ali, J.R. and Anderson, C.D., 1995a. Cenozoic Motion of the Philippine Sea Plate - Paleomagnetic Evidence from Eastern Indonesia. Tectonics, 14(5): 1117-1132.
Hall, R., Ali, J.R., Anderson, C.D. and Baker, S.J., 1995b. Origin and motion history of the Philippine Sea Plate. Tectonophysics, 251(1): 229-250.
Hall, R. and Spakman, W., 2002. Subducted slabs beneath the eastern Indonesia-Tonga region: insights from tomography. Earth and Planetary Science Letters, 201(2): 321-336.
Hall, R. and Spakman, W., 2003. Mantle structure and tectonic evolution of the region north and east of Australia. Geological Society of America Special Papers, 372: 361-381.
Hall, R. and Spakman, W., 2015. Mantle structure and tectonic history of SE Asia. Tectonophysics, 658: 14-45.
Hamilton, W.B., 1979. Tectonics of the Indonesian region. US Govt. Print. Off.
Haq, B.U., Hardenbol, J. and Vail, P.R., 1987. Chronology of fluctuating sea levels since the Triassic. Science, 235(4793): 1156-1167.
Hébert, R., Bezard, R., Guilmette, C., Dostal, J., Wang, C.S. and Liu, Z.F., 2012. The Indus–Yarlung Zangbo ophiolites from Nanga Parbat to Namche Barwa syntaxes, southern Tibet: First synthesis of petrology, geochemistry, and geochronology with incidences on geodynamic reconstructions of Neo-Tethys. Gondwana Research, 22(2): 377-397.
Heine, C. and Müller, R.D., 2005. Late Jurassic rifting along the Australian North West Shelf: margin geometry and spreading ridge configuration. Australian Journal of Earth Sciences, 52(1): 27-39.
Heine, C., Müller, R.D. and Gaina, C., 2004. Reconstructing the lost eastern Tethys ocean basin: convergence history of the SE Asian margin and marine gateways. Continent-Ocean Interactions Within East Asian Marginal Seas, Geophys. Monogr. Ser, 149: 37-54.
Hellinger, S.J., 1981. The uncertainties of finite rotations in plate tectonics. Journal of Geophysical Research: Solid Earth (1978–2012), 86(B10): 9312-9318.
Herold, N., Buzan, J., Seton, M., Goldner, A., Green, J.A.M., Müller, R.D., Markwick, P. and Huber, M., 2014. A suite of early Eocene (~ 55 Ma) climate model boundary conditions. Geoscientific Model Development, 7(5): 2077-2090.
Hilde, T.W.C. and Chao-Shing, L., 1984. Origin and evolution of the West Philippine Basin: a new interpretation. Tectonophysics, 102(1): 85-104.
Hill, K.C. and Hall, R., 2003. Mesozoic–Cenozoic evolution of Australia's New Guinea margin in a west Pacific context. Geological Society of Australia Special Publications, 22: 265-289.

Hill, K.C. and Raza, A., 1999. Arc‐continent collision in Papua Guinea: Constraints from fission track thermochronology. Tectonics, 18(6): 950-966.
Holm, R.J., Spandler, C. and Richards, S.W., 2014. Continental collision, orogenesis and arc magmatism of the Miocene Maramuni arc, Papua New Guinea. Gondwana Research.
Hopper, J.R., Mutter, J.C., Larson, R.L. and Mutter, C.Z., 1992. Magmatism and rift margin evolution: Evidence from northwest Australia. Geology, 20(9): 853-857.
Hu, X., Garzanti, E., Moore, T. and Raffi, I., 2015. Direct stratigraphic dating of India-Asia collision onset at the Selandian (middle Paleocene, 59±1 Ma). Geology, 43(10): 859-862.
Huber, M. and Goldner, A., 2012. Eocene monsoons. Journal of Asian Earth Sciences, 44: 3-23.
Hutchison, C.S., 1975. Ophiolite in Southeast Asia. Geological Society of America Bulletin, 86(6): 797-806.
Hutchison, C.S., 1996. The 'Rajang accretionary prism'and 'Lupar Line'problem of Borneo. Geological Society, London, Special Publications, 106(1): 247-261.
Hutchison, C.S., 2004. Marginal basin evolution: the southern South China Sea. Marine and Petroleum Geology, 21(9): 1129-1148.
Hutchison, C.S., 2010. Oroclines and paleomagnetism in Borneo and South-East Asia. Tectonophysics, 496(1): 53-67.
Hutchison, C.S., Bergman, S.C., Swauger, D.A. and Graves, J.E., 2000. A Miocene collisional belt in north Borneo: uplift mechanism and isostatic adjustment quantified by thermochronology. Journal of the Geological Society, 157(4): 783-793.
Jagoutz, O., Macdonald, F.A. and Royden, L., 2016. Low-latitude arc–continent collision as a driver for global cooling. Proceedings of the National Academy of Sciences, 113(18): 4935-4940.
Jagoutz, O., Royden, L., Holt, A.F. and Becker, T.W., 2015. Anomalously fast convergence of India and Eurasia caused by double subduction. Nature Geoscience, 8(6): 475-478.
Jagoutz, O. and Schmidt, M.W., 2012. The formation and bulk composition of modern juvenile continental crust: the Kohistan arc. Chemical Geology, 298: 79-96.
Jahn, B.-M., Chen, P.Y. and Yen, T.P., 1976. Rb-Sr ages of granitic rocks in southeastern China and their tectonic significance. Geological Society of America Bulletin, 87(5): 763-776.
Jarvis, G.T. and Lowman, J.P., 2005. Sinking slabs below fossil subduction zones. Physics of The Earth and Planetary Interiors, 152(1-2): 103-115.
Jarvis, G.T. and Lowman, J.P., 2007. Survival times of subducted slab remnants in numerical models of mantle flow. Earth and Planetary Science Letters, 260(1-2): 23-36.
Ji, W.-Q., Wu, F.-Y., Chung, S.-L., Li, J.-X. and Liu, C.-Z., 2009. Zircon U–Pb geochronology and Hf isotopic constraints on petrogenesis of the Gangdese batholith, southern Tibet. Chemical Geology, 262(3): 229-245.
Jolivet, L., Faccenna, C., D'Agostino, N., Fournier, M. and Worrall, D., 1999. The kinematics of back-arc basins, examples from the Tyrrhenian, Aegean and Japan Seas. Geological Society, London, Special Publications, 164(1): 21-53.
Jolivet, L., Huchon, P. and Rangin, C., 1989. Tectonic setting of Western Pacific marginal basins. Tectonophysics, 160(1): 23-47.
Katili, J.A., 1971. A review of the geotectonic theories and tectonic maps of Indonesia. Earth-Science Reviews, 7(3): 143-163.
Katili, J.A., 1975. Volcanism and plate tectonics in the Indonesian island arcs. Tectonophysics, 26(3): 165-188.
Kendrick, R.D., 2000. Structure, tectonics and thermochronology of the Irian Jaya Fold Belt, Irian Jaya, Indonesia, La Trobe University.
Khan, S.D., Walker, D.J., Hall, S.A., Burke, K.C., Shah, M.T. and Stockli, L., 2009. Did the Kohistan-Ladakh island arc collide first with India? Geological Society of America Bulletin, 121(3-4): 366.

Klootwijk, C., Giddings, J., Pigram, C.J., Loxton, C., Davies, H., Rogerson, R. and Falvey, D., 2003. North Sepik region of Papua New Guinea: palaeomagnetic constraints on arc accretion and deformation. Tectonophysics, 362: 273-301.
Kobayashi, K., 2004. Origin of the Palau and Yap trench-arc systems. Geophysical Journal International, 157(3): 1303-1315.
Lambeck, K., Smither, C. and Johnston, P., 1998. Sea level change, glacial rebound and mantle viscosity fornorthern Europe. Geophysical Journal International, 134(1): 102-144.
Le Pichon, X., 1968. Sea-floor spreading and continental drift. Journal of Geophysical Research, 73(12): 3661-3697.
Lee, C.-T.A., Shen, B., Slotnick, B.S., Liao, K., Dickens, G.R., Yokoyama, Y., Lenardic, A., Dasgupta, R., Jellinek, M. and Lackey, J.S., 2013. Continental arc–island arc fluctuations, growth of crustal carbonates, and long-term climate change. Geosphere, 9(1): 21-36.
Lee, T.Y. and Lawver, L.A., 1994. Cenozoic plate reconstruction of the South China Sea region. Tectonophysics, 235(1-2): 149-180.
Lee, T.Y. and Lawver, L.A., 1995. Cenozoic plate reconstruction of Southeast Asia. Tectonophysics, 251(1-4): 85-138.
Leith, C., 1926. The mineral resources of the Far East. Foreign Affairs, 4(3): 433-442.
Leng, W. and Gurnis, M., 2015. Subduction initiation at relic arcs. Geophysical Research Letters, 42.
Li, C., van der Hilst, R.D., Engdahl, E.R. and Burdick, S., 2008. A new global model for P wave speed variations in Earth's mantle. Geochemistry, Geophysics, Geosystems, 9(5): 21.
Li, X., 2000. Cretaceous magmatism and lithospheric extension in Southeast China. Journal of Asian Earth Sciences, 18(3): 293-305.
Li, Z.-H., Xu, Z., Gerya, T. and Burg, J.-P., 2013. Collision of continental corner from 3-D numerical modeling. Earth and Planetary Science Letters, 380: 98-111.
Lithgow‐Bertelloni, C. and Richards, M.A., 1998. The dynamics of Cenozoic and Mesozoic plate motions. Reviews of Geophysics, 36(1): 27-78.
Liu, L. and Gurnis, M., 2008. Simultaneous inversion of mantle properties and initial conditions using an adjoint of mantle convection. Journal of Geophysical Research B, 113(B08405): 17.
Lohman, D.J., de Bruyn, M., Page, T., von Rintelen, K., Hall, R., Ng, P.K., Shih, H.-T., Carvalho, G.R. and von Rintelen, T., 2011. Biogeography of the Indo-Australian archipelago. Annual Review of Ecology, Evolution, and Systematics, 42: 205-226.
Mathews, D.C., 2014. The Absolute Motion of Trenches and Age of the Subducting Slab. Master's Thesis, Department of Earth Science. Rice University: 49.
Matthews, D., 1990. Serendipity or economics? Tin and the theory of mineral discovery and development, 1800–1920. Business History, 32(3): 15-48.
Matthews, K.J., Müller, R.D. and Sandwell, D.T., 2016. Oceanic microplate formation records the onset of India–Eurasia collision. Earth and Planetary Science Letters, 433: 204-214.
Matthews, K.J., Müller, R.D., Wessel, P. and Whittaker, J.M., 2011. The tectonic fabric of the ocean basins. Journal of Geophysical Research, 116(B12): B12109.
Matthews, K.J., Seton, M. and Müller, R.D., 2012. A global-scale plate reorganization event at 105– 100 Ma. Earth and Planetary Science Letters, 355: 283-298.
McCourt, W.J., Crow, M.J., Cobbing, E.J. and Amin, T.C., 1996. Mesozoic and Cenozoic plutonic evolution of SE Asia: evidence from Sumatra, Indonesia. Geological Society, London, Special Publications, 106(1): 321-335.
McDermid, I.R.C., Aitchison, J.C., Davis, A.M., Harrison, T.M. and Grove, M., 2002. The Zedong terrane: a Late Jurassic intra-oceanic magmatic arc within the Yarlung–Tsangpo suture zone, southeastern Tibet. Chemical Geology, 187(3): 267-277.
McElhinny, M.W., Embleton, B.J.J., Ma, X.H. and Zhang, Z.K., 1981. Fragmentation of Asia in the Permian. Nature, 293(5829): 212-214.

McKenzie, D.P., 1969. Speculations on the consequences and causes of plate motions. Geophysical Journal International, 18(1): 1-32.
McKenzie, D.P. and Parker, R.L., 1967. The North Pacific: an example of tectonics on a sphere. Nature, 216: 1276-1280.
McNamara, A.K. and Zhong, S., 2005. Thermochemical structures beneath Africa and the Pacific Ocean. Nature, 437(7062): 1136-1139.
Metcalfe, I., 1988. Origin and assembly of south-east Asian continental terranes. Geological Society, London, Special Publications, 37(1): 101-118.
Metcalfe, I., 1994. Gondwanaland origin, dispersion, and accretion of East and Southeast Asian continental terranes. Journal of South American Earth Sciences, 7(3): 333-347.
Metcalfe, I., 1999. Gondwana dispersion and Asian accretion: an overview. In: I. Metcalfe (Editor), Gondwana dispersion and Asian Accretion. A.A. Balkema, Rotterdam, pp. 9-28.
Metcalfe, I., 2002. Permian tectonic framework and palaeogeography of SE Asia. Journal of Asian Earth Sciences, 20(6): 551-566.
Metcalfe, I., 2006. Palaeozoic and Mesozoic tectonic evolution and palaeogeography of East Asian crustal fragments: The Korean Peninsula in context. Gondwana Research, 9(1-2): 24-46.
Metcalfe, I., 2009. Late Palaeozoic and Mesozoic tectonic and palaeogeographical evolution of SE Asia. Geological Society, London, Special Publications, 315(1): 7-23.
Metcalfe, I., 2011. Tectonic framework and Phanerozoic evolution of Sundaland. Gondwana Research, 19(1): 3-21.
Metcalfe, I. and Irving, E., 1990. Allochthonous Terrane Processes in Southeast Asia [and Discussion]. Philosophical Transactions of the Royal Society of London A: Mathematical, Physical and Engineering Sciences, 331(1620): 625-640.
Miller, M.S., Kennett, B.L.N. and Toy, V.G., 2006. Spatial and temporal evolution of the subducting Pacific plate structure along the western Pacific margin. Journal of Geophysical Research: Solid Earth, 111(B2).
Milsom, J., 2000. Stratigraphic constraints on suture models for eastern Indonesia. Journal of Asian Earth Sciences, 18(6): 761-779.
Mitchell, A., Chung, S.-L., Oo, T., Lin, T.-H. and Hung, C.-H., 2012. Zircon U–Pb ages in Myanmar: Magmatic–metamorphic events and the closure of a neo-Tethys ocean? Journal of Asian Earth Sciences, 56: 1-23.
Monnier, C., Girardeau, J., Maury, R.C. and Cotten, J., 1995. Back-arc basin origin for the East Sulawesi ophiolite (eastern Indonesia). Geology, 23(9): 851-854.
Monnier, C., Girardeau, J., Pubellier, M. and Permana, H., 2000. The central ophiolite belt of Irian Jaya (Indonesia): petrological and geochemical evidence for a back-arc basin origin. Comptes Rendus de l'Academie des Sciences Series IIA Earth and Planetary Science, 331(11): 691-699.
Monod, L. and Prendini, L., 2015. Evidence for Eurogondwana: the roles of dispersal, extinction and vicariance in the evolution and biogeography of Indo‐Pacific Hormuridae (Scorpiones: Scorpionoidea). Cladistics, 31(1): 71-111.
Montelli, R., Nolet, G., Dahlen, F.A. and Masters, G., 2006. A catalogue of deep mantle plumes: new results from finite-frequency tomography. Geochemistry, Geophysics, Geosystems, 7(11): Q11007.
Morley, C.K., 2012a. Late Cretaceous-early Palaeogene tectonic development of SE Asia. Earth-Science Reviews, 115(1-2): 37-75.
Morley, R.J., 2012b. A review of the Cenozoic palaeoclimate history of Southeast Asia. Biotic evolution and environmental change in Southeast Asia. The Systematics Association Special, 82: 79-114.
Morra, G., Seton, M., Quevedo, L. and Müller, R.D., 2013. Organization of the tectonic plates in the last 200 Myr. Earth and Planetary Science Letters, 373: 93-101.
Mubroto, B., Briden, J.C., McClelland, E. and Hall, R., 1994. Palaeomagnetism of the Balantak ophiolite, Sulawesi. Earth and Planetary Science Letters, 125(1): 193-209.

Müller, R.D., Royer, J.Y. and Lawver, L.A., 1993. Revised plate motions relative to the hotspots from combined Atlantic and Indian Ocean hotspot tracks. Geology, 21(3): 275.
Müller, R.D., Sdrolias, M., Gaina, C., Steinberger, B. and Heine, C., 2008. Long-term sea-level fluctuations driven by ocean basin dynamics. Science, 319(5868): 1357.
Müller, R.D., Seton, M., Zahirovic, S., Williams, S.E., Matthews, K.J., Wright, N.M., Shephard, G., Maloney, K.T., Barnett-Moore, N., Hosseinpour, M., Bower, D.J. and Cannon, J., 2016. Ocean basin evolution and global-scale plate reorganization events since Pangea breakup. Annual Review of Earth and Planetary Sciences, 44.
Norton, I.O., 1999. Global plate reconstruction model. ExxonMobil Exploration.
Obayashi, M., Yoshimitsu, J., Nolet, G., Fukao, Y., Shiobara, H., Sugioka, H., Miyamachi, H. and Gao, Y., 2013. Finite frequency whole mantle P wave tomography: Improvement of subducted slab images. Geophysical Research Letters, 40(21): 5652-5657.
Page, R.W., 1976. Geochronology of igneous and metamorphic rocks in the New Guinea Highlands. Australian Government Publ. Service.
Parkinson, C.D., Miyazaki, K., Wakita, K., Barber, A.J. and Carswell, D.A., 1998. An overview and tectonic synthesis of the pre‐Tertiary very‐high‐pressure metamorphic and associated rocks of Java, Sulawesi and Kalimantan, Indonesia. Island Arc, 7(1‐2): 184-200.
Patriat, P. and Achache, J., 1984. India-Eurasia collision chronology has implications for crustal shortening and driving mechanism of plates. Nature, 311: 615-621.
Paulson, A., Zhong, S. and Wahr, J., 2007. Inference of mantle viscosity from GRACE and relative sea level data. Geophysical Journal International, 171(2): 497-508.
Pedersen, R.B., Searle, M.P., Carter, A. and Bandopadhyay, P.C., 2010. U–Pb zircon age of the Andaman ophiolite: implications for the beginning of subduction beneath the Andaman–Sumatra arc. Journal of the Geological Society, 167(6): 1105-1112.
Penrose, R., 1903. The tin deposits of the Malay Peninsula with special reference to those of the Kinta district. The Journal of Geology, 11(2): 135-154.
Permana, H., 1998. Dynamique de la mise en place des ophiolites d'Irian Jaya (Indonesie), PhD thesis of the Universite de Nantes, 314 pp.
Petterson, M.G., 2010. A review of the geology and tectonics of the Kohistan island arc, north Pakistan. Geological Society, London, Special Publications, 338(1): 287-327.
Petterson, M.G. and Windley, B.F., 1985. Rb Sr dating of the Kohistan arc-batholith in the Trans-Himalaya of north Pakistan, and tectonic implications. Earth and Planetary Science Letters, 74(1): 45-57.
Pieters, P.E., Pigram, C.J., Trail, D.S., Dow, D.B., Ratman, N. and Sukamto, R., 1983. The stratigraphy of western Irian Jaya.
Pigram, C.J. and Panggabean, H., 1984. Rifting of the northern margin of the Australian continent and the origin of some microcontinents in eastern Indonesia. Tectonophysics, 107(3): 331-353.
Pigram, C.J. and Symonds, P.A., 1991. A review of the timing of the major tectonic events in the New Guinea Orogen. Journal of Southeast Asian Earth Sciences, 6(3): 307-318.
Polvé, M., Maury, R.C., Bellon, H., Rangin, C., Priadi, B., Yuwono, S., Joron, J.L. and Atmadja, R.S., 1997. Magmatic evolution of Sulawesi (Indonesia): constraints on the Cenozoic geodynamic history of the Sundaland active margin. Tectonophysics, 272(1): 69-92.
Pubellier, M., Ali, J. and Monnier, C., 2003. Cenozoic Plate interaction of the Australia and Philippine Sea Plates:"hit-and-run" tectonics. Tectonophysics, 363(3): 181-199.
Pubellier, M., Monnier, C., Maury, R. and Tamayo, R., 2004. Plate kinematics, origin and tectonic emplacement of supra-subduction ophiolites in SE Asia. Tectonophysics, 392(1): 9-36.
Pubellier, M. and Morley, C.K., 2014. The basins of Sundaland (SE Asia): Evolution and boundary conditions. Marine and Petroleum Geology, 58: 555-578.
Pudsey, C.J., 1986. The Northern Suture, Pakistan: margin of a Cretaceous island arc. Geological Magazine, 123(04): 405-423.

Pudsey, C.J., Schroeder, R. and Skelton, P.W., 1985. Cretaceous (Aptian/Albian) Age for Island-Arc Volcanics, Kohistan, N Pakistan. In: V. Gupta (Editor), Geology of Western Himalayas. Hindustan Publishing Corporation, pp. 150-168.

Pusok, A.E. and Kaus, B.J.P., 2015. Development of topography in 3‐D continental‐collision models. Geochemistry, Geophysics, Geosystems.

Queano, K.L., Ali, J.R., Milsom, J., Aitchison, J.C. and Pubellier, M., 2007. North Luzon and the Philippine Sea Plate motion model: Insights following paleomagnetic, structural, and age-dating investigations. Journal of Geophysical Research, 112(B5): B05101.

Rangin, C., Jolivet, L. and Pubellier, M., 1990. A simple model for the tectonic evolution of southeast Asia and Indonesia region for the past 43 my. Bulletin de la Société géologique de France, 6(6): 889-905.

Ratnaswamy, V., Stadler, G. and Gurnis, M., 2015. Adjoint-based estimation of plate coupling in a non-linear mantle flow model: theory and examples. Geophysical Journal International, 202(2): 768-786.

Rehault, J.P., Moussat, E. and Fabbri, A., 1987. Structural evolution of the Tyrrhenian back-arc basin. Marine Geology, 74(1): 123-150.

Rehman, H.U.R., Seno, T., Yamamoto, H. and Khan, T., 2011. Timing of collision of the Kohistan-Ladakh Arc with India and Asia: Debate. Island Arc, 20(3): 308-328.

Replumaz, A., Karason, H., van der Hilst, R.D., Besse, J. and Tapponnier, P., 2004. 4-D evolution of SE Asia's mantle from geological reconstructions and seismic tomography. Earth and Planetary Science Letters, 221(1-4): 103-115.

Richards, M.A., Bunge, H.P. and Lithgow‐Bertelloni, C., 2000. Mantle convection and plate motion history: toward general circulation models. The history and dynamics of global plate motions: 289-307.

Richter, C. and Ali, J.R., 2015. Philippine Sea Plate motion history: Eocene-Recent record from ODP Site 1201, central West Philippine Basin. Earth and Planetary Science Letters, 410: 165-173.

Rickwood, F.K., 1954. The geology of the western highlands of New Guinea. Journal of the Geological Society of Australia, 2(1): 63-82.

Rock, N.M.S., Aldiss, D.T., Aspden, J.A., Clarke, M.C.G., Djunuddin, A., Miswar, W.K., Thompson, S.J. and Whandoyo, R., 1983. The Geology of the Lubuksikaping Quadrangle, Sumatra. Geol. Survey of Indonesia, Bandung.

Rohrman, M., 2015. Delineating the Exmouth mantle plume (NW Australia) from denudation and magmatic addition estimates. Lithosphere, 7(4): L445. 1.

Rolland, J., Condamine, F.L., Beeravolu, C.R., Jiguet, F. and Morlon, H., 2015. Dispersal is a major driver of the latitudinal diversity gradient of Carnivora. Global Ecology and Biogeography, 24(9): 1059-1071.

Romanowicz, B., 2008. Using seismic waves to image Earth's internal structure. Nature, 451(7176): 266-268.

Rosenbaum, G., 2014. Geodynamics of oroclinal bending: Insights from the Mediterranean. Journal of Geodynamics, 82: 5-15.

Royer, J.Y. and Chang, T., 1991. Evidence for relative motions between the Indian and Australian plates during the last 20 my from plate tectonic reconstructions: implications for the deformation of the Indo-Australian plate. Journal of Geophysical Research, 96(B7): 11779-11,802.

Ryan, W.B., Carbotte, S.M., Coplan, J.O., O'Hara, S., Melkonian, A., Arko, R., Weissel, R.A., Ferrini, V., Goodwillie, A. and Nitsche, F., 2009. Global Multi‐Resolution Topography synthesis. Geochemistry, Geophysics, Geosystems, 10(3).

Sandiford, M., 2007. The tilting continent: a new constraint on the dynamic topographic field from Australia. Earth and Planetary Science Letters, 261(1): 152-163.

Schaltegger, U., Frank, M. and Burg, J.-P., 2003. A 120 million years record of magmatism and crustal melting in the Kohistan Batholith, EGS-AGU-EUG Joint Assembly, pp. 6816.

Schärer, U., Hamet, J. and Allègre, C.J., 1984. The Transhimalaya (Gangdese) plutonism in the Ladakh region: a U Pb and Rb Sr study. Earth and Planetary Science Letters, 67(3): 327-339.
Schellart, W. and Lister, G., 2005. The role of the East Asian active margin in widespread extensional and strike-slip deformation in East Asia. Journal of the Geological Society, 162(6): 959-972.
Schellart, W.P. and Spakman, W., 2015. Australian plate motion and topography linked to fossil New Guinea slab below Lake Eyre. Earth and Planetary Science Letters, 421: 107-116.
Scotese, C., Boucot, A. and McKerrow, W., 1999. Gondwanan palaeogeography and pal1 oclimatology. Journal of African Earth Sciences, 28(1): 99-114.
Scotese, C.R., Gahagan, L.M. and Larson, R.L., 1988. Plate tectonic reconstructions of the Cretaceous and Cenozoic ocean basins. Tectonophysics, 155(1): 27-48.
Sdrolias, M. and Müller, R.D., 2006. Controls on back‐arc basin formation. Geochemistry, Geophysics, Geosystems, 7(4).
Sdrolias, M., Roest, W.R. and Müller, R.D., 2004. An expression of Philippine Sea plate rotation: the Parece Vela and Shikoku basins. Tectonophysics, 394(1): 69-86.
Searle, M.P., Whitehouse, M.J., Robb, L.J., Ghani, A.A., Hutchison, C.S., Sone, M., Ng, S.W.P., Roselee, M.H., Chung, S.-L. and Oliver, G.J.H., 2012. Tectonic evolution of the Sibumasu-Indochina terrane collision zone in Thailand and Malaysia: constraints from new U-Pb zircon chronology of SE Asian tin granitoids. Journal of the Geological Society, 169: 489.
Şengör, A.M.C., Altıner, D., Cin, A., Ustaömer, T. and Hsü, K.J., 1988. Origin and assembly of the Tethyside orogenic collage at the expense of Gondwana Land. Geological Society, London, Special Publications, 37(1): 119-181.
Şengör, A.M.C. and Natal'in, B.A., 1996. Paleotectonics of Asia: Fragments of a synthesis. In: A. Yin and T.M. Harrison (Editors), The Tectonic Evolution of Asia. Cambridge Univ. Press New York, pp. 486-640.
Seton, M., Gaina, C., Müller, R.D. and Heine, C., 2009. Mid-Cretaceous seafloor spreading pulse: Fact or fiction? Geology, 37(8): 687-690.
Seton, M., Müller, R.D., Zahirovic, S., Gaina, C., Torsvik, T.H., Shephard, G., Talsma, A., Gurnis, M., Turner, M., Maus, S. and Chandler, M., 2012. Global continental and ocean basin reconstructions since 200 Ma. Earth-Science Reviews, 113(3-4): 212-270.
Seton, M., Whittaker, J.M., Wessel, P., Müller, R.D., DeMets, C., Merkouriev, S., Cande, S., Gaina, C., Eagles, G. and Granot, R., 2014. Community infrastructure and repository for marine magnetic identifications. Geochemistry, Geophysics, Geosystems, 15(4): 1629-1641.
Sevastjanova, I., Hall, R., Rittner, M., Paw, S.M.T.L., Naing, T.T., Alderton, D.H. and Comfort, G., 2015. Myanmar and Asia united, Australia left behind long ago. Gondwana Research.
Shemenda, A.I., 1993. Subduction of the lithosphere and back arc dynamics: Insights from physical modeling. Journal of Geophysical Research, 98(B9): 16167-16185.
Shi, G., Cui, W., Cao, S., Jiang, N., Jian, P., Liu, D., Miao, L. and Chu, B., 2008. Ion microprobe zircon U–Pb age and geochemistry of the Myanmar jadeitite. Journal of the Geological Society, 165(1): 221-234.
Shi, G., Lei, W., He, H., Ng, Y.N., Liu, Y., Liu, Y., Yuan, Y., Kang, Z. and Xie, G., 2014. Superimposed tectono-metamorphic episodes of Jurassic and Eocene age in the jadeite uplift, Myanmar, as revealed by 40 Ar/39 Ar dating. Gondwana Research, 26(2): 464-474.
Shi, H. and Li, C.-F., 2012. Mesozoic and early Cenozoic tectonic convergence-to-rifting transition prior to opening of the South China Sea. International Geology Review, 54(15): 1801-1828.
Simmons, N., Myers, S., Johannesson, G., Matzel, E. and Grand, S., 2015. Evidence for long‐lived subduction of an ancient tectonic plate beneath the southern Indian Ocean. Geophysical Research Letters, 42(21): 9270-9278.
Simmons, N.A., Forte, A.M., Boschi, L. and Grand, S.P., 2010. GyPSuM: A joint tomographic model of mantle density and seismic wave speeds. Journal of Geophysical Research: Solid Earth (1978–2012), 115(B12).

Smyth, H.R., Hamilton, P.J., Hall, R. and Kinny, P.D., 2007. The deep crust beneath island arcs: Inherited zircons reveal a Gondwana continental fragment beneath East Java, Indonesia. Earth and Planetary Science Letters, 258(1-2): 269-282.
Soeria-Atmadja, R., Noeradi, D. and Priadi, B., 1999. Cenozoic magmatism in Kalimantan and its related geodynamic evolution. Journal of Asian Earth Sciences, 17(1): 25-45.
Spasojevic, S. and Gurnis, M., 2012. Sea level and vertical motion of continents from dynamic earth models since the Late Cretaceous. AAPG bulletin, 96(11): 2037-2064.
Spasojevic, S., Liu, L. and Gurnis, M., 2009. Adjoint models of mantle convection with seismic, plate motion, and stratigraphic constraints: North America since the Late Cretaceous. Geochemistry, Geophysics, Geosystems, 10(5).
Stampfli, G.M. and Borel, G.D., 2002. A plate tectonic model for the Paleozoic and Mesozoic constrained by dynamic plate boundaries and restored synthetic oceanic isochrons. Earth and Planetary Science Letters, 196(1-2): 17-33.
Stauffer, P.H., 1983. Unraveling the mosaic of Paleozoic crustal blocks in Southeast Asia. Geologische Rundschau, 72(3): 1061-1080.
Steinberger, B. and Calderwood, A.R., 2006. Models of large-scale viscous flow in the Earth's mantle with constraints from mineral physics and surface observations. Geophysical Journal International, 167(3): 1461-1481.
Steinberger, B. and O'Connell, R.J., 1998. Advection of plumes in mantle flow: implications for hotspot motion, mantle viscosity and plume distribution. Geophysical Journal International, 132(2): 412-434.
Steinberger, B. and Torsvik, T.H., 2008. Absolute plate motions and true polar wander in the absence of hotspot tracks. Nature, 452(7187): 620-623.
Steinberger, B., Torsvik, T.H. and Becker, T.W., 2012. Subduction to the lower mantle-a comparison between geodynamic and tomographic models. Solid Earth, 3(2): 415.
Stern, R.J., Reagan, M., Ishizuka, O., Ohara, Y. and Whattam, S., 2012. To understand subduction initiation, study forearc crust: To understand forearc crust, study ophiolites. Lithosphere, 4(6): 469-483.
Sukamoto, R. and Westermann, G., 1992. The Jurassic of the Circum- Pacific. Indonesia and Papua New Guinea. Cambridge University Press.
Tapponnier, P., Peltzer, G., Le Dain, A.Y., Armijo, R. and Cobbold, P., 1982. Propagating extrusion tectonics in Asia: New insights from simple experiments with plasticine. Geology, 10(12): 611-616.
Taylor, B. and Hayes, D.E., 1980. The tectonic evolution of the South China Basin. The tectonic and geologic evolution of Southeast Asian seas and islands: 89-104.
Taylor, B. and Hayes, D.E., 1983. Origin and history of the South China Sea basin. The Tectonic and Geologic Evolution of Southeast Asian Seas and Islands: Part 2: 23-56.
Torsvik, T.H., Müller, R.D., van der Voo, R., Steinberger, B. and Gaina, C., 2008. Global plate motion frames: toward a unified model. Reviews of Geophysics, 46(3).
Tovaglieri, F. and George, A.D., 2014. Stratigraphic architecture of an Early–Middle Jurassic tidally influenced deltaic system (Plover Formation), Browse Basin, Australian North West Shelf. Marine and Petroleum Geology, 49: 59-83.
Treloar, P.J., Petterson, M.G., Jan, M.Q. and Sullivan, M., 1996. A re-evaluation of the stratigraphy and evolution of the Kohistan arc sequence, Pakistan Himalaya: implications for magmatic and tectonic arc-building processes. Journal of the Geological Society, 153(5): 681-693.
Turcotte, D.L. and Oxburgh, E.R., 1972. Mantle convection and the new global tectonics. Annual Review of Fluid Mechanics, 4(1): 33-66.
Valenti, G.L., 1993. P'nyang Field: discovery and geology of a gas giant in the western Papuan Fold Belt, Western Province, Papua New Guinea, Proceedings of the Second PNG Petroleum Convention, pp. 413-430.

van der Meer, D.G., Spakman, W., van Hinsbergen, D.J.J., Amaru, M.L. and Torsvik, T.H., 2010. Towards absolute plate motions constrained by lower-mantle slab remnants. Nature Geoscience, 3: 36-40.
van der Meer, D.G., Zeebe, R.E., van Hinsbergen, D.J.J., Sluijs, A., Spakman, W. and Torsvik, T.H., 2014. Plate tectonic controls on atmospheric CO2 levels since the Triassic. Proceedings of the National Academy of Sciences, 111(12): 4380-4385.
van der Voo, R., Spakman, W. and Bijwaard, H., 1999a. Mesozoic subducted slabs under Siberia. Nature, 397(6716): 246-249.
van der Voo, R., Spakman, W. and Bijwaard, H., 1999b. Tethyan subducted slabs under India. Earth and Planetary Science Letters, 171(1): 7-20.
van Dongen, M., Weinberg, R.F., Tomkins, A.G., Armstrong, R.A. and Woodhead, J.D., 2010. Recycling of Proterozoic crust in Pleistocene juvenile magma and rapid formation of the Ok Tedi porphyry Cu–Au deposit, Papua New Guinea. Lithos, 114(3–4): 282-292.
van Hinsbergen, D.J.J., Lippert, P.C., Dupont-Nivet, G., McQuarrie, N., Doubrovine, P.V., Spakman, W. and Torsvik, T.H., 2012. Greater India Basin hypothesis and a two-stage Cenozoic collision between India and Asia. Proceedings of the National Academy of Sciences, 109(20): 7659-7664.
van Hinsbergen, D.J.J., Steinberger, B., Doubrovine, P.V. and Gassmöller, R., 2011. Acceleration and deceleration of India-Asia convergence since the Cretaceous: roles of mantle plumes and continental collision. Journal of Geophysical Research - Solid Earth, 116(B06101).
van Hunen, J. and Allen, M.B., 2011. Continental collision and slab break-off: a comparison of 3-D numerical models with observations. Earth and Planetary Science Letters, 302(1): 27-37.
van Leeuwen, T.M., 1981. The geology of southwest Sulawesi with special reference to the Biru area. The geology and tectonics of Eastern Indonesia, 2: 277-304.
van Ufford, A.Q. and Cloos, M., 2005. Cenozoic tectonics of New Guinea. AAPG bulletin, 89(1): 119-140.
Veevers, J.J., 2004. Gondwanaland from 650–500 Ma assembly through 320 Ma merger in Pangea to 185–100 Ma breakup: supercontinental tectonics via stratigraphy and radiometric dating. Earth-Science Reviews, 68(1-2): 1-132.
Vérard, C., Flores, K. and Stampfli, G., 2012. Geodynamic reconstructions of the South America–Antarctica plate system. Journal of Geodynamics, 53: 43-60.
von Rad, U. and Exon, N.F., 1983. Mesozoic-Cenozoic sedimentary and volcanic evolution of the starved passive continental margin off northwest Australia. In: J. Watkins and C. CDrake (Editors), Studies in Continental Margin Geology: AAPG Mem., pp. 252-281.
von Rad, U., Exon, N.F. and Haq, B.U., 1992. 46. Rift-To-Drift History Of The Wombat Plateau, Northwest Australia: Triassic To Tertiary Leg 122 Results.
Wajzer, M., Barber, A. and Hidayat, S., 1991. Accretion, collision and strike-slip faulting: the Woyla group as a key to the tectonic evolution of North Sumatra. Journal of Southeast Asian Earth Sciences, 6(3-4): 447-461.
Wakita, K., 2000. Cretaceous accretionary–collision complexes in central Indonesia. Journal of Asian Earth Sciences, 18(6): 739-749.
Wakita, K. and Metcalfe, I., 2005. Ocean plate stratigraphy in East and Southeast Asia. Journal of Asian Earth Sciences, 24(6): 679-702.
Wakita, K., Miyazaki, K., Zulkarnain, I., Sopaheluwakan, J. and Sanyoto, P., 1998. Tectonic implications of new age data for the Meratus complex of south Kalimantan, Indonesia. Island Arc, 7(1 – 2): 202-222.
Wang, P., 2004. Cenozoic Deformation and the History of Sea - Land Interactions in Asia. Continent-Ocean Interactions Within East Asian Marginal Seas: 1-22.
Wen, D.-R., Chung, S.-L., Song, B., Iizuka, Y., Yang, H.-J., Ji, J., Liu, D. and Gallet, S., 2008a. Late Cretaceous Gangdese intrusions of adakitic geochemical characteristics, SE Tibet: petrogenesis and tectonic implications. Lithos, 105(1): 1-11.

Wen, D.-R., Liu, D., Chung, S.-L., Chu, M.-F., Ji, J., Zhang, Q., Song, B., Lee, T.-Y., Yeh, M.-W. and Lo, C.-H., 2008b. Zircon SHRIMP U–Pb ages of the Gangdese Batholith and implications for Neotethyan subduction in southern Tibet. Chemical Geology, 252(3): 191-201.
Wennekers, J.H.L., 1958. South Sumatra Basinal Area: Far East, SP 18: Habitat of Oil. AAPG Special Volumes, pp. 1347-1358.
Wessel, P., Smith, W.H.F., Scharroo, R., Luis, J. and Wobbe, F., 2013. Generic Mapping Tools: Improved Version Released. Eos, Transactions American Geophysical Union, 94(45): 409-410.
Whittaker, J.M., Müller, R.D., Sdrolias, M. and Heine, C., 2007. Sunda-Java trench kinematics, slab window formation and overriding plate deformation since the Cretaceous. Earth and Planetary Science Letters, 255(3): 445-457.
Widiyantoro, S., Kennett, B. and Van der Hilst, R., 1998. Extending shear-wave tomography for the lower mantle using S and SKS arrival-time data. Earth, planets and space, 50(11-12): 999-1012.
Widiyantoro, S. and van der Hilst, R.D., 1996. Structure and evolution of subducted lithosphere beneath the Sunda arc, Indonesia. Science Reports, 271(5255): 1566-1570.
Williams, S.E., Whittaker, J.M. and Müller, R.D., 2011. Full‐fit, palinspastic reconstruction of the conjugate Australian‐Antarctic margins. Tectonics, 30(6): 21.
Worthen, J., Stadler, G., Petra, N., Gurnis, M. and Ghattas, O., 2014. Towards adjoint-based inversion for rheological parameters in nonlinear viscous mantle flow. Physics of the Earth and Planetary Interiors, 234: 23-34.
Worthing, M.A. and Crawford, A.J., 1996. The igneous geochemistry and tectonic setting of metabasites from the Emo Metamorphics, Papua New Guinea; a record of the evolution and destruction of a backarc basin. Mineralogy and Petrology, 58(1-2): 79-100.
Wu, J., Suppe, J., Lu, R. and Kanda, R., 2016. Philippine Sea and East Asian plate tectonics since 52 Ma constrained by new subducted slab reconstruction methods. Journal of Geophysical Research: Solid Earth.
Xu, C., Boucot, A., Scotese, C. and Junxuan, F., 2012. Pangaean aggregation and disaggregation with evidence from global climate belts. Journal of Palaeogeography, 1: 5-13.
Yang, S., Hu, S., Cai, D., Feng, X., Chen, L. and Gao, L., 2004. Present-day heat flow, thermal history and tectonic subsidence of the East China Sea Basin. Marine and petroleum geology, 21(9): 1095-1105.
Yang, T., Gurnis, M. and Zahirovic, S., 2016. Mantle‐induced subsidence and compression in SE Asia since the early Miocene. Geophysical Research Letters.
Yin, A. and Harrison, T.M., 2000. Geologic evolution of the Himalayan-Tibetan orogen. Annual Review of Earth and Planetary Sciences, 28(1): 211-280.
Yirgu, G., Ebinger, C.J. and Maguire, P.K.H., 2006. The afar volcanic province within the East African Rift System: introduction. Geological Society, London, Special Publications, 259(1): 1-6.
Yoshida, M. and Hamano, Y., 2015. Pangea breakup and northward drift of the Indian subcontinent reproduced by a numerical model of mantle convection. Scientific reports, 5.
Yumul, G.P., Dimalanta, C.B., Marquez, E.J. and Queaño, K.L., 2009. Onland signatures of the Palawan microcontinental block and Philippine mobile belt collision and crustal growth process: A review. Journal of Asian Earth Sciences, 34(5): 610-623.
Yuwono, Y.S., Priyomarsono, S., Maury, R.C., Rampnoux, J.P., Soeria-Atmadja, R., Bellon, H. and Chotin, P., 1988. Petrology of the Cretaceous magmatic rocks from Meratus Range, southeast Kalimantan. Journal of Southeast Asian Earth Sciences, 2(1): 15-22.
Zahirovic, S., Flament, N., Müller, R.D., Seton, M. and Gurnis, M., In Press. Large fluctuations of shallow seas in low-lying Southeast Asia driven by mantle flow. Geochem. Geophys. Geosys.

2780 Zahirovic, S., Müller, R.D., Seton, M. and Flament, N., 2015. Tectonic speed limits from plate
2781 kinematic reconstructions. Earth and Planetary Science Letters, 418: 40-52.
2782 Zahirovic, S., Müller, R.D., Seton, M., Flament, N., Gurnis, M. and Whittaker, J., 2012. Insights on
2783 the kinematics of the India-Eurasia collision from global geodynamic models. Geochemistry
2784 Geophysics Geosystems, 13(Q04W11).
2785 Zahirovic, S., Seton, M. and Müller, R., 2014. The Cretaceous and Cenozoic tectonic evolution of
2786 Southeast Asia. Solid Earth (EGU), 5: 227-273.
2787 Zaman, H., Otofuji, Y.-i., Khan, S.R. and Ahmad, M.N., 2013. New paleomagnetic results from the
2788 northern margin of the Kohistan Island Arc. Arabian Journal of Geosciences, 6(4): 1041-
2789 1054.
2790 Zaman, H. and Torii, M., 1999. Palaeomagnetic study of Cretaceous red beds from the eastern
2791 Hindukush ranges, northern Pakistan: palaeoreconstruction of the Kohistan–Karakoram
2792 composite unit before the India–Asia collision. Geophysical Journal International, 136(3):
2793 719-738.
2794 Zaw, K., Meffre, S., Lai, C.-K., Burrett, C., Santosh, M., Graham, I., Manaka, T., Salam, A.,
2795 Kamvong, T. and Cromie, P., 2014. Tectonics and metallogeny of mainland Southeast
2796 Asia—A review and contribution. Gondwana Research, 26(1): 5-30.
2797 Zhang, K.-J., Zhang, Y.-X., Tang, X.-C. and Xia, B., 2012. Late Mesozoic tectonic evolution and
2798 growth of the Tibetan plateau prior to the Indo-Asian collision. Earth-Science Reviews,
2799 114(3): 236-249.
2800 Zhao, D., Maruyama, S. and Omori, S., 2007. Mantle dynamics of Western Pacific and East Asia:
2801 insight from seismic tomography and mineral physics. Gondwana Research, 11(1): 120-131.
2802 Zhong, S., Zuber, M.T., Moresi, L. and Gurnis, M., 2000. Role of temperature-dependent viscosity
2803 and surface plates in spherical shell models of mantle convection. Journal of Geophysical
2804 Research, 105(B5): 11063.
2805

2806